UNIVERSITY OF PADOVA

Institution: University of Padova

Department of Biomedical Sciences

Graduate School**: BIOCHEMISTRY AND BIOTECHNOLOGIES**

Specialization area**: BIOCHEMISTRY AND BIOPHYSICS**

XXIII CYCLE

Relationship between mitochondrial ROS formation and myofibrillar protein oxidation in contractile dysfunction.

School Director: Ch.mo Prof. Giuseppe Zanotti

Coordinator: Ch.ma Prof.ssa Maria Catia Sorgato

Supervisor: Ch.mo Prof. Fabio Di Lisa

PhD Candidate: Sara Menazza

31 gennaio 2011

INDEX

ABBREVIATIONS

APS, ammonium persulphate

BSA, bovine serum albumin

cTnI, cardiac Troponin I

Da, dalton

DCB, disulfide cross-bridge

DHE, dihydroethidium

DMSO, dimethyl sulfoxide

dNTP, deoxyribonucleotide triphosphate

EDTA, ethylene diamine tetraacetic acid

EGTA, ethylene glycol tetraacetic acid

EF, ejection fraction

FITC, fluorescein isothiocyanate

FS, fractional shortening

GSH, reduced glutathione

GSSG, oxidized glutathione

GR, glutathione reductase

HF, heart failure

H_2O_2, hydrogen peroxide

HRP, horseradish peroxidase

LVEDD, LV end-diastolic diameter

LVEF, left ventricular ejection fraction

LVSF, left ventricular shortening fraction

MAO, monoamine oxidase

MD, muscular dystrophy

MMP, metalloproteinase

MP, myofibrillar protein

mRNA, messenger ribonucleic acid

NADPH, nicotinamide adenine dinucleotide phosphate

NEM, N-etilmaleimide

NF, non failure

NO, nitric oxide

NOS, nitric oxide synthase

p66Shc, src homology 2 domain containing transforming protein 1

PBS, phosphate buffered saline

PCR, polymerase chain reaction

PTP, permeability transition pore

ROS, reactive oxygen species

SDS, sodium dodecyl sulphate

SOD, superoxide dismutase

Sp1, specificity protein1, transcription factor

TEMED, N,N,N',N'-tetramethylethylene dinamine

Tm, tropomyosin

TUNEL, Terminal deoxynucleotidyl transferase-mediated dUTP nick end labeling

1. SUMMARY

Oxidative stress has been related in numerous cardiovascular and muscular pathologies, but the causal relationship between ROS accumulation and contractile impairment is not clear yet. We hypothesized that upon oxidative stress myofibrillar proteins (MPs) are oxidized providing a relevant contribution to the decrease of contractile performance. Initially, ROS accumulation and MP oxidation were assessed in a rabbit model of heart failure (HF), caused by rapid left ventricular pacing. We found that ROS is increased causing oxidation of MPs that has been detected by means of anti-tropomyosin (Tm) immunoblotting under non reducing conditions. The link between ROS formation and Tm oxidation is further supported by the observation that antioxidant treatment with vitamins C and E reduces both ROS accumulation and Tm oxidation. Then, we extended this study to human failing hearts. We focused our attention on protein carbonylation, an irreversible modification that occurs during severe oxidative stress. Using the oxyblot method we detected an increase of Tm and actin carbonylation in end-stage of human failing hearts compared to non-failing hearts. Interestingly, the degree of Tm and actin carbonylation significantly correlated with contractile impairment and TnI plasma release, a marker of cell viability. Under mild stress proteins can be modified at the level of Cys residues. Thus, we analyzed disulfide cross bridge (DCB) formation in Tm also in human HF. We detected an increased Tm oxidation in HF-group compared to non failure-group (NF), but the correlation between this modification and contractile impairment is less remarkable compared to the correlation with protein carbonylation. This might be because our study analyzed samples collected at end-stage failure, whereas DCB formation is likely to occur at an earlier stage. Considering the large body of evidence related to the

involvement of nitric oxide in HF we investigated whether Tm is also a target of reactive nitrogen species *in vitro*. We demonstrated by mass spectrometry that purified Tm underwent S-nitrosylation when incubated with increasing concentrations of S-nitrosoglutathione, a nitric oxide donor. Based upon this *in vitro* evidence, the occurrence and extent of MP S-nitrosylation were assessed in biopsies from HF- and NF-group by means of the biotin switch technique. Several MPs underwent S-nitrosylation in HF-group compared to NF-group and one of these bands corresponds to Tm. These findings provide the first evidence of S-nitrosylation of a specific MP in human failing hearts. However, Tm nitrosylation did not correlate with cTnI and LVEF. A number of intracellular sources of ROS has already been identified. Mitochondria, and especially mitochondrial respiratory chain, are considered as major intracellular sources of ROS. However, other mitochondrial components resulted to be equally important for ROS generation, such as monoamine oxidase (MAO). In fact, previous studies in Di Lisa's laboratory demonstrated that MAO plays a major role in the amplification of oxidative stress in cardiac disease. Thus, in the second part of this thesis it has been studied the role of MAO in muscle dystrophies (MDs), investigating the contribution of MAO-dependent ROS to contractile dysfunction. We found that in two models of dystrophic mice the activity and the protein level of MAO-A is increased compared to wild-type mice and demonstrated that its inhibition ameliorates the dystrophic phenotype, reducing apoptosis, degeneration/regeneration cycling of the fibers, inflammation, normalizing the fiber area distribution and the contractile impairment. Interestingly, MAO inhibition prevents Tm oxidation, demonstrating that also in MDs Tm oxidation is a link between ROS production and contractile impairment. Taken together, these data

demonstrated for the first time that MAO-dependent ROS accumulation causes MP oxidation with consequent contractile impairment in two models of MD, suggesting that MAO inhibition may represent a new therapeutic tool for these pathologies.

1. SOMMARIO

Lo stress ossidativo è stato riconosciuto come uno dei meccanismi alla base di molte patologie cardiovascolari e muscolari, ma non è ancora stata chiarita quale possa essere la relazione tra l'elevato accumulo di ROS e la disfunzione contrattile. Noi abbiamo ipotizzato che in presenza di stress ossidativo le proteine miofibrillari (MPs) possano venire ossidate, contribuendo cosi al danno contrattile.

Inizialmente abbiamo studiato l'accumulo di ROS e l'ossidazione delle MPs in un modello di scompenso cardiaco causato da stimolazione ad alta frequenza del ventricolo sinistro di coniglio. Utilizzando la tecnica di Immunoblotting è stata individuata, nei cuori scompensati, una maggiore ossidazione delle MPs, in particolare della Tropomiosina (Tm), causata da un elevato accumulo di ROS. Il trattamento antiossidante (con vitamina C ed E) ha validato questo risultato, riducendo sia la presenza di ROS che l'ossidazione della Tm nei conigli con scompenso cardiaco. Successivamente abbiamo esteso questo studio a biopsie di pazienti con scompenso cardiaco. Abbiamo focalizzato la nostra attenzione sulla carbonilazione delle proteine, una modifica irreversibile che avviene in presenza di un marcato stress ossidativo. Utilizzando la tecnica dell'oxyblot abbiamo determinato un aumento di proteine carbonilate nelle biopsie dei pazienti scompensati ed in particolare abbiamo individuato due proteine suscettibili a questa modifica, Tm e actina. Da notare che il grado di carbonilazione di entrambe le proteine correla sia con la disfunzione contrattile che con la diminuita vitalità cellulare. Poiché in presenza di uno stress ossidativo blando le proteine sono sottoposte a modifiche reversibili,

che avvengo a livello dei residui cisteinici, abbiamo analizzato la formazione di ponti disolfuro (DCB) nella Tm anche nei cuori dei pazienti scompensati. Abbiamo individuato un aumento dell'ossidazione della Tm nel cuore umano con scompenso cardiaco, ma la correlazione tra questa modifica e la disfunzione contrattile è meno marcata rispetto alla correlazione con la carbonilazione delle proteine. Questo potrebbe essere dovuto al fatto che il nostro studio analizza campioni provenienti da pazienti con un marcato scompenso cardiaco, mentre la formazione di DCB potrebbe avvenire ad uno stadio di stress ossidativo precedente. Infine, considerando l'elevata presenza dell'ossido nitrico nello scompenso cardiaco, abbiamo valutato la possibilità che la Tm potesse essere un bersaglio anche delle specie reattive dell'azoto. Abbiamo cosi dimostrato, *in vitro*, utilizzando la spettrometria di massa, che la Tm viene nitrosilata se incubata con S-nitrosoglutatione, un donatore di ossido nitrico. Basandoci su queste evidenze *in vitro*, abbiamo analizzato la nitrosilazione delle MPs nelle biopsie di cuori scompensati utilizzando la tecnica del "Biotin Switch". Sono state individuate molte proteine nitrosilate nello scompenso cardiaco ed una è risultata essere la Tm. Comunque la nitrosilazione della Tm non correla con la disfunzione contrattile e la vitalità cellulare.

Sono numerosi i siti intracellulari di produzione di ROS finora individuati. I mitocondri ed in particolare la catena respiratoria mitocondriale sono considerati la maggior fonte di ROS nella cellula. Ciononostante, altri componenti del mitocondrio sono risultati essere ugualmente importanti per la generazione dei ROS, come la monoamino ossidasi (MAO). Infatti, lavori recenti condotti nel laboratorio del Prof. Di Lisa dimostrano che la MAO ha

un ruolo importante nell'amplificare lo stress ossidativo nelle patologie cardiache. Cosi, nella seconda parte della tesi è stato caratterizzato il ruolo della MAO nelle distrofie muscolari (MDs), analizzando quanto importante possa essere il contributo dei ROS prodotti dalla MAO nella disfunzione contrattile. Abbiamo individuato, in due modelli murini di MD, un' elevata attività ed espressione proteica della MAO A rispetto ai topi controllo e dimostrato che la sua inibizione farmacologica migliora il fenotipo distrofico, riducendo l'apoptosi, la rigenerazione delle fibre, l'infiammazione e la disfunzione contrattile. Inoltre, l'inibizione della MAO previene l'ossidazione della Tm, dimostrando che anche nelle MDs la Tm mette in relazione la produzione di ROS con la disfunzione contrattile.

L'insieme di questi dati dimostra per la prima volta che i ROS prodotti dalla MAO sono responsabili dell'ossidazione delle MPs causando disfunzione contrattile in due modelli di MD e suggerendo un nuovo approccio terapeutico per queste patologie.

2. INTRODUCTION

2.1 Reactive oxygen species and reactive nitrogen species

Oxygen is an indispensable molecule for the aerobic organisms; however it can become toxic when it is partially reduced. In that case, unstable and reactive intermediates are formed and it has been demonstrated that they are involved in numerous pathophysiological conditions, such as aging, cancer, myocardial infarction, neurodegenerative diseases and many others (1). Atoms or molecules with unpaired electrons are designated as free radicals and are highly reactive entities that can readily participate in a variety of chemical and biochemical reactions. In the aerobic environment, cells generate energy at mitochondrial level, reducing molecular oxygen to water during the electron transport in the mitochondrial respiratory chain. Molecular oxygen is found in nature as a diatomic molecule, presenting two unpaired electrons with parallel spin in its outermost shell (triplet oxygen) and this configuration makes it a non-reactive and weak oxidant. The complete reduction of one molecule of oxygen to 2 molecules of water requires the transfer of 4 electrons. However, partial reduction of oxygen during this process can generate reactive intermediates, known as reactive oxygen species (ROS) (2,3).

The products of partial oxygen reduction are following:

- Singlet oxygen (O_2): it is the molecular oxygen in its first excited singlet state, presenting both electrons in the same molecular orbital with paired spins. It is generated by the transfer of energy to the triplet molecular oxygen and it has been postulated to be an important intermediate in a

range of biological systems. Most commonly, singlet oxygen is formed following exposure to UV or visible light in the presence of chromophores that can act as sensitizing agents, such as tryptophan, tyrosine or cysteine. However, it can also be formed by a range of peroxidase enzymes or during the reaction of H_2O_2 with peroxynitrite. O_2 interacts with a wide range of biological targets, including DNA, RNA, proteins, lipids and sterols. In proteins, it has been demonstrated to interact with tryptophan, tyrosine, histidine, methionine and cysteine side chains (4).

- Superoxide anion ($O_2^{\bullet-}$) : it is formed following a single electron donation to molecular oxygen.

$$O_2 + e^- \rightarrow O_2^{\bullet-}$$

The biological toxicity of superoxide is due to its capacity to inactivate iron-sulfur cluster containing enzymes, critical in a wide variety of metabolic pathways, thereby liberating free iron in the cell, which can undergo Fenton chemistry and generate the highly reactive hydroxyl radical. In its $HO_2^{\bullet}$ form (hydroperoxyl radical), superoxide can also initiate lipid peroxidation of polyunsaturated fatty acids (5). It also reacts with carbonyl compounds and halogenated carbons to create toxic peroxy radicals. Superoxide can also react with $NO^{\bullet}$ to form peroxynitrite. As such, superoxide is one of the main causes of oxidative stress. Superoxide can also produce hydrogen peroxide through a dismutation reaction catalyzed by superoxide dismutase.

However, this may be followed by hydroxyl radical formation through the Haber-Weiss reaction (6).

$$2O_2^{\bullet-} + H^+ \rightarrow O_2 + H_2O_2$$

$$O_2^{\bullet-} + H_2O_2 \rightarrow OH^{\bullet-} + OH^- + O_2$$

- Nitric oxide ($NO^{\bullet}$): It reacts with molecular oxygen (O_2) and its derivatives (ROS) to generate a range of oxidation products (NO_x) whose downstream reactivities greatly increase the breadth of what is termed “NO signaling”. These reactive nitrogen species (RNS) differentially induce biomolecule oxidation, nitration (addition of NO_2) and nitrosation (addition of NO). One well-characterized RNS-forming reaction is that of $NO^{\bullet}$ with $O_2^{\bullet-}$ to produce peroxynitrite ($ONOO^-$). It is strongly oxidizing, and when protonated produce hydroxyl radical ($OH^{\bullet-}$) and nitrogen dioxide ($NO_2^{\bullet}$) (7). Moreover, $ONOO^-$ reacts with CO_2 to form nitrosoperoxycarbonate ($ONOOCO_2^-$), a reaction that leads to the formation of a carbonate radical ($HCO_3^{\cdot}$). Through its own activity and that of its byproducts, $ONOO^-$ engages in lipid and protein oxidation and nitration, enabling signal transduction and changes in cellular function (8).
- Hydrogen peroxide (H_2O_2): it is formed when two electrons are donated to molecular oxygen according to the reaction:

$$O_2 + 2e^- + 2H^+ \rightarrow H_2O_2$$

Otherwise, it is formed by superoxide anion dismutation. It is lipid soluble and thus able to diffuse across membranes. Depending on concentrations, H_2O_2 can act as a signaling molecule. However, it can be a dangerous species for the biological systems, as in the presence of ions such as Fe^{2+} e Cu^+, it can generate highly reactive hydroxyl radical according to the Fenton reaction (9):

$$H_2O_2 + Fe^{2+} \rightarrow OH^{\bullet-} + OH^- + Fe^{3+}$$

- Hydroxyl radical ($OH^{\bullet}$): it is the most dangerous ROS for the biological systems, as it can not be neutralized by enzymatic antioxidant systems. It is formed following the reaction of H_2O_2 with ferrous ions during the Fenton reaction, as a product of a reaction between superoxide and H_2O_2 (Haber-Weiss reaction) or during water radiolysis induced by electromagnetic irradiation. The hydroxyl radical cannot be eliminated by an enzymatic reaction, as this would require its diffusion to the enzyme's active site. As diffusion is slower than the half-life of the molecule, it will react with any oxidizable compound in its vicinity. It can damage virtually all types of macromolecules: carbohydrates, nucleic acids (mutations), lipids (lipid peroxidation) and amino acids (e.g. conversion of Phe to m-Tyrosine and o-Tyrosine, carbonyl formation see par. 2.5 and (10)). The only means to protect important cellular structures is the use of effective repair systems and antioxidants.

2.2 Mitochondrial formation of reactive oxygen species

ROS are produced both enzymatically and non-enzymatically by several intracellular sources. Enzymatic sources include NADPH oxidase, located on the cell membrane, cytochrome P_{450}-dependent oxygenases, xanthine oxidase (XO) and nitric oxide synthase that, when uncoupled, can become a powerful ROS generator.

However, the largest amount of intracellular ROS is formed within the mitochondria, although a major and unsolved issue is where ROS are generated in mitochondria (3,11-13). The majority of oxygen delivered to mitochondria is fully

reduced to water at the level of complex IV of the respiratory chain. Nevertheless, electrons flowing through the respiratory chain can be donated to oxygen at other sites resulting in a formation of partially reduced oxygen species, such as superoxide anion. Indeed, superoxide is formed at the level of Complex I and III and rapidly dismutated into H_2O_2 by Mn-SOD.

However other mitochondrial components contribute to ROS generation, such as monoamine oxidase (MAO), p66shc and NOX4 (14,15). These additional mitochondrial proteins produce significant amount of ROS. For example, Davies and coworkers demonstrated that in brain mitochondria the highest rate of H_2O_2 formation from respiratory chain is 48-fold lower than that originating from MAO activity (16).

2.2.1 Respiratory Chain

Although the mitochondrial electron transport chain is a very efficient system for the production of ATP, the nature of the alternating oxidation-reduction reactions it catalyzes, predisposes each electron carrier to side reactions with molecular oxygen. The superoxide anion radical (O_2•R) and hydrogen peroxide (H_2O_2), the products of the univalent and bivalent reduction of oxygen respectively, are produced during normal aerobic metabolism and constitute physiological intracellular metabolites. The physiological rate of the mitochondrial production of O_2•R and H_2O_2 associated with the electron transfer chain is dependent on the mitochondrial metabolic state: the resting mitochondrial state 4 is characterized by a relatively slow rate of respiration and no availability of ADP and is associated with a relatively high rate of O_2•R and H_2O_2 production, probably as a consequence of the high reduction state of the components of the respiratory chain (16). Conversely, the active mitochondrial respiratory state 3, with a high

rate of oxygen uptake and ample availability of ADP, shows a relatively slow rate of O_2•R and H_2O_2 production due to the highly oxidized state of the components of the respiratory chain. Evidence indicate that, *in vitro*, mitochondria convert 1–2% of the oxygen molecules consumed into superoxide anions. Given that these initial estimates were made on isolated mitochondria in the presence of high, nonphysiological concentrations of oxygen, the *in vivo* rate of mitochondrial superoxide production is undoubtedly considerably less. The production of mitochondrial superoxide radicals occurs primarily at two discrete points in the electron transport chain, namely at complex I (NADH dehydrogenase) and at complex III (ubiquinone–cytochrome *c* reductase) (Fig. 1) (17,18). However, given the potentially harmful effects of ROS, mitochondria possess efficient systems for their neutralization. Superoxide produced at the level of Complex I and III is rapidly transformed into H_2O_2 by Mn-SOD present in the mitochondrial matrix. ROS production in mitochondria is however increased in various pathological conditions such as hypoxia, ischemia and reperfusion, ageing and following the inhibition of the mitochondrial respiratory chain.

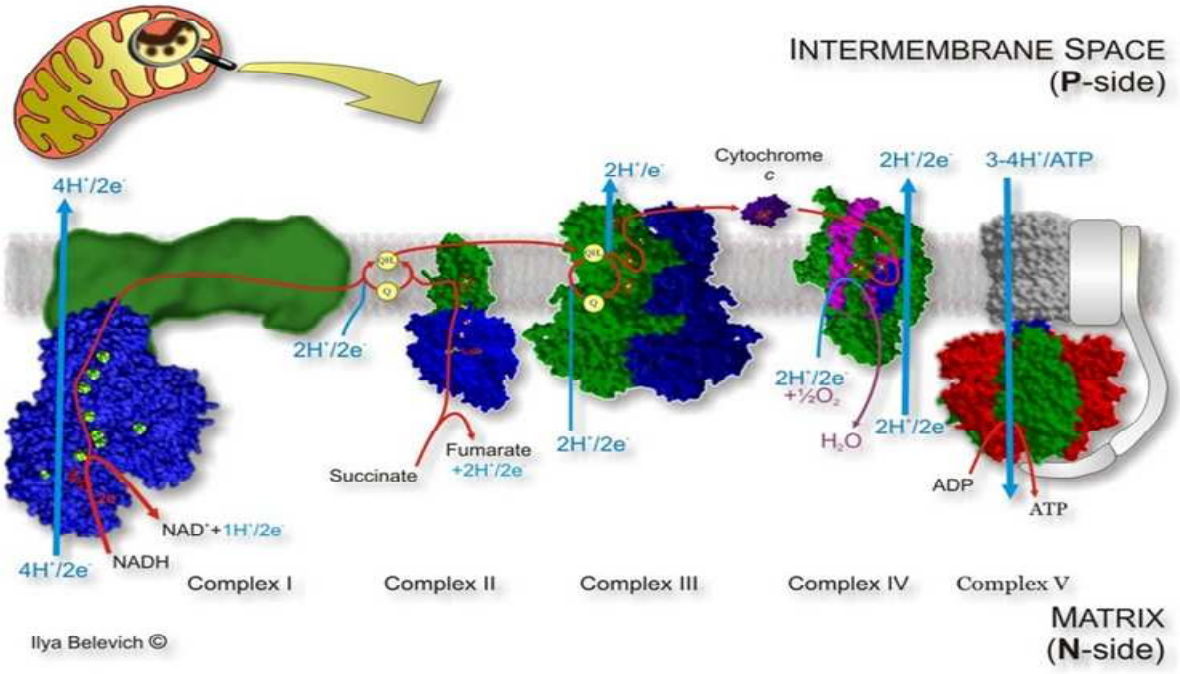

Figure 1. Schematic representation of mitochondria respiratory chain.
The major sources of ROS are Complex I and III.

2.2.2 p66shc

P66shc is a vertebrate splice variant of p52shc and p46shc, two cytoplasmic adaptor proteins involved in the propagation of intracellular signals from activated tyrosine kinases to Ras (19). However, p66shc is not involved in Ras regulation, but rather functions in the intracellular pathways that regulates ROS metabolism and apoptosis (20). In fact, when pKCbeta phosphorylation of p66shc cause its translocation into the mitochondria, the ROS formation is enhanced (21,22). Several studies demonstrated clearly that ROS formation is reduced in cell lacking p66shc, and that systemic and intracellular markers of oxidative stress are diminished in p66 $shc^{-/-}$ mice (21,23,24).

2.2.3 Monoamine oxidases (MAO)

MAO is a flavoenzyme located within the outer mitochondrial membrane, responsible for the oxidation of neurotransmitters and dietary amines. There are two isoforms, MAO-A and MAO-B that differ for subtrate specificity and inhibitor sensitivity (25). MAO-A catalyzes preferentially the oxidative deamination of norepinefrine (NE), and serotonine (5-HT) and is inhibited by low concentration of clorgyline. In contrast, MAO-B has higher affinity for phenylethylamine and benzylamine, and is inhibited by selegiline (26). Both the isoform catalyze the deamination of dopamine, tyramine, octopamine, tryptamine and are inhibited by pargyline. MAO inhibitors can be classified in three groups: (i) irreversible and non selective inhibitors, such as phenelzine, tranylcypromine and tyramine; (ii) irreversible and selective inhibitors, such as seleginine for MAO-B and clorgyline for MAO-A; (iii) reversible and selective inhibitors, such as moclobemide for MAO-A and lazabemide for MAO-B.

These two enzymes show 70% homology in their primary sequence (25,27,28) and both contain the pentapeptide Ser-Gly-Gly-Cys-Tyr, where the obligatory cofactor FAD is covalently bound through a thioether linkage to the cysteine residue (27,28) namely Cys406 in MAO-A and Cys397 in MAO-B (29,30). This flavin moiety is the only redox factor necessary for the explication of their activity. MAO-A and B are integrated proteins of the outer membrane of mitochondria, anchored through a C-terminal α-helix segment that protrudes from the basal face of the structure and is highly hydrophobic, therefore facilitating the insertion into the membrane. For that reason, their crystallization has been difficult and human enzymes have been crystallized only recently (31,32) (Fig. 2).

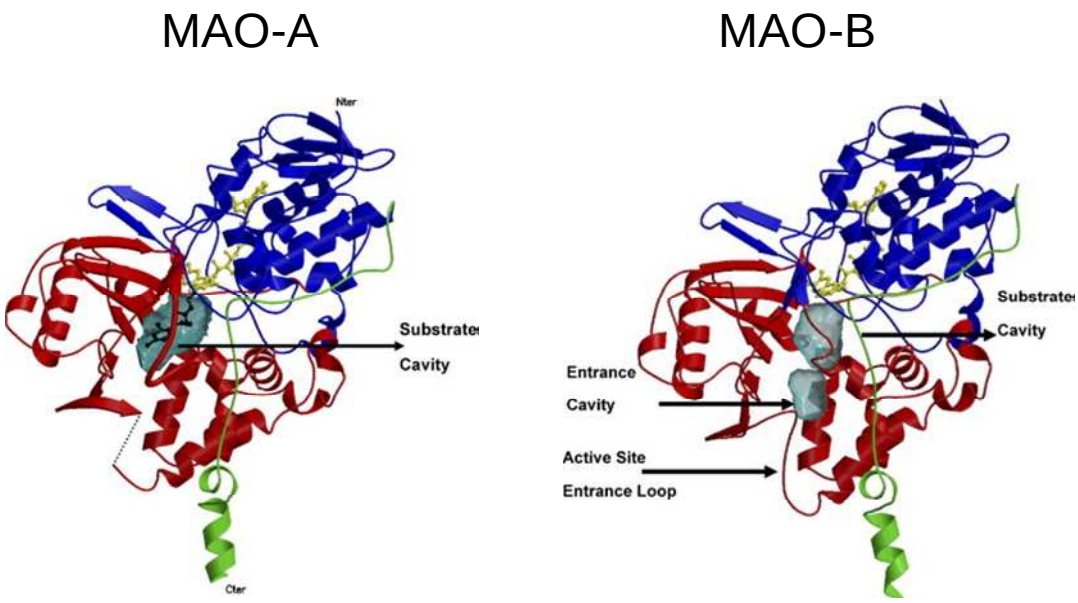

Figure 2. Ribbon diagram of human MAO-A and –B structures.
The covalent flavin moiety is shown in a ball and stick model in yellow. The flavin binding domain is in blue, the substrate domain in red and the membrane binding domain in green. *From Edmondson et al, 2007.*

MAO-B crystallizes as a dimer, with each monomer presenting a C-terminal membrane bound domain, FAD binding domain and a substrate binding domain (31,33). For a substrate molecule to reach the flavin center, it must first negotiate a protein loop at the entrance to one of the two cavities before reaching the flavin coenzyme. The first cavity is very hydrophobic in nature and has been named the “entrance cavity”. Separating the “entrance cavity” from a similarly hydrophobic “substrate cavity” is an Ile199 side chain which serves as a gate between the two cavities. At the end of the “substrate cavity” is the FAD coenzyme (34). In contrast to human MAO-B, human MAO-A crystallizes as a monomer (32). It has only single substrate binding cavities with protein loops at the entrances of either cavity. The single cavity in MAO-A displays a rounder shape and is larger in volume than the substrate cavity in MAO-B. Analysis of residue side chains in either active site shows the substrate to have less freedom for rotation in the

MAO-B site than in MAO-A. The structural basis for this difference can be partially attributed to the conformational differences of the 200-215 residue segment that constitutes the “cavity shaping loop” in both isoforms. This loop is in a more extended conformation in MAO-A and in a more compact conformation in MAO-B.

MAO catalyze the following reaction:

$RCH_2NR'R'' + O_2 + H_2O \rightarrow RCHO + NR'R'' + H_2O_2$

Kinetic studies have shown that the binding of the amine group to the enzyme precedes the binding of oxygen (35). In a cystein residue of MAO there is a covalent bind with FAD (29). In a first moment, the reduction of the cofactor FAD yields an aldehyde intermediate and ammonia, while in a second moment the oxidized form of the prosthetic group is restored with the concomitant production of hydrogen peroxide.

$RCH_2NH_2 + MAO \rightarrow RCHO + NH_3 + MAO\text{-reduced}$

$MAO\text{-reduced} + O_2 \rightarrow MAO + H_2O_2$

The aldehyde intermediates are rapidly metabolized to the corresponding acid by the action of aldehyde dehydrogenase (ALDH).

The distribution of MAO in various tissues of different species has been investigated by use of specific inhibitors, immunohistochemistry, enzyme autoradiography and *in situ* hybridization (36-38). Their distribution has been particularly studied in the brain, where MAO-A has been prevalently found in noradrenergic neurons whereas MAO-B has been detected in serotoninergic and

histaminergic neurons and in glial cells (39-42). In peripheral tissues, MAO-A has been found in placenta, liver, intestine and thyroid gland, while platelets, liver and kidney contain mainly MAO-B. Human cardiomyocytes contain both enzymes, although MAO-A is the predominant isoform (43-45).

Differential expression of MAO-A and B genes might be due to differences in their core promoter regions. MAO-B, but not MAO-A, expression is regulated by mitogen-activated protein kinase (MAPK) pathway that includes PKC, the small G protein Ras, ERK, MEK3, MEK7, ERK2, JNK1 and p38 (46). Progesterone, testosterone, corticosterone and glucocorticoids increase the levels of MAO-A, but have little or no effect on MAO-B (47,48). Likewise, MAO-A is elevated in the endometrium, reproductive tissue and the brain where levels of progesterone are high during the oestrous cycle. Castration leads to a threefold increase in MAO-A activity and this increase can be prevented the administration of oestradiol or testosterone. Both MAO-A and B promoters are GC-rich and are regulated by Sp1 family of transcription factors (46). However, they have distinctly different features. MAO-B gene, but not MAO-A gene, has TATA box and MAO-B promoter contains two clusters of overlapping Sp1 sites, the CACCC repressor element (Fig. 3). Another interesting feature of human MAO-A and MAO-B promoters is the fact that they appear to have the cAMP responsive element, which suggests that their expression might be regulated by the activation of receptors coupled to adenylate cyclase (49,50).

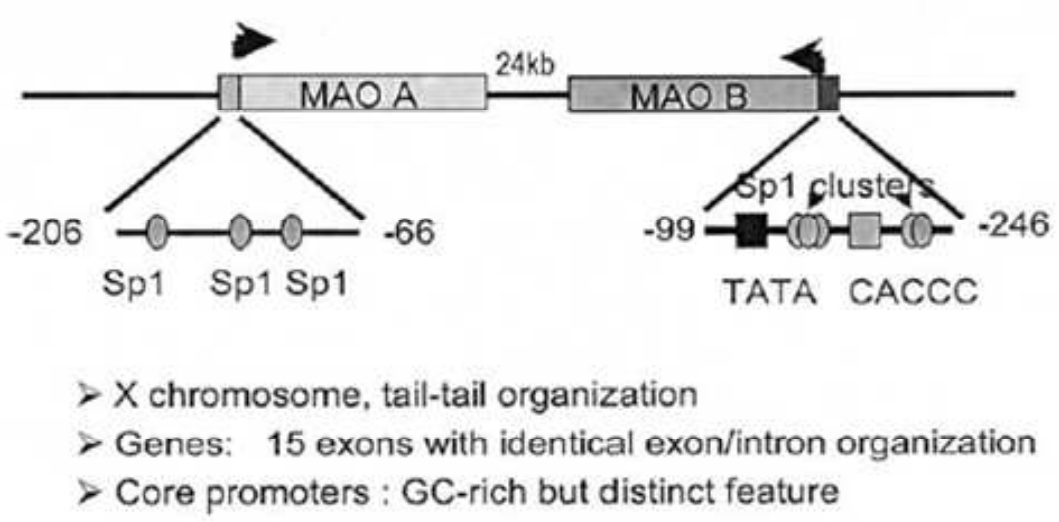

Figure 3. Schematic representation of MAO and –B genes and their core promoters. *From Shih et al, 2004.*

Deletion of MAO-B in human causes a rare form of disease, the so-called Norrie disease, thus indicating that MAO is not essential for survival (51). Gene deletion has shown that MAO-A activity is important during development. A compulsive-aggressive behaviour results from lack of MAO-A function in human (52) and in mice (53). This effect, which might reflect the importance of serotonin during development, can be mimicked by the administration of MAO-A inhibitor clorgyline during the early postnatal period.

MAO is involved in numerous pathologies, in particular in neuronal and psychiatric disorders. MAO-B appears to be involved in the loss of dopaminergic neurons that occurs in Parkinson's disease, most likely due to the increased dopamine catabolism, resulting in elevated production of ROS responsible for the oxidative damage at the level of nigrostriatal neurons. An increased in MAO-B activity in brain is also associated to Alzheimer's and Huntington's diseases. In contrast, MAO-A isoform has been shown to play a relevant role in myocardial injury caused by post-ischemic reperfusion (54) and also in the maladaptive evolution of

myocardial hypertrophy into failure (55). Moreover, MAO-A activity increased with aging (56).

2.2.4 nox4

NADPH oxidases (nox) are a family of transmembrane enzymes dedicated to produce $O_2^{\bullet-}$ by transferring an electron from NAD(P)H to molecular oxygen. Interestingly, only nox 4 is localized primarily at mitochondria in cardiac myocytes, and its upregulation upon hypertrophic stimuli enhances $O_2^{\bullet-}$ production, and mitochondria dysfunction (57).

2.3 Mitochondria antioxidant defences

ROS are constantly formed, even under physiological conditions. However, their production is counterbalanced by several cellular mechanisms, including enzymatic and non enzymatic pathways (58). Among the best characterized enzymatic systems are:

1. Superoxide dismutase (SOD): in eukaryotic cells, $O_2^{\bullet-}$ can be metabolized to hydrogen peroxide by two metal-containing SOD isoenzymes, an 80-kDa tetrameric Mn-SOD present in mitochondria (59), and the cytosolic 32- kDa dimeric Cu/Zn-SOD (60). In the reaction catalyzed by SOD, two molecules of superoxide form hydrogen peroxide and molecular oxygen and are thereby a source of cellular hydrogen peroxide. The reaction catalyzed by SOD is extremely efficient, limited in essence only by diffusion.

$$O_2\bullet^- + O_2\bullet^- + 2H^+ \rightarrow H_2O_2 + O_2$$

2. Catalase: catalases of many organisms are mainly heme-containing enzymes. This enzyme is predominantly localized in mitochondria and peroxisomes, where it catalyzes the dismutation of hydrogen peroxide to water and molecular oxygen:

$$2H_2O_2 \rightarrow 2H_2O + O_2$$

Catalase is also involved in detoxifying different substrates, e.g., phenols and alcohols, via coupled reduction of hydrogen peroxide:

$$H_2O_2 + RH_2 \rightarrow 2H_2O + R$$

One antioxidative role of catalase is to lower the risk of hydroxyl radical formation from H_2O_2 via the Fenton-reaction catalyzed by Cu^+ or Fe^{2+} ions. Catalase binds NADPH, which protects the enzyme from inactivation and increases its efficiency.

3. Glutathione peroxidase (GPx) and glutathione reductase (GR): There are at least four different GPx in mammals (GPx1–4), all of them containing selenocysteine (61). GPx1 and GPx4 (or phospholipid hydroperoxide GPx) are both cytosolic enzymes abundant in most tissues. GPx is also localized at the mitochondrial level where it catalyzes the reduction of H_2O_2 produced by Mn-SOD, using glutathione as substrate. This system affords protection against low levels of oxidative stress, while catalase is more efficient when oxidative burden is increased (62). They can also reduce other peroxides

(e.g., lipid peroxides in cell membranes) to alcohols. In physiological conditions, reduced glutathione (GSH) is used for the 32 reduction of H_2O_2 and is transformed into oxidized glutathione (GSSH). GR is the flavoenzyme that restores GSH.

4. Thioredoxin system: is constituted from thioredoxin (Trx), thioredoxin reductase (TrxR) and NAPDH and operates as a powerful protein disulfide oxidoreductase system. Trx is a 12 kDa protein containing a dithioldisulfide active site. It acts as antioxidant by facilitating the reduction of other proteins by cysteine thiol-disulfide exchange. The oxidized Trx is reduced and regenerated by the flavoenzyme TrxR, in a NADPH-dependent reaction. Thioredoxins act as electron donors to peroxidases and can catalyze the regeneration of many antioxidant molecules, including ubiquinone, lipoic acid and ascorbic acid (Fig. 4).

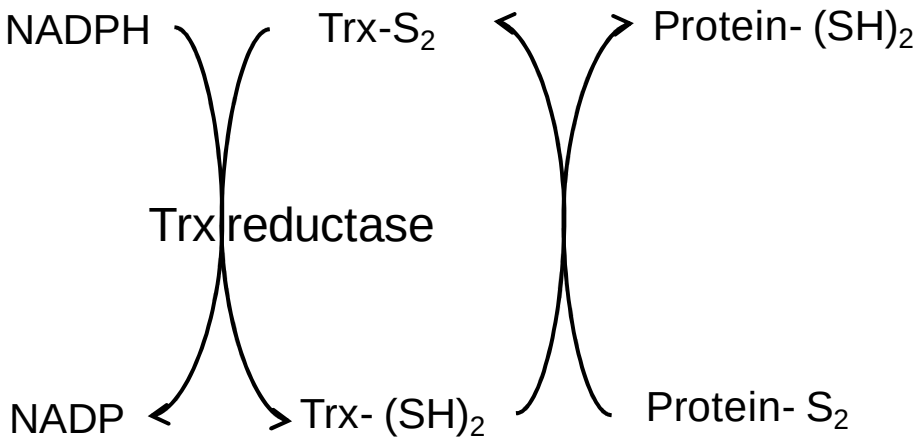

Figure 4. The thioredoxin system.
Thioredoxin reduces disulfides and methionine sulfoxides in oxidizied proteins with a concomitant oxidation of cysteine moieties. The corresponding disulfide is, in turn, reduced by thioredoxin reductase.

Besides the enzymatic systems, there is a number of intracellular antioxidants that act as scavengers:

1. Vitamin E (P-tocopherol): it is the most studied of the fat-soluble antioxidant vitamins as it has the highest bioavailability, with the body preferentially absorbing and metabolizing this form. It has been suggested that the P-tocopherol form is the most important lipid-soluble antioxidant, and that it protects membranes from oxidation by reacting with lipid radicals produced in the lipid peroxidation chain reaction (63).

$$VitE\text{-}OH + LOO\bullet \rightarrow VitE\text{-}O\bullet + LOOH$$

This removes the free radical intermediates and prevents the propagation reaction from continuing. The tocopheril radical that is formed is fairly stable, not reactive and does not contribute to the formation of other radicals. The oxidized P-tocopheroxyl radicals produced in this process may be recycled back to the active reduced form through reduction by ascorbate, retinol or ubiquinol. The functions of the other forms of vitamin E are less well-studied, although T-tocopherol is a nucleophile that may react with electrophilic mutagens, and tocotrienols may have a specialized role in neuroprotection.

2. Vitamin C (ascorbic acid): it is a water soluble antioxidant found in both animals and plants. In cells, it is maintained in its reduced form by reaction with glutathione, which can be catalyzed by protein disulfide isomerase and glutaredoxins (64). Ascorbic acid is a reducing agent and can easily donate

a hydrogen atom form the hydroxyl group bound to carbon 2 and thereby neutralize ROS such as hydrogen peroxide.

3. Glutathione (GSH): is a cysteine containing peptide (Glu-Cys-Gly). Glutathione has antioxidant properties since the thiol group in its cysteine moiety is a reducing agent and can be reversibly oxidized and reduced. In cells, glutathione is maintained in the reduced form by the enzyme glutathione reductase and in turn reduces other metabolites and enzyme systems as well as reacting directly with oxidants (Fig. 5). Due to its high concentration and its central role in maintaining the cell redox state, glutathione is one of the most important cellular antioxidants.

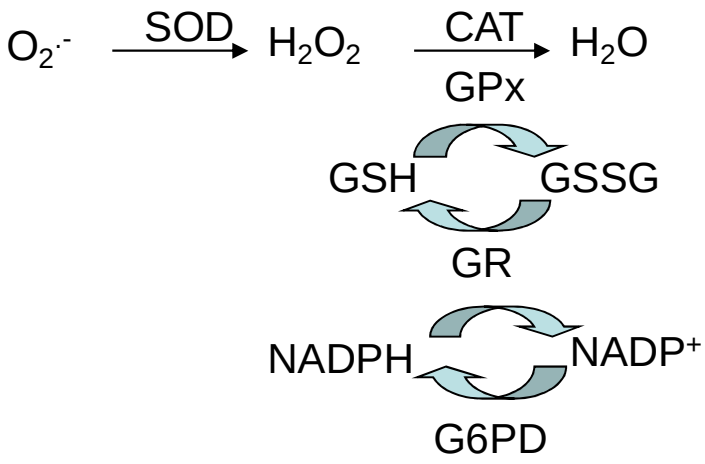

Figure 5. Glutathione redox cycle.
Hydrogen peroxide is reduced to water with the concomitant oxidation of glutathione (GSH) to glutathione disulfide (GSSG). Considering that intracellular amounts of GSH are limited, the reduced form is restored by the action of the enzyme glutathione reductase.

4. Bilirubin: is the end product of heme catabolism in mammals that can efficiently scavenge peroxyl radical (65). Heme oxygenase is a stress-inducible enzyme that catalyzes the degradation of heme to liberate, among other products, biliverdin IX, a hydrophilic compound that is reduced by

biliverdin reductase to bilirubin. There is evidence that bilirubin can protect cells and LDL against lipid peroxidation and contribute to the antioxidant capacity of jaundiced newborn infants. The antioxidant mechanism by which bilirubin deactivates peroxyl radicals, the main chain-carrying radicals in lipid peroxidation, is still not completely clear. However, the proposed mechanisms include hydrogen atom transfer from the methylene at position C-10 to peroxyl radicals, peroxyl radical addition to the pyrroles, and single electron transfer.

5. Uric acid: derives from purine metabolism and it is the most abundant aqueous antioxidant in humans. Local concentrations of uric acid have been shown to increase during acute oxidative stress and ischemia, likely reflecting a compensatory mechanism that confers protection against increased free radical activity (66). Uric acid is particularly effective in quenching hydroxyl, superoxide and peroxynitrite radicals, and may serve a protective physiological role by preventing lipid peroxidation.

2.4 ROS/RNS Targets

“Oxidative stress” is an expression used to describe various deleterious processes resulting from an imbalance between the excessive formation of ROS and/or RNS and limited antioxidant defences (Fig. 6). While small fluctuations in the steady-state concentration of these oxidants may actually play a role in intracellular signalling, uncontrolled increases in the steady-state concentrations of these oxidants lead to free radical-mediated chain reactions which can be dangerous for

biological systems for their capacity to interact with numerous macromolecules, such as proteins, lipids and DNA.

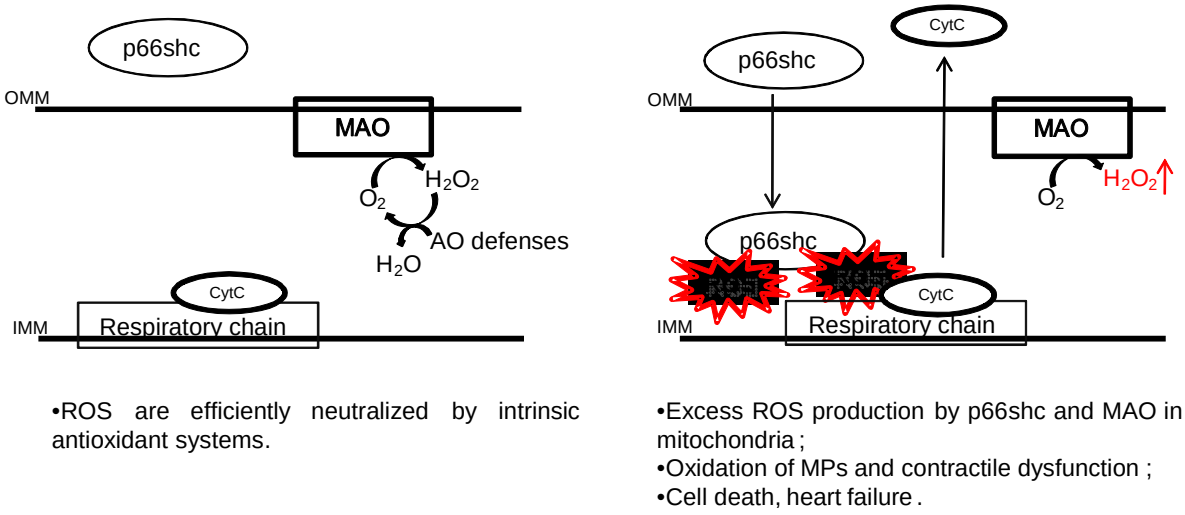

Figure 6. Mitochondrial sources of reactive oxygen species (ROS).
Under physiological conditions (left panel), p66Shc is localized in the cytosol while ROS production by MAO is neutralized by antioxidant defenses. However, pathological stimuli (such as ischemia/reperfusion injury, right panel) or diseases may trigger signaling pathways that mediate p66Shc translocation into the mitochondria and an increased activity of MAO. Both these events result in increased ROS production that may overwhelm cellular antioxidant defenses leading to contractile dysfunction, PTP opening, cell death, and heart failure. OMM outer mitochondrial membrane, IMM inner mitochondrial membrane, cyt c cytochrome c, MAO monoamine oxidase, AO defenses antioxidant defenses. *From Di Lisa et al, 2009.*

Three types of reaction can occur: extraction of an H• from an organic molecule; addition of OH•; and electron transfer. The common feature of these reactions is that the initial reaction is always amplified due to the formation of another radical, resulting in a chain reaction. Therefore, these molecules are dangerous not only because of their reactivity, but also because of their capacity to trigger chain reactions, resulting in formation of secondary radicals that can diffuse and lead to the propagation of the damage. These reactions can terminate only when free radicals are in the presence of a similar molecule, able to neutralize them (i.e. scavenger), or an enzymatic system, able to metabolize them.

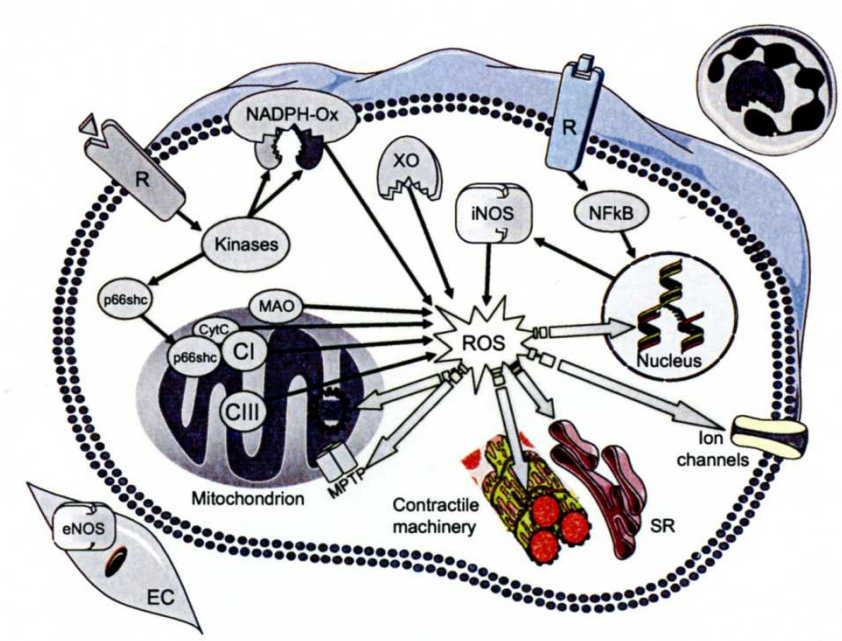

Figure 7. Origin and targets of reactive oxygen species (ROS).
Cyt C = cytochrome c, EC = endothelial cell, eNOS = endothelial nitric oxide synthase, iNOS = inducibile nitric oxide synthase, MAO = monoamine oxidase, MPO = myeloperoxidase, MPTP = mitochondrial permability transition pore, NF = nuclear factor, R = receptor, SR = sarcoplasmic reticulum, XO = xanthine oxidase. *From Heusch and Schulz, 2011 (67).*

Following are some examples of ROS induced damage:

• Oxidative damage of DNA: ROS have been shown to be mutagenic (68), an effect that should be derived from chemical modification of DNA. A number of alterations (e.g., cleavage of DNA, DNA-protein cross links, oxidation of purines, etc.) are due to reactions with ROS, especially hydroxyl radical. If the DNA-repair systems are not able to immediately regenerate intact DNA, a mutation will result from erroneous base pairing during replication. This mechanism may partly explain the high prevalence of cancer in individuals exposed to oxidative stress. Of the oxidative lesions, the most dangerous are double-strand breaks, as these are difficult to repair and can produce point mutations, insertions and deletions from the DNA sequence, as well as chromosomal translocations (58).

• Oxidative damage to proteins: once they are oxidized, proteins cannot be repaired. Extensive studies have revealed that oxidized proteins are recognized by proteases and completely degraded (to amino acids), and entirely new replacement protein molecules are then synthesized de novo (16). It seems that oxidized amino acids within oxidatively modified proteins are eliminated or used as carbon sources for intermediate metabolism and consequent energy synthesis. Because an oxidatively modified protein may contain only two or three oxidized amino acids, it seems probable that most of the amino acids from an oxidized and degraded protein are re-utilized for protein synthesis. Thus, during oxidative stress many proteins that are synthesized are likely to contain a high percentage of recycled amino acids. During periods of particularly high oxidative stress the proteolytic capacity of cells may not be sufficient to cope with the number of oxidized protein molecules being generated. A similar problem may occur in ageing, or with certain disease states, when proteolytic capacity may decline below a critical threshold of activity required to cope with normal oxidative stress levels (69). Under such circumstances oxidized proteins may accumulate and cross-link with one another or form extensive hydrophobic bonds. Such aggregates of damaged proteins are detrimental and may lead to cell dysfunction (70).

• Oxidative damage of lipids: membrane lipids are rich in polyunsaturated fatty acids that can easily be oxidized by ROS, because of their multiple double bonds. Such oxidation is also involved in the generation of atherosclerotic plaques (71). Their oxidation results in excess formation of carbonyl compounds, such as prostanoid and aldehydes that are toxic metabolites that can impinge on numerous pathologies.

2.5 Oxidation of myofibrillar proteins

Structural integrity of a sarcomere is essential for normal contractile function, as exemplified by various familiar hypertrophic cardiomyopathies resulting from genetic mutations in myofibrillar proteins (MPs) (as reviewed by Marian (72). Although the damage to the contractile apparatus is clearly sufficient to induce myocardial dysfunction, the effects of heart failure on MPs structure and function have not been fully characterized. MPs are markedly susceptible to oxidative damage both *in vitro* and *in vivo*, and recent data suggest that oxidation of MPs is a significant contributor to dysfunction of skeletal and cardiac muscle. Proteins undergo a variety of oxidative modifications, including irreversible carbonylation at the level of lysine, arginine, and proline residues (10); tyrosine nitration; reversible thiol oxidation; and disulfide cross-bridge (DCB) formation (73). In fact, various studies have suggested that H_2O_2 causes the oxidation of sulfhydryl groups and/or the formation of carbonyls, specifically affecting actin, tropomyosin (Tm) and, in skeletal muscle, myosin heavy chain (74,75). Moreover, Canton et al. demonstrated that, in experimental models of coronary microembolization, the resultant contractile dysfunction was related to DCB formation in Tm (76).

Consensus Symbols

RED	Small (small+ hydrophobic (incl.aromatic -Y))
BLUE	Acidic
MAGENTA	Basic
GREEN	Hydroxyl + Amine + Basic - Q

An alignment will display by default the following symbols denoting the degree of conservation observed in each column:

"*" means that the residues or nucleotides in that column are identical in all sequences in the alignment.

":" means that conserved substitutions have been observed, according to the COLOUR table above.

"." means that semi-conserved substitutions are observed.

Figure 7. Multiple sequence alignments of the mouse striated muscle Tm isoforms.
The complete protein sequence (amino acids 1–284) for the striated muscle α-Tm, β-Tm, and γ-Tm isoforms were aligned. Comparisons of the amino acid biophysical properties are color coded and indicated by dots below the amino acid sequence, as designated in the legend. *From Wieczorec 2010.*

Tm plays a key role in controlling calcium regulated sarcomeric contraction through its interactions with actin and the troponin complex. At low calcium, Tm localizes to the outer domain of actin and sterically blocks the myosin binding site

on actin to prevent myosin-actin interaction and sarcomeric contraction (77). Calcium release from the sarcoplasmic reticulum and its binding by troponin C helps to alleviate this blocked state of Tm on the myosin binding site. There are 3 principle striated muscle isoforms of Tm: α-Tm, β-Tm, and δ-Tm. These proteins share a high degree of amino acid homology: α-Tm and β-Tm are 87% identical, α-tm and δ-tm are 91% identical, and β-Tm and δ-Tm are 86% identical (Fig. 8) (78,79). Isoforms differ also for the cysteine contents: α- and δ-Tm have a single cysteine (Cys190), and β-Tm has two cysteines (Cys190 and Cys36). Isoform expression changes in different muscles and animal models. In fact, previous study demonstrated that the heart expresses α- and β-Tm during embryogenesis and fetal development, but β-Tm expression decreases soon after birth (78). Thus the adult myocardium essentially has homogenous expression of only striated muscle α-Tm. Moreover, in the heart of small animals (rabbit, rat, mouse) is present only the α isoform, while in bigger animals, such as sheep, pig and also in human heart there is 20 % of β isoform of Tm (80). The δ-Tm is not expressed in myocardium, but is expressed in embryonic, newborn, and adult skeletal musculature, in particular δ-Tm is expressed in slow twitch skeletal muscle (i.e. soleus). Previous studies determined that TnT bind to Tm in 2 distinct regions: at the carboxyl end of the molecule (amino acids 258-284), and internally in the region of amino acids 175-190 (Fig. 9) (81). Canton and co-workers demonstrated that Cys190 of cardiac α-Tm plays a key role in the regulation of the contractility. In the presence of ROS Cys190 forms disulfide cross-bridges with another Tm or another protein and this oxidation is associated with contractile dysfunction in experimental models of coronary microembolization (76). That Tm is an essential protein has been demonstrated also by murine knockout models of Tm. Results

show that when α-Tm is removed from the murine genome by homologous recombination, the developing mouse dies between 10 and 14 embryonic days (82). Furthermore, knockout of the low molecular weight non-muscle δ-Tm isoforms results in a failure of both embryonic development and cell survival (83); when β-Tm is knocked out, there is a failure in early developmental processes (79). These results illustrate that Tm expression occurs early in development, remains active throughout the lifespan of the mouse, and is essential for development and viability of the mouse. Also in human striated muscle Tm mutations have been found and associated with skeletal and cardiac muscle diseases. Mutations in α-Tm are associated with familiar hypertrophic cardiomyopathy (FHC) and dilated cardiomyopathy (DCM) (84).

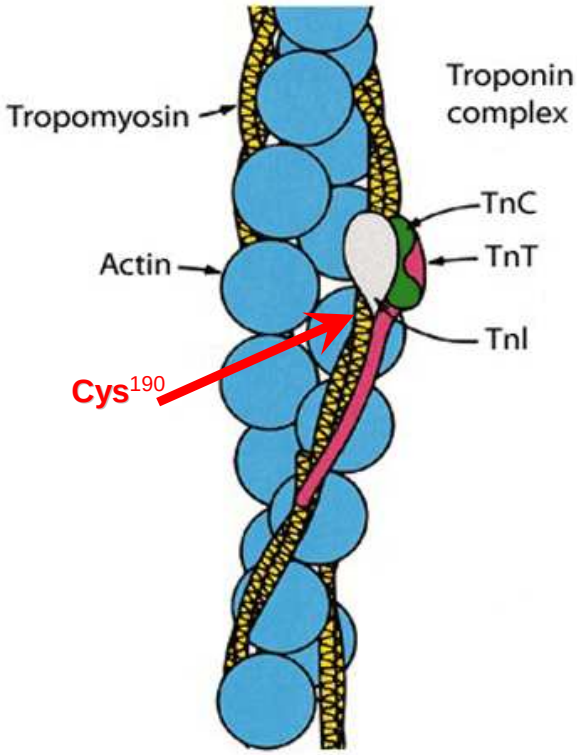

Figure 9.Tm plays a key role in controlling calcium regulated sarcomeric contraction through its interactions with actin and the troponin complex.
CardiacTm has a single Cysteine (Cys190) localized near the Troponin complex bind.

2.6 ROS production in pathophysiology

A characteristic component of pathophysiology in many organ systems is increased levels of ROS. It has been demonstrated that oxidative stress is involved in several pathophysiological conditions, such as aging, cancer, myocardial infarction, neurodegenerative diseases, muscular dystrophy and many others (1,85,86). During this thesis we investigated the role of ROS in models of cardiac and skeletal disease (87,88).

2.6.1 Heart diseases

It is well-known that oxidative stress is elevated in most cardiovascular diseases, including hypertrophy, ischemia-reperfusion, myocardial infarction, and heart failure (HF) (89).

ROS may contribute to the myocardial remodelling in a number of ways, including activating MMPs that participate in reconfiguration of the extracellular matrix; acting as signalling kinases and transcription factors in the development of compensatory hypertrophy; and contributing to myocyte loss via apoptosis or other cell death mechanisms (90).

Kaludercic and co-workers demonstrated an increased presence of ROS in cardiac hypertrophy and reported a beneficial effect in MAO knockout mice (see par. 2.2.3) (55). Recent studies suggest that hypertrophic effects of angiotensin are mediated through ROS generation. Nakamura et al reported that AT II induced ROS generation in neonatal rat myocytes and that pretreatment with antioxidants could abolish AT II-mediated hypertrophy (91). It was also demonstrated that this mechanism involves H_2O_2 dependent activation of Ras/Raf/ERK mitogen activated protein kinase (MAPK) pathway and activation of the transcription factor NFkB.

Norepinephrine (NE) interacts with α- and β-adrenergic receptors and both receptor subtypes have been implicated in NE-induced ROS generation and hypertrophy (92). In neonatal rat myocytes, NE increased the level of intracellular ROS and this effect was inhibited by α-adrenergic receptor blockade and antioxidants. Incubation with catalase, was able to prevent NE-induced increase in ROS and RNA and protein content.

In some cases, effects similar to those of ischemia or I/R have been reported after the exogenous addition of H_2O_2 (75). Wrang et al. (93) reported that H_2O_2 causes left ventricular dysfunction in rat hearts in a Ca^{2+}-independent manner, concluding that the alteration in the function of the contractile elements is the principle mechanism of ROS-induced contractile dysfunction. ROS impair contractile function by a number of mechanisms, including (i) decreased nitric oxide bioavailability, (ii) decreased ß-adrenoceptor expression (94) and ion channel activity (95), (iii) activation of protein kinases (96,97), and (iv) oxidation of MPs. In fact, many studies demonstrated that ROS cause oxidation of MPs altering cardiac sarcomere function in different models of cardiac disease (76,98). Apart from post-myocardial infarction remodelling, HF also results from hypertension (99), valvular disease (100), idiopathic cardiomyopathy or myocarditis (101) and occasionally tachycardia (102). In addition, the loss of cardiomyocytes (post-myocardial infarction or cardiomyocyte apoptosis), alterations in excitation-contraction coupling (103,104) and oxidative modification of contractile myofilaments contribute to myocardial dysfunction (75,76,105-107). In failing hearts, the formation of ROS is increased in both, non-cardiomyocyte cells (endothelial cells, fibroblasts, inflammatory cells, platelets) and cardiomyocytes (108). Moreover, the causal relationship of ROS formation with contractile dysfunction and their

molecular targets and links with intracellular signaling are not clear in detail. Among other protein kinases, ROS activate p38 MAPK (96,97). In rabbit hearts, p38 MAPK is activated after myocardial infarction and its activation correlates with increased oxidative stress (109). Once activated, p38 MAPK contributes to left ventricular (LV) remodeling and HF development (110), including LV hypertrophy, fibrosis and inflammation (111) as well as cardiomyocyte apoptosis (112). Therefore, p38 MAPK provides an interesting target for HF therapy (113). Indeed, pharmacological blockade of p38 MAPK (114,115) or its genetic knockout (116) improves LV function and attenuate morphological alterations following myocardial infarction. p38 MAPK is also activated in myocardial biopsies from HF patients, (117), and the improvement of LV function by resynchronization therapy is associated with reduced p38 MAPK phosphorylation in human hearts (118). The mechanism underlying the improvement in LV function following blockade of p38 MAPK activation in failing hearts, however, remains unclear. Under physiological conditions, contractile function was reported to be reduced by pharmacological blockade of p38 MAPK in rat cardiomyocytes (119) or its genetic knockout in mice hearts in vivo (120), whereas in other models reduced contractile function was not observed (121,122). In contrast, during post-ischemic reperfusion or HF p38 MAPK inhibition invariably improves contractile function and myocardial viability (123). In this thesis we investigated (i) the effect of p38 MAPK inhibition on MP oxidation and p38 MAPK activation in a rabbit HF model of rapid left ventricular pacing in collaboration with Prof. Schulz (Essen, Germany) and (ii) the correlation between contractile impairment and increased ROS accumulation in human HF in collaboration with Prof. Pepe (Melburne, Australia).

2.6.2 Muscular dystrophy

The muscular dystrophies (MDs) are inherited disorders that mostly affect striated muscles, involving progressive weakness, degeneration of skeletal muscle, difficulties in breathing and premature death. Duchenne muscular dystrophy (DMD) is the most common and severe form of MD worldwide. This progressive and lethal X-linked myopathy is characterized by deficiency of dystrophin, a subsarcolemmal protein critical in membrane stabilization and prevention of contraction-induced cell membrane damage (Fig.10). Another family of MDs is due to inherited mutations in genes encoding collagen VI and cause two muscle diseases in humans, namely Bethlem myopathy and Ullrich congenital muscular dystrophy. Since 1980, many theories have considered the pathogenic mechanisms leading to muscle degeneration in MDs. These hypotheses include disorders of intracellular Ca^{2+} homeostasis, disruption of membrane function and oxidative stress. Several studies documented the key role of ROS in dystrophic muscular damage (124,125). Evidence of oxidative stress have been shown in three-week-old mdx mice, an age when signs of muscle damage are not yet evident (125). Therefore ROS accumulation appears as a primary event rather than a consequence of muscle degeneration caused by other mechanisms. These derangements might suggest the possible involvement of mitochondria. In fact, recent studies provided clear evidence of the crucial role of mitochondria in MDs. This concept is supported by genetic or pharmacological reduction of the open probability of the mitochondrial permeability transition pore, that has been demonstrated to prevent myofiber injury characterizing experimental models of MDs (126-128). Besides the respiratory chain, a relevant source of ROS in mitochondria is represented by monoamine oxidases (MAO). Data available in

literature, as well as data previously obtained in Prof. Di Lisa's laboratory, demonstrated the important role of MAO in cardiac diseases (54,55).

During this thesis we analyzed the pathological contribution of MAO-dependent ROS accumulation in two different model of MDs, namely mdx mice, a model of DMD, and Col61a$^{-/-}$ mice, a model of Bethlem and Ullrich myopathy. (87,129).

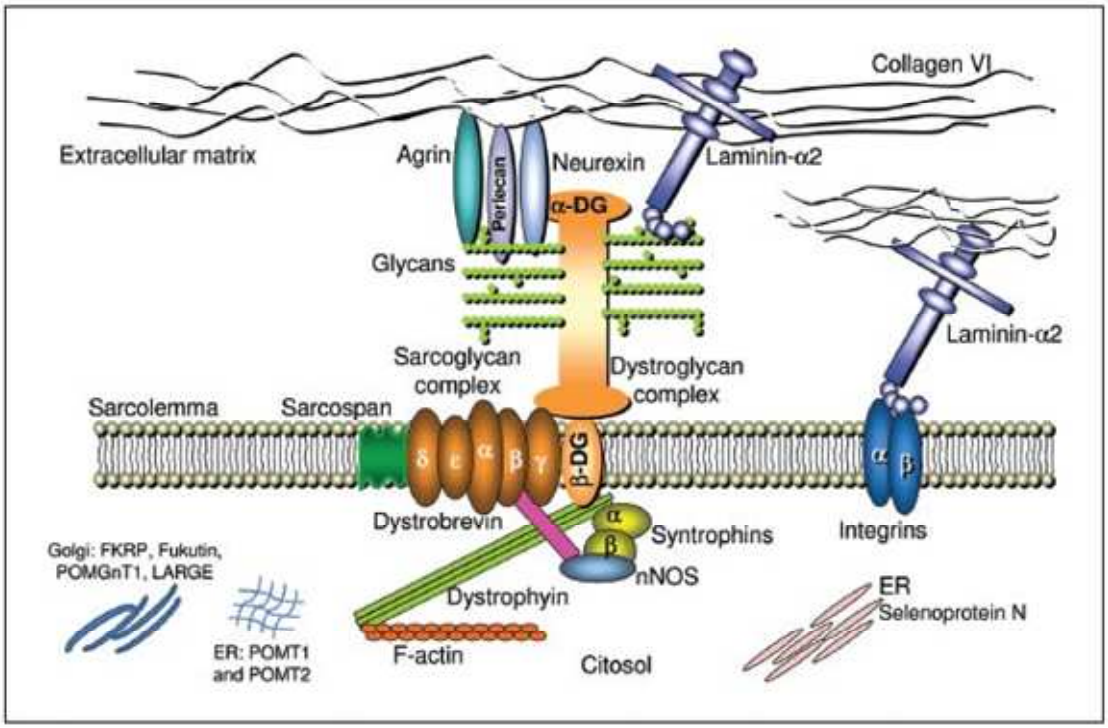

Figure 10. Schematic representation of the main proteins involved in congenital muscular dystrophies. *From Lisi and Cohn.*

3. AIMS OF THE STUDY

Although several studies documented the key role of oxidative stress along with mitochondrial dysfunction in heart failure (HF) and muscular dystrophy (MDs), the sources of ROS are still controversial as well as their molecular targets. In particular, we will investigate the role of mitochondria, and especially of MAO, in ROS formation and of myofibrillar proteins (MPs) as targets of oxidative stress that might be relevant in contractile dysfunction.

Thus, the aims of this study will be developed as follows:

- We will evaluate whether MPs represent important intracellular targets of ROS in cardiac and skeletal muscles and whether MP oxidation correlates to contractile impairment. To this aim, we will analyse the role of oxidative stress in a rabbit model of HF and in human biopsies from patients affected by end-stage HF. Our hypothesis is that protein modifications, caused by an increased accumulation of ROS, will correlate with contractile dysfunction. We will focus our attention on irreversible modifications, which occur during severe oxidative stress, and reversible modifications occurring upon mild stress. Thus, initially we will analyze irreversible modifications, such as carbonylation, because previous results demonstrated the occurrence of protein carbonylation in the ischemic heart. In addition, since HF is associated with a large formation of NO that can bind cysteinyl residues to form s-nitrosothiols (S-NO), we will analyze the occurrence of protein S-nitrosylation in human failing hearts. Moreover, we will investigate the reversible modifications, in particular at the level of cysteine residues, by immunoblotting under non

reducing conditions. Since previous studies demonstrated that Tm is particular susceptible to oxidative modifications we will investigate whether Tm oxidation can be a diagnostic tool because it is likely to occur at earlier stages. We will assess whether MP oxidation can occur also in two murine models of MD and whether these modifications can be related to contractile dysfunction.

- We will investigate the role of MAO as a mitochondrial source of ROS in MDs. The rationale is based on previous results obtained in Di Lisa's laboratory in experimental model of cardiac injury. We hypothesize that MAO-dependent ROS might contribute to contractile dysfunction and myofiber apoptosis in MDs. To this aim, we will assess the effects of pharmacological MAO inhibition on oxidative stress, alterations of muscle structure and function, and loss of cell viability in *Col6a1*$^{-/-}$ *and mdx* mice.

4. MATERIAL AND METHODS

4.1 Models

4.1.1 Patient samples and clinical measures

The use of discarded explanted failing heart tissue biopsies was approved by the Alfred Hospital Human Ethics Committee for Discarded Tissue Research. The NF donor hearts that were excluded from transplantation were approved for research by donor family consent and the Victorian Organ Donation Service, Australian Red Cross. Clinical measures were performed by Prof. Pepe. Biopsies were snap-frozen in liquid nitrogen within approximately 3 h of aortic crossclamp for cardiac explantation. Plasma cardiac troponin I (cTnI) levels were measured within a few days prior to explantation using an automated chemiluminescent microparticle immunoassay as per the assay manufacturer (Architect ci8200 Integrated System, Abbott Laboratories, Abbott Park, Illinois). Ejection fraction was estimated by the Simpson biplane method at echocardiography. Septal and posterior wall thickness, LV end-diastolic diameter, and LV end-systolic diameter were measured in the parasternal long-axis view, whereas left atrial area and right atrial area were measured in the apical 4-chamber view at end-systole (130). When multiple measures per patient were available for cTnI or echocardiography, the last recorded values (closest to cardiac explantation) were used Protein analysis by gel electrophoresis (Western blot).

4.1.2 Rabbit experimental model and protocols

The experimental model and clinical measures were performed by Prof. Schulz. Instrumentation of male Chinchilla rabbits (Charles River, Kisslegg, Germany) weighing 3–4 kg body weight was performed as described in detail elsewhere (131,132). HF was induced by LV pacing (400 bpm) for 1 (HF1, n = 7), 2 (HF2, n = 7) or 3 weeks (HF3, n = 8) respectively. Seven sham-operated rabbits (Sham) served as controls. HF was evident from clinical signs, such as ascites and cachexia and echocardiographic parameters, such as a reduction of LV shortening fraction (LVSF) and an increase in LV end-diastolic diameter (LVEDD). After euthanasia of the rabbits, samples (50 mg each) were taken from the LV free wall and either frozen in liquid nitrogen and stored at -70℃ or fixed in formalin and embedded in paraffin.

Vitamins C and E treatment. In four additional groups, rabbits received either placebo or vitamins C (100 mg·kg-1·day-1p.o.) and E (200 mg·day-1p.o.) for 3 weeks without (Sham, n = 7 or Sham-Vit, n = 7) or with LV pacing (HF3, n = 8 or HF3-Vit, n = 6).

SB281832 treatment. In four additional groups, rabbits received either placebo or the p38 MAP kinase inhibitor SB281832 at a dose of 50 mg·kg-1·day-1p.o. for 3 weeks without (Sham, n = 7 or Sham-SB, n = 7) or with LV pacing (HF3, n = 8 or HF3-SB, n = 6). To detect potential blood pressure changes following p38 MAP kinase blockade, measurements of systolic and diastolic blood pressures were performed using a sphygmomanometer cuff (Memoprint, Babenhausen, Germany) in five rabbits of each group, while conscious. Echocardiography. Heart rate and LV function were measured (Supervision 7000, Toshiba, Neuss, Germany) as described in detail elsewhere (131,132). LVSF was calculated from LVEDD and end-systolic diameter: (LVEDD - endsystolic diameter)/LVEDD ¥ 100.

4.1.2 Mice experimental model and treatment

Col6a1$^{+/-}$ mice were backcrossed in the inbred C57BL/6J strain for eight generations as described (129), and data were obtained by comparing *Col6a1*$^{-/-}$ mice with their wild-type littermates. Wild-type C57BL/10 mice and *mdx* (in the C57BL/10 background) were obtained from Charles River and Jackson Laboratories, respectively. Pargyline (50 mg/kg/d) or vehicle (phosphate buffered saline, PBS) were administered by daily intraperitoneal injection for 7 days in 6-month-old *Col6a1*$^{-/-}$ and C57BL/6J male mice or 5-week-old *mdx* and C57BL/10 male mice. During the treatment, mice were placed in separate cages with running-wheel. At the end of the treatment, mice were sacrificed and muscles were removed and stored in liquid nitrogen until use. All *in vivo* experiments were approved by the competent Authority of the University of Padova.

4.2 Protein analysis by gel electrophoresis

4.2.1 Protein extraction from muscle

MPs were isolated in the presence of protease inhibitors, and the entire procedure was performed at 4℃. Cryosections from frozen tiss ue were homogenized in 1 ml of ice-cold PBS, pH 7.2 containing 5 mM EDTA, added with an antiprotease mixture (10 μM leupeptin, 10 mM pepstatin, and 0.2 mM phenylmethylsulfonyl fluoride). The solutions were prepared with bidistilled water to limit free metal ion contamination. Just before use, the solution was stirred under vacuum and then bubbled with argon to maximally reduce the oxygen tension. The protein

suspension was centrifuged at 12,000 g for 10 min by means of a Beckman microcentrifuge, and the resulting pellet was resuspended in sample buffer (2% SDS, 5% glycerol, 1% β-mercaptoethanol, 125 mM Tris–HCl, pH 6.8) and denatured by 10 min boiling. This procedure referred to as reducing condition was compared with the non-reducing condition obtained without β-mercaptoethanol. The supernatant collected was a protein solution enriched in MPs. To avoid artefacts due to the oxidation of thiol groups in vitro, non-reducing conditions were performed in the presence of 1 mM N-ethylmaleimide. Aliquots of this extract were assayed for protein concentration (Bradford Bio-Rad Protein Assay, Bio-Rad Laboratories).

4.2.2 SDS-polyacrylamide gel electrophoresis (SDS-PAGE)

Electrophoresis was performed on polyacrylamide gel, at a 12% concentration in the *separating* gel and 5% concentration in the *stacking* gel, prepared in glass slabs 0.75 mm thick. Following solutions were used for the preparation of the gel:

- Acrylamide/bisacrylamide: 30% acrylamide and 0.8%bisacrylamide
- Lower Tris-HCl (4x): 1.5 M Tris-HCl and 0.4% SDS, pH 8.8
- Upper Tris-HCl (4x): 0.5 M Tris-HCl and 0.4% SDS, pH 6.8
- Running buffer (4x): 0.1 M Tris-HCl, 0.77 M Glycine and 0.4% SDS, pH 8.3

The polymerization of the gel was obtained by the addition of TEMED (Sigma) and APS (0.1mg/ml) (Amersham Biosciences). SDS–PAGE was performed in mini gel format (7 cm gel size) using the BioRad Protean II Electrophoresis system (Bio-Rad, Hercules, CA, USA). Samples were run on the gel at room temperature using

the Electrophoresis Power Supply ST504D (Apelex) which provided a constant voltage of 100V in the stacking gel and 150V in the separating gel.

4.2.3 Coomassie staining of the gel

As indicate, to verify the protein loading, gels were run in duplicate, one stained with EZBlue-Coomassie brilliant blue G-250 (Sigma-Aldrich, St. Louis, Missouri) and the second one used for immunoblotting or oxyblot assay.

4.2.4 Immunoblotting

In order to make the proteins accessible to antibody detection, they were moved from within the gel onto a nitrocellulose membrane. Immunoblotting was performed according to Towbin (133). A 0.45 micron nitrocellulose membrane (Bio-Rad Laboratories) was placed on top of the gel, avoiding creating bubbles, and a stack of tissue papers placed on top. This stack was then inserted into a transfer box filled with transfer buffer ,containing 25 mM Tris–HCl, 192 mM glycine, and 20% methanol, so that the gel is oriented towards the cathode and the membrane towards the anode. When a current is applied to the electrodes, this causes the proteins to migrate from the negatively charged cathode to the positively charged anode, i.e. towards the membrane. The best efficiency of transfer was observed when a 150 mA current was applied (Hoefer EPS2A200) overnight at 4℃.

The efficiency of transfer to nitrocellulose membrane was checked by staining with Red Ponceau S (Sigma Chemical Co., St Louis, MO, USA).

Once the transfer was carried out, the membrane was saturated using a blocking solution with 3% BSA for 1 hour at room temperature.

The antibodies used for the proteins of interest were diluited in the blocking solution. The following primary antibodies were used:

- Anti-tropomyosin monoclonal antibody (CH1 clone, Sigma Chemical Co.), dilution 1:500
- Anti-MAO A (Santa Cruz), dilution 1:1000;
- Anti-MAO B (Sigma), dilution 1:1000;
- Anti–alphasarcomeric actin 5C5 clone (Sigma-Aldrich), dilution 1:1000;
- Anti-desmin DE-B-5 clone (Oncogene Science, Massachusetts), dilution 1:1000;
- Anti–myosin light chain MY-21 clone (SigmaAldrich), dilution 1:1000;
- Anti-TnI (Mab 8I-7, Spectral Diagnostic, Toronto, Canada), dilution 1:1000;
- Anti-TnC (Biodesign, Saco,Maine), dilution 1:1000;
- Anti-DNP, (Intergen), dilution 1:100.

All the primary antibody incubations were carried out for 2 hours or overnight at 4℃. Following the incubation, membranes were washe d three times with the washing buffer composed of 50 mM Tris-HCl, 85 mM NaCl, 0.1% Tween 20, pH 7.4 (10 minutes each wash). Secondary antibodies were diluted in blocking solution and incubated with the membrane for 1 hour at room temperature. Secondary antibodies used were:

- Anti mouse (Pierce), dilution 1:3000
- Anti rabbit (Pierce), dilution 1:3000

Secondary antibody in conjugated to a reporter enzyme, namely HRP. When in the presence of a chemiluminescent agent, they can interact and the reaction

product produces luminescence in proportion to the amount of protein. Prior to the detection, membrane was washed three times (10 minutes each wash).

4.2.5 Chemiluminescent detection

Membrane was exposed to SuperSignal West Pico or Femto Chemiluminescent Substrate (Pierce) for 1 minute. This incubation causes the generation of luminous signal due to the oxidation of the substrate by HRP bound to the secondary antibody. The light, emitted at max 340 nm, was detected by a CCD camera (Image Station 440 CF, Kodak).

4.2.6 Densitometry

Images of the western blot acquired were analyzed using the ImageJ software (National Institutes of Health, Bethesda, Maryland). This program allows the quantification of the optical density of the bands that are directly proportional to the protein content.

Quantitative analysis of the degree of tropomyosin oxidation was performed on the densitometric values of the bands detected in immunoblots. In particular, the density of additional bands with high molecular weight, that appeared only under non reducing conditions reflecting the formation of disulphide cross-bridges, were normalized to Red Ponceau staining to take differences in sample loading into account.

Carbonylated actin and Tm were quantified by normalizing the bands of actin and Tm in the Oxyblot for the corresponding band stained with EZBlue-Coomassie brilliant blue G-250 (Sigma-Aldrich, St. Louis, Missouri).

4.2.7 Oxyblot procedure.

Total myocardial protein carbonylation was measured using the Oxyblot protein oxidation detection kit (Chemicon, Temecula, California) according to the manufacturer's protocol. Carbonyl groups were derivatized by reaction with 2,4-dinitrophenylhydrazine (DNPH) for 15 min. The reaction was stopped immediately or after incubation times by neutralization with 2 M Tris base and 30% glycerol. The same samples were prepared in the absence of DNPH as a control. One-dimensional electrophoresis was promptly carried out on 12% SDS-polyacrylamide resolving gels at 4℃ with 6.5 μg of derivatized protein loaded per lane. Dinitrophenylated protein molecular mass standards were purchased from Intergen. Proteins were transferred to a polyvinylidene fluoride membrane at 400 mA constant current for 2 h. The membranes were blocked by incubation with 3% BSA for 1 h and then incubated for 90 min at room temperature with anti-DNP (1:100, Intergen). Blots were washed three times for 10 min and were subsequently incubated for 1 h with peroxidase-labeled anti-rabbit immunoglobulins (at 1:300 dilution). Blots were developed by using a chemiluminescence detection system.

The membranes were stripped with Restore Western blot stripping buffer (Thermo Scientific, Waltham, Massachusetts) and reprobed with anti-alpha-sarcomeric actin 5C5 clone and anti-Tm CH1 clone antibodies (Sigma-Aldrich).

4.2.8 2-D electrophoresis

Myofibrillar proteins were extracted and subjected to 2D gel electrophoresis followed by oxyblot analyses. To this aim protein extracts were prepared from human heart tissues as described (134). Protein samples (120 µg) were resolved by isoelectric focusing on 11-cm immobilized pH gradient strips (pH 3-10) followed by in-strip DNP derivatization (reacting with protein carbonyls) as described (135). Second-dimensional separation was performed by electrophoresis on SDS-PAGE (12% porosity polyacrylamide). After electrophoresis, the proteins were transferred overnight to nitrocellulose membranes (Bio-Rad) at 150 mA. The membranes were incubated with anti-DNP antibody, as reported in 4.2.7 of Methods section.

4.2.9 Detection of protein S-nitrosylation in human samples

Heart biopsies were stored in liquid nitrogen and then homogenized in ice-cold PBS, pH 7.2 containing 1 mM EDTA and 0.1 mM neocuproine. Just before use, the solution was stirred under vacuum and bubbled with argon to maximally reduce the oxygen tension. The protein suspension was centrifuged at 12 000 g for 5 min at 4℃. The resulting pellet was subjecte d to the Biotin switch assay according to the S-nitrosylation detection kit. In brief the assay consists in three-step process: in the first step protein free thiols were blocked by incubation with thiol-specific agent methylmethanethiosulfonate (MMTS), then S-nitrosothiols were selectively reduced to yield free thiols with ascorbate, which were reacted with N-[6-(biotinamido)hexyl]-3'-(2'-pyridyldithio)-propionamide (biotin-HPDP), a sulfhydryl-specific biotinylating reagent. The addition of ascorbate is essential to provide this method with specificity. In fact, ascorbate generates a thiol from S-

nitrosothiols but not from alternatively S-oxidized thiols (e.g., disulfides, sulfenic acids) (136). This assay was performed in the dark. Finally the pellet was resuspended in wash buffer and divided in two aliquots: (i) one was added with sample buffer (2% SDS, 5% glycerol, 125 mM Tris–HCl, pH 6.8), denatured by 10 min boiling and used for anti-biotin western blot, (ii) the other was used for immunoprecipitation (IP) with anti-Tm. To this aim, the biotinylated proteins were incubated overnight with anti-Tm antibody (CH1 clone, Sigma Chemical Co) at 4℃, and then precipitated by protein G-PLUS Agarose for 3 h at 4℃. Finally the precipitates were probed with anti-biotin and anti-Tm antibodies, respectively. Gel electrophoresis and Western blotting were performed under nonreducing conditions, followed by enhanced chemiluminescence detection. Densitometry was performed on scanned immunoblots using ImageJ software (National Institutes of Health).

4.2.10 Detection of S-Nitrosylation in purified Tm

Rat cardiac Tm was purified by high-pressure liquid chromatography (HPLC) Agilent 1100 series (Agilent Technologies, Santa Clara, California) using a Jupiter-C18 column (Phenomenex, Torrance, California) and incubated with 0.1 or 0.5 mM S-nitrosoglutathione (Sigma-Aldrich) for 1 h at room temperature in the dark. The occurrence of S-nitrosylated Tm was assessed by means of the biotin-switch assay (137) using the S-nitrosylation protein detection kit (Cayman Chemical, Ann Arbor, Michigan). This method is aimed at converting nitrosylated cysteines into biotinylated cysteines.

Before immunoblot analysis, the biotinylated/S-nitrosylated Tm was precipitated with avidin agarose beads and eluted with 1 mM dithiothreitol. Finally, Tm was resuspended in sample buffer, denaturated by 10 min boiling for: (i) anti-Tm western blotting analysis and (ii) mass spectrometric analysis.

Protein identification by mass spectrometric analysis performed by Prof. Polverino De Laureto. To prepare the sample for mass spectrometric analysis, denaturated Tm was subjected to SDS-PAGE and the gel was stained by Coomassie Brilliant Blue G-250 (Bio-Rad). The resulting peptides were extracted from gel. The identity of the protein was determined by mass spectrometry of the protein material purified by reverse-phase HPLC. Mass determination was obtained with an electrospray-ionization mass spectrometer with a Q-Tof analyzer micro from Micromass (Manchester, United Kingdom). The measurements were conducted at a capillary voltage of 2.5 to 3 kV and a cone voltage of 30 to 35 V. The molecular masses of protein samples were estimated using Mass-Lynx software 4.1 (Micromass).

4.2.11 Tricine gel

Tricine gels are commonly used for peptides at low molecular weight. Electrophoresis was performed on polyacrylamide gel, at a 16,5% concentration of acrilamide, Gel Buffer (3M tris-HCl, 0.3% SDS, pH 8.45), 10% (v/v) glycerol in the *separating* gel and 4% concentration of acrilamide and Gel Buffer in the *stacking* gel.

The polymerization of the gel was obtained by the addition of TEMED (Sigma) and 10% (w/v) APS (Amersham Biosciences). Electrophoresis was performed using two buffer:

- Cathode buffer: 100 mM Tris, 100 mM tricine,0.1% SDS, pH 8.25
- Anodic buffer: 0.2 M Tris-HCl, pH 8.9

Samples were run on the gel at room temperature a constant voltage of 75V for 5 hours.

4.2.12 Dot Blot assay

The aliquots obtained from Tm digestion were analyzed by the Dot Blot method. A polyvinylidene fluoride membrane was dived into small squares by drawing lines and 2µl of sample are placed in each square. The membranes were stored dry at room temperature and detected by anti-Tm antibody.

4.3 Fluorescence Microscopy

Experiments involving microscopy were performed using an inverted microscope (Olympus IMT-2) equipped with a xenon lamp as a fluorescence light (75W), a 12 bit digital cooled CCD camera provided with a cooling system (Miromax, Princeton Instruments), a 20x air objective and appropriate excitation and emission filters.

4.3.1 Immunohistochemistry

Cryosections from rabbit heart were incubated with anti-tropomyosin monoclonal antibodies (CH1 clone) for 30 min (1:25 in PBS containing 0.3% BSA). After several rinses with PBS, sections were incubated with fluorescein-conjugated secondary antibodies (1:50, Dako). For detection of the fluorescein fluorescence, 488+25 nm excitation and 522 nm longpass emission filter settings were used. Data were acquired and analysed using Metamorph software (Universal Imaging, West Chester, PA, USA).

4.3.2 Determination of oxidative stress by DHE staining

Skeletal muscle cryosectioned to 10 micron thick slices using a LEICA CM 1850 microtome, termostated at -24℃. Sections were attached to polylysine precoated slides and dried to prepare them for further analysis. ROS production was determined measuring variations in fluorescence intensity of the probe dihydroethidium (DHE). Once inside the cell, this probe can be oxidized by ROS to the fluorescent compound ethidium and irreversibly bind to nuclear DNA, a process that results in a further increase in fluorescence. DHE (Sigma) was prepared as a 1 mM stock solution in DMSO and then diluted to a final concentration of 5 μM in degassed PBS. Considering that the solution is photosensible, all the operations were carried out in dark. The cryosections previously prepared were covered with a sufficient amount of DHE solution and incubated for 30 minutes at 37℃ in humid atmosphere. Afterwards, slides were washed in PBS to remove excess DHE solution (to reduce the background fluorescence). Slides were mounted with a 90% glycerol solution and covered with

a cover slide. Slides were examined using a fluorescence microscope and a 20x air objective at 568 nm and 585 nm excitation and emission wavelengths respectively.

4.3.3 IgG detention

Membrane permeability of skeletal muscle was directly visualized by immunohistochemical staining with IgG. Cryosections (10-µm thick) were incubated with anti-mouse fluorescein isothiocyanate-conjugated IgG, washed twice with PBS, mounted and visualized with an Olympus IMT-2 inverted microscope using excitation/emission cubes of 488/525±25 nm bandpass.

4.3.4 Image analysis

Images were analyzed using the Metamorph imaging software. Variations of fluorescence intensities were analyzed and reported as mean of the variations in all regions analyzed.

4.4 Light microscopy

4.4.1 Haematoxylin and eosin

Cross-sections (7-µm thick) were prepared and processed for haematoxylin and eosin (H&E) staining. H&E staining was used for determination of hypertrophied fibres, proportion of centrally nucleated fibers, and area of degeneration. For the morphometric analysis of myofiber cross-sectional areas and central nucleation,

we counted approximately 2000 fibers per mouse for each muscle type by means of ImageJ software. At least three sections from each muscle were analyzed. Images were taken using a Leica DC300 digital camera and a Leica DMR microscope.

4.4.2 Terminal deoxynucleotidyl transferase-mediated dUTP nick end labeling (TUNEL) method

TUNEL was performed on paraffin-embedded sections (7-μm thick) using the ApopTag *in situ* apoptosis detection kit (Chemicon). Samples were stained with peroxidase diaminobenzidine to detect TUNEL-positive nuclei and counterstained with Hoechst 33258 to identify all nuclei. The total number of nuclei and number of TUNEL-positive nuclei were determined in randomly selected fibers using a Zeiss Axioplan microscope equipped with a Leica DC 500 camera.

4.4.3 Evans Blue

Evans blue dye staining of muscles *in vivo* was performed by i.p. injection with 0.2 ml Evans blue (10 mg/ml in phosphate-buffered saline, Sigma). Mice were sacrificed after 16-18 h and diaphragms were fixed with 4% paraformaldehyde overnight at 4℃. After fixation, the samples were observed by means of light microscopy (Leica DC300 digital camera and a Leica DMR microscope).

4.5 MAO activity

Frozen quadriceps and gastrocnemius muscles were cut on a cryostat at -25℃ and were rapidly placed in liquid nitrogen. MAO activity was measured in the mitochondrial fraction obtained as briefly described. The muscles cryosections were suspended in phosphate buffer saline and centrifuged at 500 g for 10 minutes at 4℃ (MPW350R, Med. Instruments, Poland), the supernatant is centrifuged again at 8000g for 10 minutes at 4℃. T he pellet was resuspended in a small volume of PBS and stored on ice until the analysis. Protein concentration was determined by the Bradford assay.

The hydrogen peroxide formed by MAO (as a by-product of the oxidation of biogenic amine) was determined using Amplex Red. Briefly, the mitochondrial proteins obtained as described above (40 μg) were incubated in phosphate buffer with 10 μM Amplex Red and 15 μg/ml HRP. The assay is based on the detection of hydrogen peroxide generated during substrate catabolism in a horseradish peroxidase (HRP) coupled reaction using 10-acetyl-3,7-dihyrdoxyphenoxazine (Amplex Red reagent, Molecular Probes). The reaction was started by the addition of 50 μM tyramine and the fluorescence intensity was recorded for 60 minutes at 37℃ using a Perkin Elmer LS-50B fluorimeter at the 544/590 nm excitation/emission wavelengths. The fluorescence intensity of Amplex Red was checked to increase linearly as known amounts of H_2O_2 were added. Parallel samples were run in the absence of substrate to evaluate a possible increase of fluorescence not due to MAO activity.

4.6 Epitope mapping of anti-Tm antibody

4.6.1 Tm extraction from rat heart

Rat hearts are conserved at -80℃ until use. Tissue s are cut and crumbled in a phosphate buffer saline with 5mM EDTA. Tm was extracted as describe in Smille at al. (138). Rat cardiac Tm was purified by high-pressure liquid chromatography (HPLC) Agilent 1100 series (Agilent Technologies, Santa Clara, California) using a Jupiter-C18 column (Phenomenex, Torrance, California). Tm was eluted at rate of 0.8 mL/min with a gradient (from 5% at 35%) of acetonitrile for 6 min and a gradient (from 35% at 45%) of acetonitrile for 28 min.

4.5.2 Proteolytic digestions of Tm

Proteolysis of Tm was performed with chymotrypsin. Digestions were carried out at a protein concentration of 1 mg/mL using an enzyme to substrate (E:S) ratio of 1:10 (by Weight). Proteolysis was stopped by alkalinization of the solutions by acidification with 4% TFA in water. The time-course digestion of Tm was followed by SDS-PAGE under reducing conditions using the Tricine buffer system (139). The proteolytic mixtures were also analyzed by RP-HPLC (Agilent 1100, Santa Clara, California) using a Jupiter-C18 column (Phenomenex, Torrance, California) and eluted with a linear gradient of acetonitrile containing 0.1% TFA from 5 to 30% in 8 min and from 30 to 50% in 28 min. The effluent of the column was monitored by absorbance measurements at 226 nm. The principal proteolytic products are freeze-dry by Speed-Vac Concentrator (Savant).

Spectrometric analysis was performed by Prof. Polverino De Laureto. Mass spectra were recorded using a time-of-flight matrix-assisted laser desorption

ionization (MALDI) mass spectrometer (Kompact Maldi-1, Kratos-Shimadzu, Manchester, United Kingdom). Speedy-dry Tm was diluted in a buffer with CH_3CN and H_2O_2 (ratio 1:1 by volume) and 1% of HCOOH. Mass determinations were also obtained with an electrospray ionization (ESI) mass spectrometer triple quadrupole (API-300) from PE-Sciex (Thornhill, Ontario, Canada), equipped with an ion spray ionization source. Spectra were deconvoluted by the software MacSpec provided by PE-Sciex.

4.5 Muscle functional assessment

All the functional analysis were performed by Reggiani's group.

4.5.1 Skinned fibers

Single myofibers were isolated from *Col6a1*$^{-/-}$ gastrocnemius muscle, chemically skinned as described (140) and tension was measured during maximal isometric activation (pCa = 4.5, T = 20℃, initial sarcomere length = 2.75 μm).

4.5.2 Force measurement in vivo

Force measurements were performed in the left and/or right gastrocnemius muscle of anaesthetized mice by electrical stimulation through the sciatic nerve, as described previously (141).

4.5.3 Running wheel

Voluntary exercise was evaluated by placing a wheel in the cage. Before the treatment, mice were placed in separate cages with wheel to acclimatize, then the average distance covered by each mouse in 24 hours during the treatment was measured using an automatic counter.

4.7 real time RT-PCR

4.7.1 RNA extraction

Total RNA extraction from gastrocnemius of *mdx* and wild-type mice was performed using TRIzol reagent (Invitrogen), a monophasic solution of phenol and guanidine isothiocyanate, according to the manufacturer instruction. Briefly, 30 mg of tissue were lysed adding 1 ml of TRIzol and passing the lysate several times through a pipette. The homogenized samples were incubated for 5 minutes at room temperature to permit the complete dissociation of nucleoprotein complexes. Then, 0.2 ml of chloroform were added, tubes shaken vigorously for 15 seconds and incubated at room temperature for 3 minutes. Samples were centrifuged at 12,000 × *g* for 15 minutes at 4℃. Following centrifugation, the mixture separated into a lower red, phenol-chloroform phase, an interphase, and a colorless upper aqueous phase which contained RNA. Aqueous phase was transferred into a new tube and RNA precipitated by the addition of 0.5 ml of isopropyl alcohol. Following 10 minutes incubation at room temperature, samples were centrifuged again at 12,000 × *g* for 15 minutes at 4℃ and supernatant was discarded. RNA precipitate was washed with 70% ethanol, briefly air dried and dissolved in 40 ml RNase free DEPC-treated water (Amersham). An aliquot was diluted in water and the absorbance of the solution was measured spectrophotometrically at 260 and 280

nm to determine the purity and the concentration of isolated RNA. Preparations with the ratio A260/A280 higher than 1.8 were considered for further analysis.

4.7.2 cDNA synthesis

Reverse transcription reactions were performed using 1 to 5 mg of total RNA pretreated with DNAse I (Invitrogen), to eliminate the contaminating DNA. After addition of dNTP and oligo dT to prime the first strand cDNA synthesis, RNA was denatured at 65℃ for 5 minutes and then placed on ice. Superscript II (Invitrogen) was the added and the mixture incubated at 42℃ for 50 minutes and 70℃ for 15 minutes to synthesize cDNA.

4.7.3 Real time PCR

Each PCR reaction was performed in a 20 ml volume combining 50 ng of cDNA, 0.25 mM of forward e reverse primers and 10 ml of 2X Sybr green Master mix (Applied Biosystems). Applied Biosystems thermal cycler was used (GeneAmp 9700).

Following were the amplification cycling conditions:

- Initial step 95℃ for 10 minutes
- Denature 95℃ for 15 seconds
- Anneal 60℃ for 1 minute
- Extend 72℃ for 30 seconds

} 40 cycles

- Dissociation stage 95℃ for 15 seconds

60℃ for 15 seconds

95℃ for 15 seconds

Primer sets for the specific target genes were designed to span one or more introns. The sequences of forward and reverse primers used for each gene that was investigated are:

- mouse MAO A F 5’ AGGTGGCTCTGGCCAAATAAGTGA 3’
  R 5’ ACCGGTGGGATGGCACTAATTACA 3’
- mouse MAO B F 5’ CGCTCTTTGTGAACCTGTGTG 3’
  R 5’ CCTGTCTGGTCAATGTGGTCA 3’
- mouse GAPDH F 5’ CATGGCCTTCCGTGTTCCTA 3’
  R 5’ CCTGCTTCACCACCTTCTTGAT 3’

The specificity of the primers was assessed examining the dissociation curves for each PCR product. Standard curves were run in parallel and their slopes and y-intercept were used for data analysis. All the samples were normalized to the expression of GAPDH gene, taken as a reference to ensure equal loading.

4.8 Statistical analysis

Results are presented as mean ±SD or means ± SEM as indicated.

Contrasts between human NF and HF groups were performed via 2-tailed unpaired Student t test and Fisher exact tests when indicated. Multiple linear regression analyses (SPSS version 17.0, SPSS, Inc., Chicago, Illinois) were

performed to determine correlation between oxidative measures and sample parameters such as LV ejection fraction (LVEF) and prior cTnI release.

Comparison of data before and during LV pacing in rabbit models was performed by one-way ANOVA. Comparison of haemodynamic data before and during the 3 weeks of pacing between the different treatment groups was performed by two-way ANOVA. Cardiomyocyte cross sectional area, the number of TUNEL-positive cardiomyocytes, b-adrenoceptor density, MAP kinase phosphorylation and activation and oxidation were compared between untreated and treated sham and HF rabbits by two way ANOVA. When a significant overall effect was detected by ANOVA, individual mean values were compared using Bonferroni's method. All statistical calculations were performed using the Prism or Origin programmes.

A P-value less than 0.05 was taken to indicate a significant difference.

5. RESULTS AND DISCUSSION

5.1 The increase in reactive oxygen species contributes to contractile dysfunction in pacing-induced heart failure in rabbit.

The incidence and prevalence of heart failure (HF) continue to increase (142-144), largely because patients survive myocardial infarction due to improved medical treatment (145). It is well-known that ROS may contribute to the myocardial injury, however, the causal relationship of ROS formation with contractile dysfunction and their molecular targets and links with intracellular signalling are not clear in detail. In HF, among other protein kinases, increased ROS formation contributes to p38 MAPK activation, but the impact of the interaction of ROS with p38 MAPK on contractile function is particularly unclear. Therefore, in the first part of this thesis we used an experimental model of HF obtained by rapid LV pacing in rabbits in collaboration with Prof. Schulz (Essen, Germany) to study (i) the time course of ROS formation and p38 MAPK activation during the progression of HF, (ii) the effect of ROS scavenging by vitamins C and E, and (iii) the effect of p38 MAPK inhibition on myofibrillar protein (MP) oxidation and MAPK activation and the resulting LV function and morphology.

	Sham	HF1	HF2	HF3
Heart rate (bpm)	224 ± 5	263 ± 10*	277 ± 10*	258 ± 15
LVEDD (mm)	17.0 ± 0.3	18.7 ± 0.4*	19.3 ± 0.3*	19.6 ± 0.5*#
Fractional shortening (%)	30.0 ± 1.7	19.1 ± 0.7*	15.9 ± 0.7*	10.3 ± 1.3*#
Cardiomyocyte cross-sectional area (μm²)	242 ± 11	266 ± 4	299 ± 8*#	334 ± 7*#$
Number of TUNEL-positive cardiomyocytes (/(1000*mm²))	4 ± 2	23 ± 5*	16 ± 4	50 ± 8*#$
Phospho p38 MAPK/total p38 MAPK (relative to sham)	1.00 ± 0.24	0.54 ± 0.09	0.65 ± 0.24	2.34 ± 0.54*#$

Table 1. Hemodynamics, morphology and p38 MAPK activation during the progression of heart failure.
mean±SEM.; Sham: sham-operated rabbits (n=7); HF1: heart failure rabbits, 1 week (n=7); HF2: heart failure rabbits, 2 weeks (n=7); HF3: heart failure rabbits, 3 weeks (n=8); LVEDD: LV end-diastolic diameter; * $p<0.05$ vs. Sham; $^{\#}$ $p<0.05$ vs. HF1; $^{\$}$ $p<0.05$ vs. HF2

A progressive increase in left ventricular end-diastolic diameter (LVEDD) and a reduction of left ventricular shortening fraction (LVSF) occurred with increasing duration of rapid LV pacing (Table 1). Cardiomyocyte cross-sectional area remained unchanged at 1 week, but increased after 2 and 3 weeks of rapid LV pacing, and the apoptosis (number of TUNEL-positive cardiomyocytes) was increased more than 12-fold after 3 weeks of rapid LV pacing. p38 MAPK phosphorylation was increased only after 3 weeks of rapid LV pacing. The ROS accumulation was significantly increased after 3 weeks of rapid LV pacing (Fig. 11A). Interestingly, myocardial ROS concentration inversely correlated to LVSF, such that any attenuation in the ROS concentration was associated with an improvement in LVSF (Fig. 11B). There is little information on the direct impact of oxidative stress on the contractile machinery (108,146). Genetic deletion of enzymes involved in ROS removal induces severe structural and functional alterations (147,148), whereas antioxidant treatments counteract adverse remodelling in several experimental models of HF (149,150).

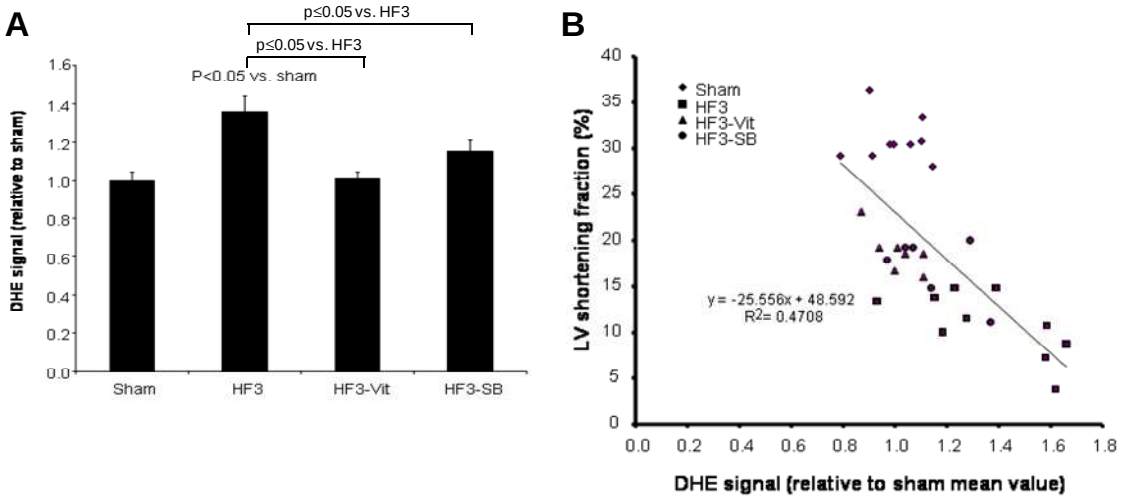

Figure 11. ROS concentration increased at 3 weeks of rapid LV pacing and correlated with contractile dysfunction.
(**A**) The myocardial ROS accumulation increased following 3 weeks of rapid LV pacing, as detected by DHE. Such an increase was prevented by pretreatment with vitamins C and E and p38MAPK inhibitor. (**B**) Relationship between ROS formation and LV shortening fraction at the end of the 3 week study protocol. There is a significant inverse relationship between ROS formation and LV shortening fraction, and the beneficial effects of vitamin C and E and p38MAPK inhibitor fall along the relationship. Vitamins C and E, vit; p38MAPK inhibitor, SB; heart failure from rabbit after 3 weeks of LV pacing,HF3. Data are expressed as mean±SEM.

Previous studies in Di Lisa's laboratory demonstrated the occurrence of Tm oxidation in isolated rat and microembolized pig hearts and related it to contractile dysfunction (75,76). Although these prior findings are consistent with the hypothesis that the reversible contractile impairment is related to covalent changes of MPs, these studies originate from models of ischemic heart, where myocyte death inevitably contributes to loss of function (75). Thus, the present study extended the previous results investigating the relationship between Tm oxidation and contractile impairment in a model of HF devoid of ischemia. The increased ROS accumulation after 3 week of pacing in rabbit hearts was associated with increased Tm oxidation, as indicated by an increased Tm dimer to monomer ratio (Fig. 12A and B). As shown by the typical example in Figure 12A, immunoblots stained with the Tm monoclonal antibody CH1 clone displayed an additional band (apparent molecular weight of 82 kDa) in biopsy samples obtained from rabbit

failing hearts. As the appearance of high molecular weight bands could also result from other cross-linking processes, such as the activation of transglutaminase (151), the attribution to DCB formation is performed by comparing the immunoblots obtained after SDS–PAGE carried out under reducing and non-reducing conditions.

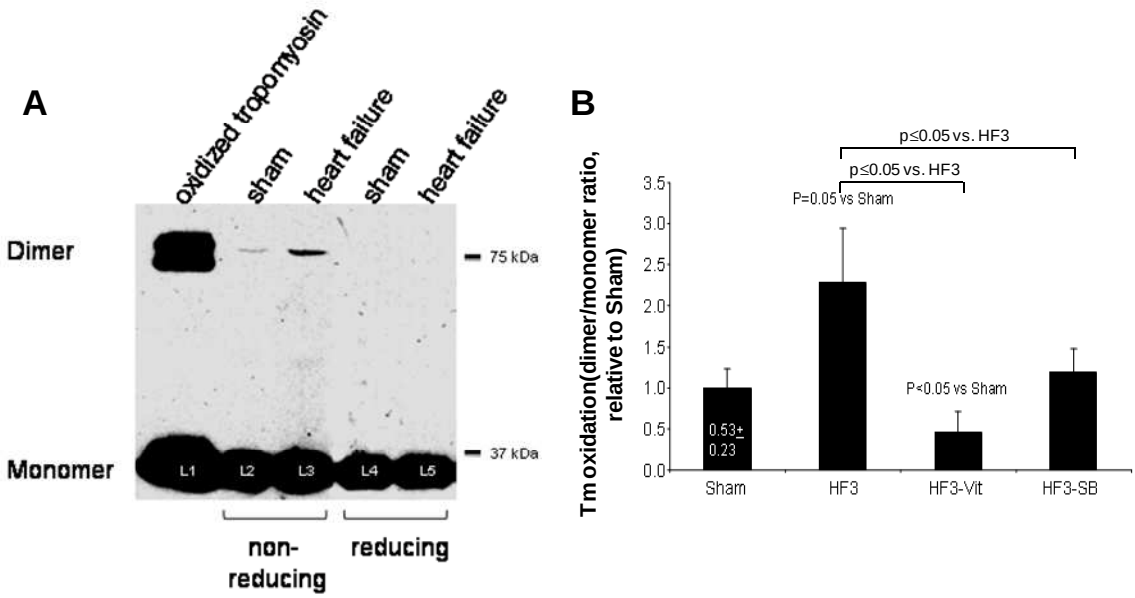

Figure 12. Oxidation of Tm increased in failing rabbit hearts.
(**A**) Representative Western blots of tropomyosin oxidation. Lanes 3 and 5 illustrate typical examples of Western blots from failing rabbit hearts after 3 weeks of rapid left ventricular pacing as compared to control hearts from sham operated rabbits (lanes 2 and 4). Isolated myofibrillar samples were denatured in the absence (non–reducing) or in the presence (reducing) of β-mercaptoethanol and then analyzed by Western blot with CH1 anti-Tm monoclonal antibody. The comparison between reducing and non-reducing electrophoresis allows the attribution of Tm dimers in lanes 2 and 3 to disulfide cross-bridge formation. Lane 1 illustrates the highest degree of oxidation obtained by adding isolated tropomyosin with 1 mM H_2O_2 for 15 min. (**B**) The amount of dimer formation was quantified by densitometry as Dimer band/Monomer band. Tm oxidation increased following 3 weeks of rapid LV pacing. Such increases in Tm oxidation were prevented by pretreatment with vitamins C and E and p38MAPK inhibitor. Vitamins C and E, vit; p38MAPK inhibitor, SB; heart failure from rabbit after 3 weeks of LV pacing,HF3; tropomyosin,Tm. Data are expressed as mean±SEM.

The appearance of this band, which was quite faint in samples obtained from non failing hearts, reflected DCB formation, because it was visible only in non-reducing electrophoresis. The formation of cross-linked products is likely to modify MPs, possibly resulting in changes of immunoreactivity. Indeed, the occurrence of such

a process has been demonstrated for another MP, troponin T, which undergoes transglutaminase-catalysed crosslinking upon post-ischaemic reperfusion (152). Therefore, we analysed Tm immunoreactivity in cryosections from HF rabbits. Figure 13 shows that Tm immunoreactivity was increased in rabbit failing hearts cryosections compared to controls. The quantitative analysis indicates a significant increase of the immunofluorescence values.

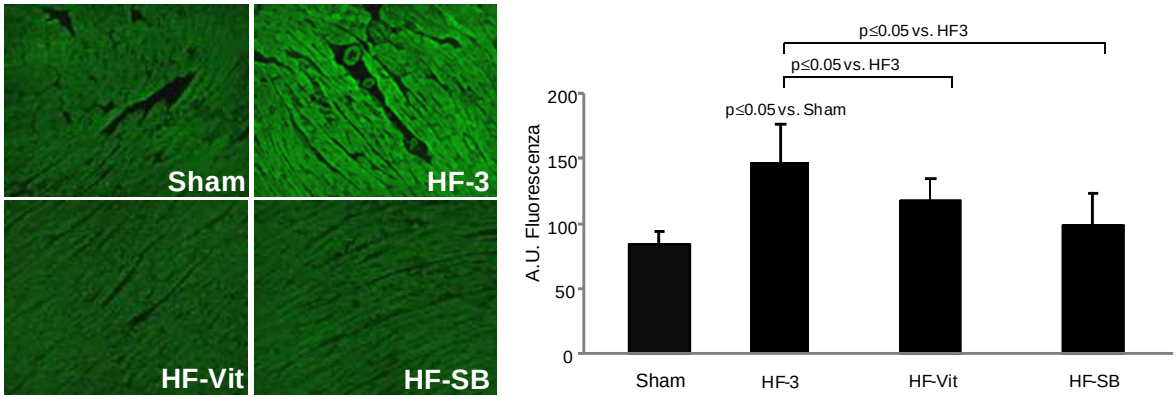

Figure 13. Tm immunostaining in rabbit hearts.
Cryosections from failing and non-failing rabbit hearts were stained with CH1 anti-Tm monoclonal antibody. Left panels show typical examples of Tm immunostaining. HF rabbit showed an increase in Tm immunoreactivity. Pretreatment of HF rabbit with vitamins and p38 MAPK inhibitor significantly decreased the Tm immunofluorescence. Right panel shows the quantitative analysis of the fluorescence intensity. Vitamins C and E, vit; p38MAPK inhibitor, SB; heart failure from rabbit after 3 weeks of LV pacing,HF3. Data are expressed as mean±SEM.

Administration of antioxidant vitamins throughout the 3 weeks of rapid LV pacing did not significantly alter any analyzed parameter in sham rabbit hearts, except that p38 MAPK phosphorylation was increased (Table 2). Antioxidant vitamin treatment completely abolished the increases in ROS formation and increased LVSF (Fig. 11 and table 2). Moreover, vitamins prevented Tm oxidation in HF rabbits visualized both by anti-Tm immunoblotting and by Tm immunofluorescence (Fig. 12 and 13). Cardiomyocyte cross-sectional area and number of TUNEL-positive cardiomyocytes were reduced following 3 weeks of rapid LV pacing with

antioxidant vitamins. In contrast, p38 MAPK phosphorylation remained elevated after 3 weeks of rapid LV pacing with antioxidant vitamins.

Blockade of p38 MAPK with SB-281832 did not alter any analyzed parameter in sham rabbit hearts (Table 3). SB-281832 abolished the increased p38 MAPK phosphorylation following 3 weeks of rapid LV pacing. The HF-induced increase in ROS concentration, Tm oxidation, and Tm immunoreactivity were abolished by SB281832 (Fig. 11, 12 and 13), and LVSF was better preserved following 3 weeks of rapid LV pacing. Cardiomyocyte hypertrophy was attenuated with SB-281832 while the increased number of TUNEL-positive cardiomyocytes remained unaffected following 3 weeks of rapid LV pacing.

	Sham	Sham-Vit	HF3	HF3-Vit
Heart rate (bpm)	223 ± 6	220 ± 4	259 ± 11*	241 ± 5
LVEDD (mm)	16.6 ± 0.2	16.7 ± 0.2	19.8 ± 0.5*	18.8 ± 0.2*
Fractional shortening (%)	31.9 ± 1.0	31.1 ± 0.7	12.9 ± 0.7*	18.7 ± 0.9*#
Cardiomyocyte cross-sectional area (μm²)	227 ± 6	211 ± 4	306 ± 6*	259 ± 9*#
Number of TUNEL-positive cardiomyocytes (/(1000*mm²))	4 ± 3	19 ± 7	64 ± 4*	18 ± 4#
Phospho p38 MAPK/total p38 MAPK (relative to sham)	1.00 ± 0.30	4.79 ± 0.80*	2.47 ± 0.71*	3.25 ± 0.55*

Table 2. Hemodynamics and morphology without and with ROS scavenging by vitamins C and E in sham and heart failure rabbits.
mean±SEM.; Sham: sham-operated rabbits (n=7); Sham-Vit (n=7); sham-operated rabbits receiving vitamins C and E, HF3: heart failure rabbits, 3 weeks (n=8); HF3-Vit: heart failure rabbits (3 weeks) receiving vitamins C and E (n=6); LVEDD: LV end-diastolic diameter; * $p<0.05$ vs. Sham; # $p<0.05$ vs. HF3

In this part of the project we demonstrated that: (i) antioxidants abolish the increases in both myocardial ROS formation and Tm oxidation otherwise seen in failing hearts, along with improvement of contractile function and prevention of apoptosis. Antioxidants, however, do not modify the pacing-induced activation of p38 MAPK; (ii) oxidation of MPs is a causal link between ROS formation and

contractile dysfunction; (iii) inhibition of p38 MAPK counteracts ROS accumulation, Tm oxidation and contractile failure, while it does not affect apoptosis, indicating that p38 MAPK activation is upstream rather than downstream of oxidative stress. In fact, scavenging of ROS did not affect p38 MAPK activity (Table 2), suggesting that other signals -apart from ROS- such as nitric oxide (153) or PKC activation (154) contribute to p38 MAPK activation in failing hearts. Moreover, ROS scavenging with vitamin C and E even increased p38 MAPK phosphorylation in sham rabbit hearts, confirming previous data (94) and suggesting a negative feedback between ROS formation and p38 MAPK phosphorylation.

	Sham	Sham-SB	HF3	HF3-SB
Heart rate (bpm)	224 ± 5	228 ± 7	258 ± 15*	264 ± 18*
LVEDD (mm)	17.0 ± 0.3	16.8 ± 0.2	19.6 ± 0.5*	18.9 ± 0.3*
Fractional shortening (%)	30.0 ± 1.7	30.3 ± 0.6	10.3 ± 1.3*	17.0 ± 1.3*#
Cardiomyocyte cross-sectional area (µm²)	242 ± 11	253 ± 6	334 ± 7*	295 ± 4*#
Number of TUNEL-positive cardiomyocytes (/(1000*mm²))	4 ± 2	14 ± 5	50 ± 8*	54 ± 14*
Phospho p38 MAPK/total p38 MAPK (relative to sham)	1.00 ± 0.24	1.01 ± 0.21	2.34 ± 0.54*	0.46 ± 0.24

Table 3. Hemodynamics and morphology without and with blockade of p38 MAPK in sham and heart failure rabbits

mean±SEM.; Sham: sham-operated rabbits (n=7); Sham-SB (n=7); sham-operated rabbits receiving SB, HF3: heart failure rabbits, 3 weeks (n=8); HF3-SB: heart failure rabbits (3 weeks) receiving SB (n=6); LVEDD: LV end-diastolic diameter; * $p<0.05$ vs. Sham; # $p<0.05$ vs. HF3

5.2 Tm Epitope mapping

Our findings indicate the possibility that the formation of cross-linked products in Tm resulted in changes of immunoreactivity. In fact, Tm immunoreactivity in cryosections from HF rabbits was increased compared to controls and vitamins treatment prevented the increased immunofluorescence (Fig.13). Thus, the increased activity is probably due an oxidative modification of Tm, because the epitope is more accessible to anti-Tm monoclonal antibody (CH1 clone). Rabbit α-Tm has a single cysteine (Cys 190), and only at this level Tm can form DCB (76,88). Moreover, Cys190 is located in a flexible region of the protein (155), and this region is also responsible for the interaction with the Troponin complex (156). We investigated whether Tm monoclonal antibody recognises this particular fragment of the protein. Tm has been extracted from rat hearts by Bailey method and purified by means of RP-HPLC (138). Cardiac Tm has been digested by chymotrypsin, a serine protease. The reaction was conducted in $CaCl_2$ 0.1 M and Tris 0.133 M a pH 7.4 for 1 hour using an enzyme/substrate ratio of 1:10. The fragments were separated by RP-HPLC, as shown in the chromatogram in Figure 14A. Aliquots from the proteolysis mixture were analyzed by SDS-PAGE according to Schagger and Von Jagow (157) and protein material tested by anti-Tm immunoblotting: only the aliquots at retention time (RT) 9.0 and 11.3 were recognized by the antibody (Fig. 14B). At RT 9.0 we found a band at low molecular weight, whereas at 11.3 we found the band at high molecular weight. This result has been confirmed by means of the *dot-blot* (Fig. 14C). Thus, the fragment at RT 9.0 was analyzed by mass spectrometry. The sequence was determined by MS-MS and was as follow: EAKAEQY. Notably, this fragment is located close to Cys 190 (fig. 14D), as observed by comparing the sequence fragment with the entire

protein sequence. Thus, we can speculate that the DCB formation at the level of Cys190 causes a conformational modification rendering the epitope more accessible to anti-Tm antibody. The sample at 11.3 is a partial digestion of Tm.

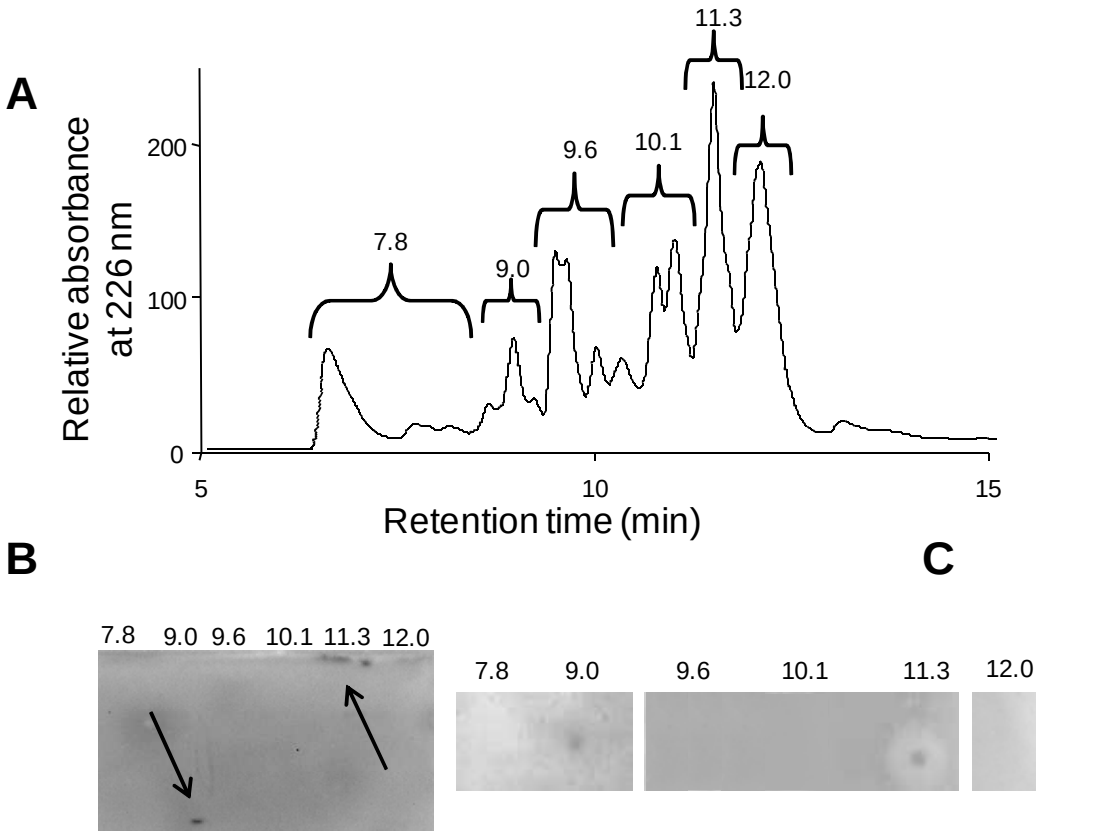

D

α-Tm sequence **9.0 Fragment : EAQAEKY**

```
        10         20         30         40         50         60
MDAIKKKMQM LKLDKENALD RAEQAEADKK AAEDRSKQLE DELVSLQKKL KGTEDELDKY
        70         80         90        100        110        120
SEALKDAQEK  LELAEKKATD AEADVASLNR RIQLVEEELD RAQERLATAL QKLEEAEKAA
       130        140        150        160        170        180
DESERGMKVI  ESRAQKDEEK MEIQEIQLKE AKHIAEDADR KYEEVARKLV IIESDLERAE
       190        200        210        220        230        240
ERAELSEGKC  AELEEELKTV TNNLKSLEAQ AEKYSQKEDK YEEEIKVLSD KLKEAETRAE
       250        260        270        280
FAERSVTKLE  KSIDDLEDEL YAQKLKYKAI SEELDHALND MTSI
```

Figure 14. Epitope mapping of the anti-Tm CH1 monoclonal antibody.
(**A**) Chromatogram showed the fragments of Tm, separated by RP-HPLC, after chymotrypsin digestion. (**B**) Anti-Tm Western blotting of the Tm fragments. Anti-Tm antibody recognised the fragments at a retention time (RT) equal to 9.0 and 11.3. (**C**) Dot Blot method confirmed that anti-Tm antibody recognised proteins corresponding to RT 9.0 and 11.3. (**D**) Mass spectrometry of the fragment at RT 9.0 demonstrated that the anti-Tm antibody recognised the fragment EAKAEQY.

5.3 Oxidation of MPs in human heart failure

Previous results demonstrated that oxidative stress induces changes of myofibrillar proteins (MPs) that are likely to cause or exacerbate the contractile impairment in experimental model of rabbit HF (158,159). Although these experimental findings suggest that augmented intracellular accumulation of ROS may cause contractile dysfunction, the occurrence and the role of MP oxidation have hardly been analyzed in clinical settings. This section of my thesis was aimed at investigating the relationship between MP oxidation and contractile impairment in heart samples from HF patients undergoing heart transplantation (New York Heart Association class IV) as compared to non-failing (NF) samples. Donor hearts are obtained following brain-death and are subject to the Cushing-reflex that may involve acute pacing/ischemia-reperfusion stress on the myocardium and thus may have contributed to oxidative modification of MPs. This effect on the heart will vary in time and severity between donors and cannot be directly controlled in the clinical setting. Although ischemic time (due to cardioplegic ischemic arrest and storage) can contribute to oxidative modifications of MPs, this was not significantly different between NF- and HF-group (Table 4). Thus, upon sample collection both failing as well as NF hearts are exposed to oxidative stress, but this ‘oxidative background’ is probably higher in donors due to the Cushing reflex that is precipitated during brain death. It is likely that, without this background, differences between NF- and HF-group would be greater.

Initially, we measured the most widely studied protein modification induced by ROS, namely carbonylation, which especially affects lysine, arginine, and proline (10). This alteration, resulting from a severe oxidative stress, has been assessed by means of Oxyblot (160). The detection of carbonyls is based on their reaction

with 2,4-dinitrophenylhydrazine (DNPH), which produces the corresponding hydrazone; the oxidized protein can be detected by Western blot analysis with anti-dinitrophenyl (DNP) antibodies. Actin is known to be especially susceptible to carbonylation. This modification has been shown to occur in isolated rat hearts subjected to post-ischemic reperfusion (75). Notably, carbonylation has been demonstrated to result in progressive disruption of actin filaments *in vitro* (161).

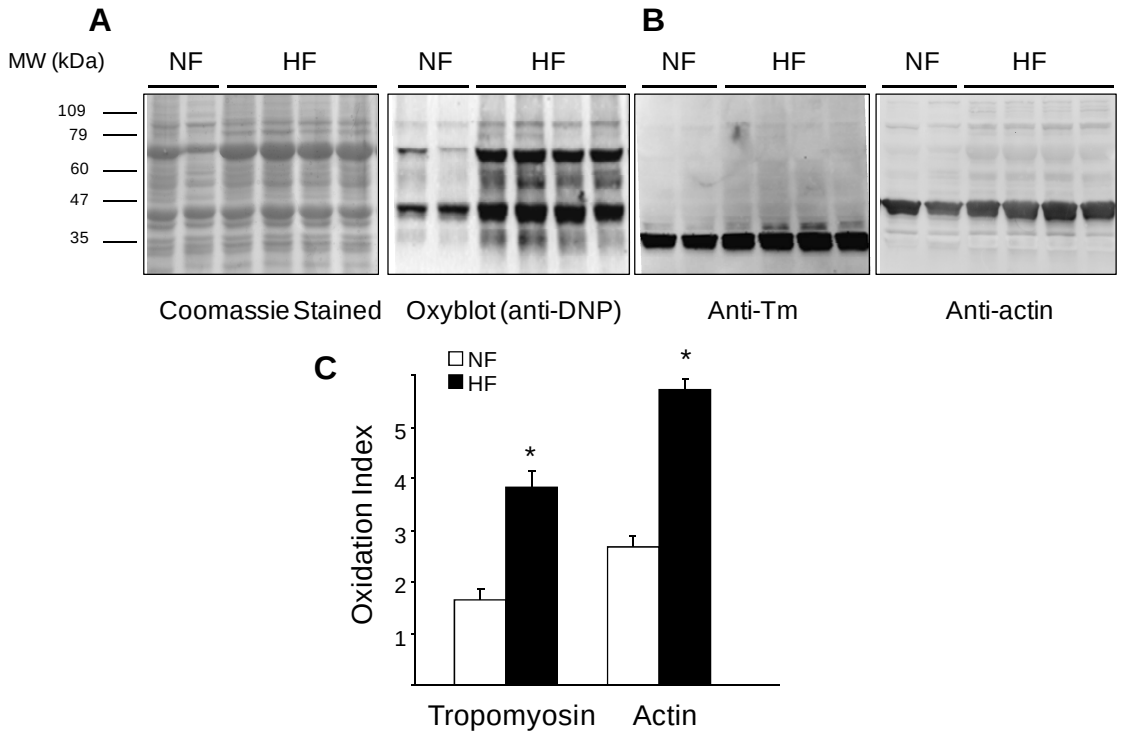

Figure 15. Tm and actin carbonylation is increased in HF.
(**A**) Total myocardial protein extracts from LV biopsies of HF(n=28)- and NF(n=20)-groups were subjected to DNP-derivatization (Oxyblot assay) to detect protein carbonylation and then analyzed by immunoblot probed with anti-DNP antibodies. Coomassie blue staining was performed for protein loading. (**B**) Actin and Tm were identified by stripping and reprobing of the membrane by anti-Tm and actin immunoblots. (**C**) The Oxidation Index is given by the ratio between the densitometric values of the actin and Tm bands in the oxyblot and those of the corresponding bands stained with Coomassie Blue. *P=0.00002 NF- vs HF-group. Data are expressed as mean±SEM.

Figure 15A shows that several proteins were carbonylated in failing hearts. We measured the degree of oxidation of two bands, whose migration corresponds to that of actin and Tm. Their identity was confirmed by stipping and reprobing of the membrane with anti Tm- and actin antibodies (Fig. 15B) and by two-dimensional

oxyblots (Fig. 16). Figure 15C shows that Tm and actin carbonylation was significantly higher in HF patients than in NF donors. Densitometric analysis was performed by normalizing the bands of actin and Tm in the oxyblot for the corresponding band stained with EZBlue-Coomassie brilliant blue G-250 using the Quantity One software. The total amount of actin and Tm was not different between failing and non-failing hearts, as shown by EZBlue-Coomassie staining in Figure 15A. Actin and Tm carbonylation appear to reflect reliably the oxidative degradation of MP.

	NF	**HF**
Age (years)	54.4±3	49.5±2
Gender (female/male)	11/25	5/46
Weight (kg)	75.4±1.0	76.2±0.6
Height (cm)	172±0.9	170±0.7
LVEF (%)	64.2±2.6	24.2±1.1*
Left Atrium Diameter (mm)	35±1.3	48±0.8*
End Diastolic Diameter (mm)	46±1.2	68±1.0*
Systolic Diameter (mm)	33±0.9	63±1.3*
Heart Rate (bpm)	70±1.1	83±1.0*
Systolic Pressure (mmHg)	118±1.4	125±1.0
Diastolic Pressure (mmHg)	65±1.1	76±0.8*
TnI (mg/L)	1.3±0.4	4.2±0.4*
Ischemic time (minutes)	180±10	139±10
Diabetes mellitus	1/25	0
Hypertension	3/25	16/46
Smoker	4/25	1/46

Table 4. NF donor and severe chronic HF patient group details.
NF donors died of subarachnoid hemorrhage-related brain death, and were free of overt cardiovascular disease. Plasma TnI was measured prior to cardiac explantation (means ± SD), *p<0.0001 vs NF. HF = heart failure; LV = left ventricular; LVEF = left ventricular ejection fraction; NF = non failing; TnI = troponin I.

In the HF-group left ventricular ejection fraction (LVEF), a functional parameter that indicates the contractile impairment, was significantly lower (Table 4, 24.2±7.2 *vs* 66.1±8.9% in the NF-group, p<0.0001). Age, gender, and cardiac ischemic time

(from aortic cross clamp to freezing of biopsy) did not differ significantly between NF- and HF-group and had no detectable impact on any of the molecular analyses as determined by multiple linear regression analyses in Table 4. We correlated protein carbonylation with this functional parameter of contractile disfunction.

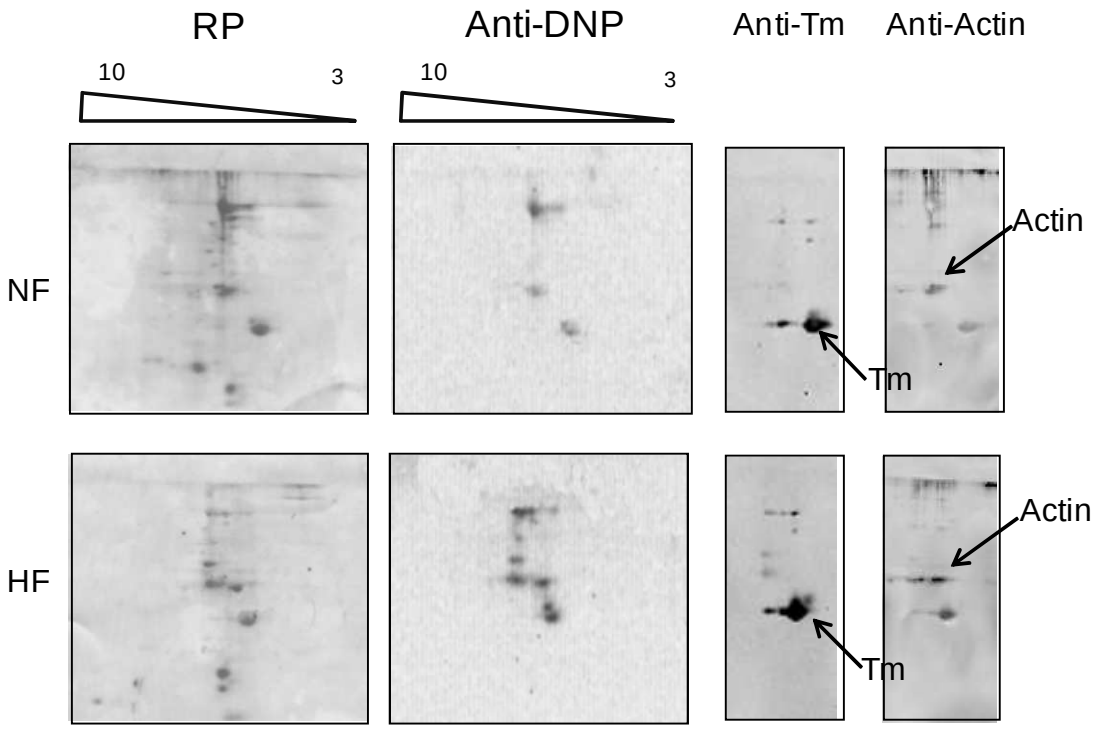

Figure 16. Identification of actin and Tm by two-dimensional oxyblot.
MPs were extracted from NF- and HF-group and subjected to two dimensional gel electrophoresis followed by detection with anti-DNP antibodies. Red Ponceau (RP) staining was performed for protein loading. The membranes were subsequently stripped and reprobed with anti-actin and anti-Tm antibodies to confirm the identity of the carbonylated proteins (indicated by the arrows).

Notably, the degree of Tm and actin carbonylation significantly correlated with the contractile impairment, as shown by a reduction of LVEF (Fig. 17A). This is the first demonstration that HF is related to oxidative changes of specific MPs in humans. Oxidative stress is well-established in causing loss of cellular viability, and TnI release into plasma is a useful clinical diagnostic marker of myocardial cell injury.

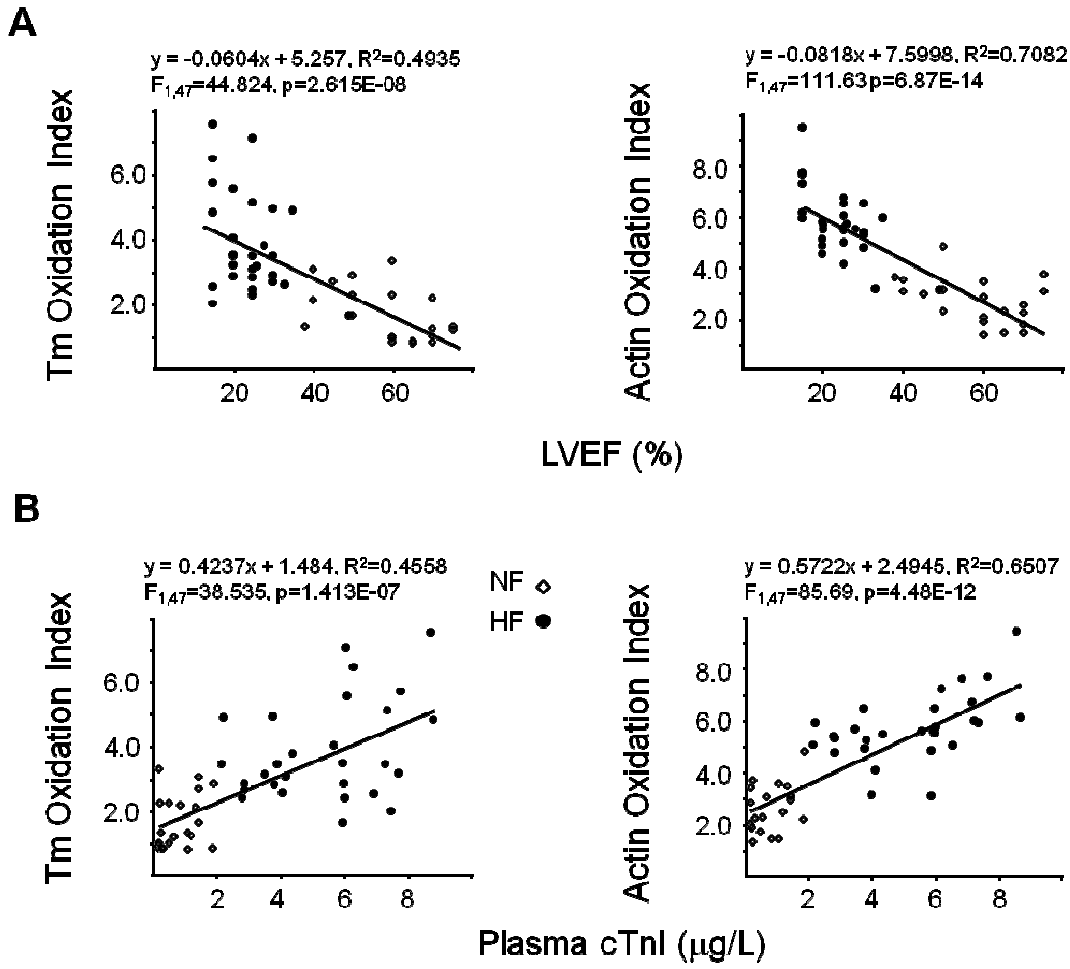

Figure 17. Tm and actin carbonylation correlates with contractile dysfunction and loss of myocardial viability.
The degree of Tm and actin oxidation significantly correlates with (**A**) left ventricular ejection fraction (LVEF) and (**B**) plasma cardiac troponin I (cTnI) when the NF- and HF-groups were combined. Open diamonds = NF, close circles = HF.

The increase of plasma cTnI levels has been documented in several cardiovascular diseases, such as acute coronary syndromes, acute decompensated HF (162), and chronic HF (163). Indeed, increased circulating cTnI levels are associated with poor clinical outcome in patients with cardiomyopathy (164) and are inversely correlated to LVEF in patients with septic shock (165). These relationships might explain the reduced calcium responsiveness of myofilaments that has been proposed to underlie HF (166). Plasma TnI levels were significantly higher in HF- than in NF-group (4.2±0.4 *vs*

1.3±0.4 μg/L, p<0.0001, Table 1) and importantly, correlated with the extent of Tm and actin carbonylation (Fig. 17B).

Carbonylation is likely to result from severe oxidative stress. Under milder stress, proteins can be oxidatively modified at the level of Cys residues. Based upon these findings that provided evidence of the correlation between contractile impairment and MP carbonylation in failing myocardium, we characterized the oxidative modifications occurring at the level of cysteine residues. In particular, we analyzed Tm oxidation, since in experimental models we previously demonstrated that this protein modification is linearly related to contractile impairment (76). Tm oxidation was detected as the appearance of high-molecular-weight peptides in immunoelectrophoreses performed under non-reducing conditions. As shown by the typical example in Figure 18A, anti-Tm immunoblots displayed additional bands in samples obtained from HF-group. The appearance of these bands reflected DCB formation, because they were visible only in non-reducing electrophoresis. The band at 82 kDa was attributed to a dimer of Tm (76), whereas the bands with an apparent molecular mass > 200 kDa are likely to reflect high-molecular-weight complexes among several monomers of Tm, or between Tm and other proteins. It is worth pointing out that in rodents, cardiac Tm contains only the α–isoform, whereas Tm from human cardiac muscle contains up to 20% of the β–isoform. At variance from the presence of a single cysteine (Cys190) in α-isoform, β-Tm contains two Cys residues that might result in the covalent aggregation of more than two proteins by means of DCB formation. Densitometric analysis illustrated in Figure 18B shows that the amount of DCB in Tm was significantly increased in the HF-group (1.12±0.1 *vs* 0.63±0.1 in the NF-group, p<0.001). Tm oxidation was quantified by assessing the density of DCB

complexes that appeared only under nonreducing conditions. The density of the bands was normalized to red Ponceau staining to take the difference in sample loading into account.

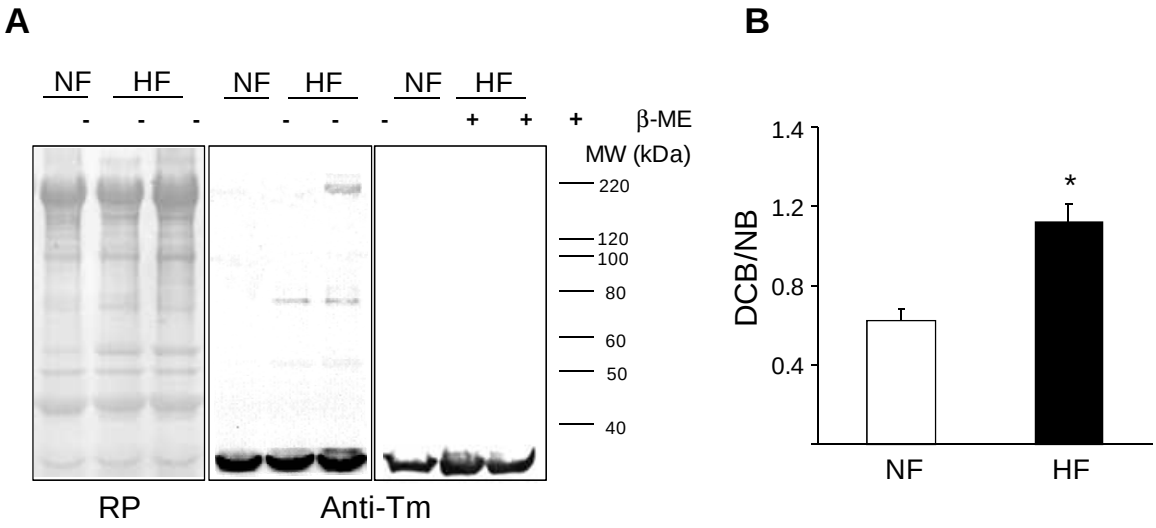

Figure 18. Tm oxidation is increased in human failing hearts.
(**A**) MPs extracted from LV biopsies of HF(n=33) patients and NF(n=15) donors were denatured in the absence (non–reducing conditions) or in the presence (reducing conditions) of β-mercaptoethanol (β-ME) and then analyzed by anti-Tm immunoblot. Two additional bands due to DCB formation were detected in HF-samples under non-reducing conditions. Equal loading was checked by Red Ponceau staining (RP). (**B**) The amount of DCB was quantified by densitometry as DCB/NB. NB = native band. Values are means ±SEM. * p=3.76E-05 NF-vs HF-group.

Interestingly, Tm appeared especially susceptible to oxidation, since we could not detect DCBs in actin and desmin (Fig. 19), although these proteins undergo oxidation both *in vitro* and in experimental models (75). Similarly also troponin C, cTnI and myosin light chain did not show DCB formation.

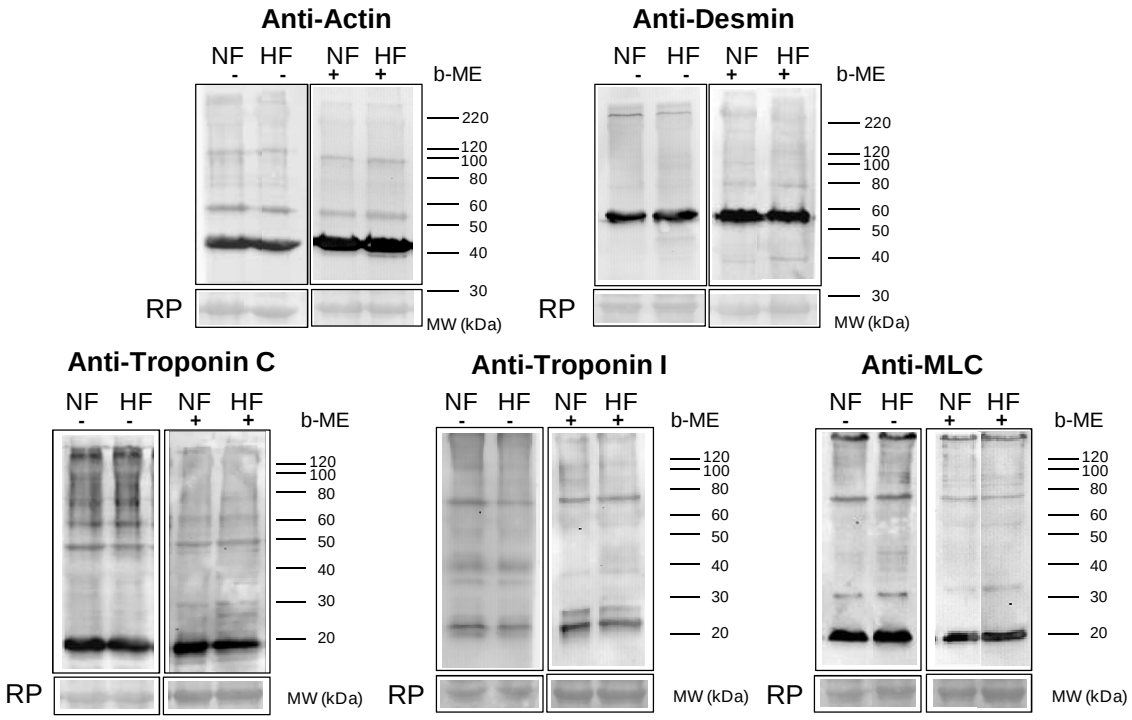

Figure 19. No evidence of DCB-related MP oxidation for sarcomeric actin, desmin, TnI, troponin-C and Myosin Light Chains (MLC).
MPs were extracted from LV biopsies of HF(n=12)- and NF(n=8)-group, denatured as reported in figure 18 and analyzed by immunoblot probed with antibodies to specific sarcomeric MPs. No evidence of DCB formation was obtained in HF- compared to NF-group because no major differences were detected between these groups under non-reducing and reducing conditions.

We then analyzed the relationship between Tm oxidation and cTnI released prior to explantation. Interestingly, Plasma cTnI levels and LVEF correlated with the extent of DCB formation in Tm when all of the samples were analyzed ($y = 0.0743x + 0.6875$, $r^2 = 0.18$,$p = 0.003$; $y = -0.0107x + 1.3364$, $r^2 = 0.20$,$p = 0.0002$, respectively) (Figure 20). This finding showed that DCB content in Tm was significantly higher in failing hearts, however, unlike carbonylation, the correlation between DCB formation and LVEF and plasma cTnI is less remarkable. This might be because our study analyzed samples collected at end-stage failure, whereas DCB formation is likely to occur at an early stage. In fact, in acute experimental setting of HF, DCB formation correlated with contractile dysfunction (76).

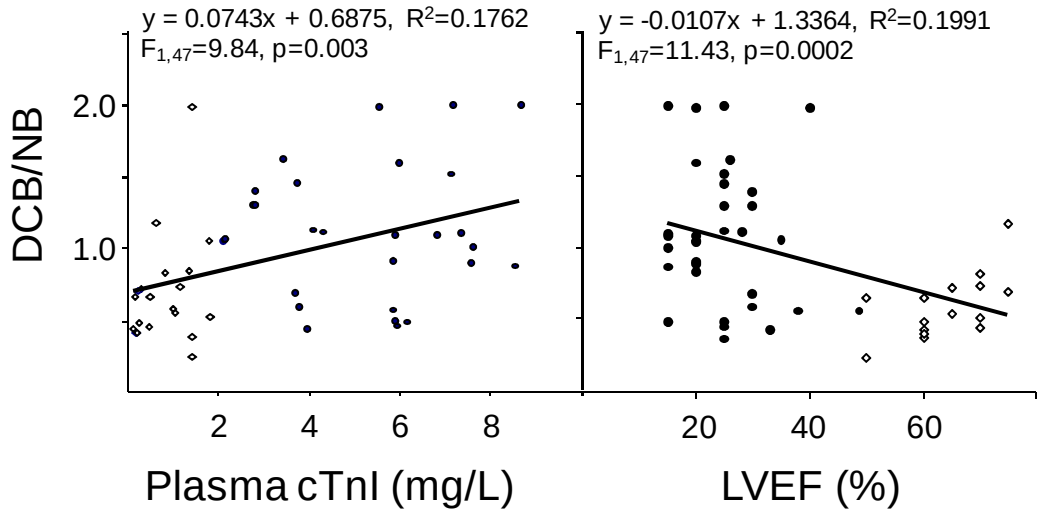

Figure 20. Correlation between Tm oxidation and myocardial injury.
The degree of Tm oxidation (DCB/NB) significantly correlated with plasma cTnI (left panel) and LVEF (right panel) when the NF and HF groups were combined. Open diamonds = NF, closed circles = HF. NB = native band.

Considering the large body of evidence related to the involvement of nitric oxide in HF we investigated whether Tm is also a target of reactive nitrogen species. Since no information was available on nitric oxide-induced changes of MPs, initially we analyzed the occurrence of S-nitrosylation, a reversible, redox-dependent protein modification in which an NO moiety is covalently attached to the free thiol of a cysteine residue, by incubating Tm purified from rat myocardium with increasing concentrations of S-nitrosoglutathione, a donor of nitric oxide. The purity of the protein was checked by Reverse-Phase HPLC and the identity was confirmed by mass spectrometry (Fig. 21A). A mass of 32722.28±0.12 Da was measured, that matches the theoretical value. Figure 21B shows that isolated Tm underwent S-nitrosylation.

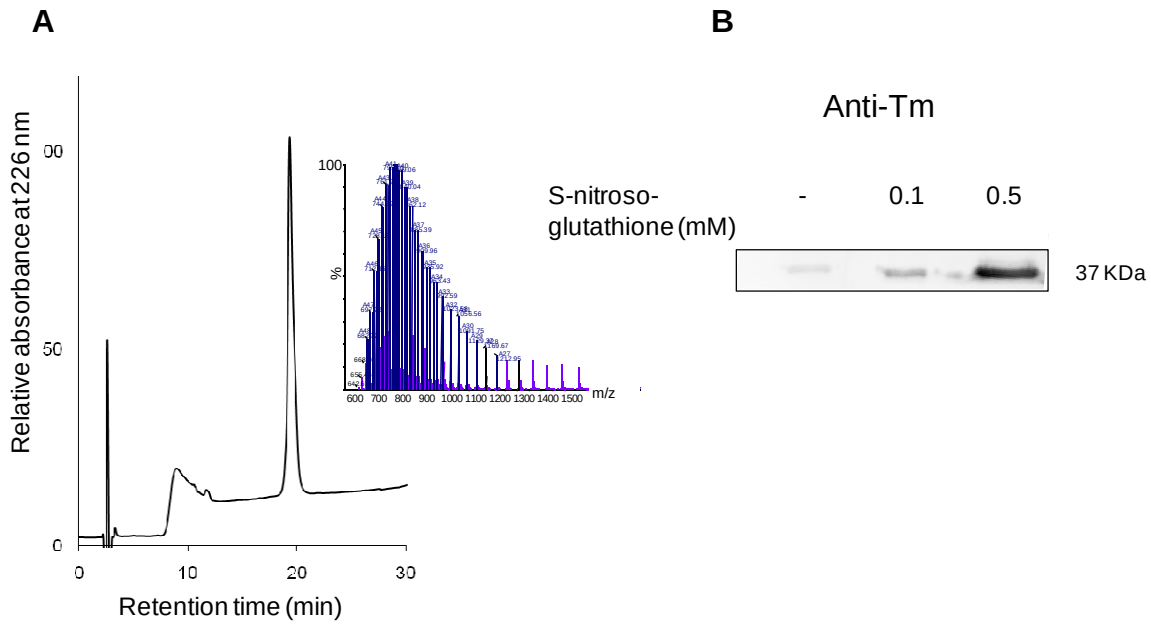

Figure 21. Tm is S-nitrosylated in vitro by S-nitrosoglutathione.
(**A**) Tm purified by HPLC from rat myocardium was incubated with S-nitrosoglutathione. (**B**) As detailed in the Methods, following the biotin-switch assay, the biotinylated/S-nitrosylated Tm was precipitated with avidin-agarose beads and the pellet was detected by anti-Tm immunoblot.

This finding might have been anticipated by analyzing the primary structure of Tm. Indeed, Cys190 in Tm is flanked by an “acid-base motif” that is crucial for the occurrence of S- nitrosylation. This process is further favored by local pH, redox tone, or presence of magnesium or calcium, which can all function as allosteric effectors to control thiol accessibility or reactivity (167).

Based upon this *in vitro* evidence, the occurrence and extent of MP S-nitrosylation were assessed in biopsies from HF- and NF-group by means of the biotin switch technique (137). In this assay nitrosylated cysteines are converted in biotinylated cysteines in three-step procedure. Briefly, protein-free thiols were blocked by incubation with a thiol-specific agent, then S-nitrosothiols were selectively reduced by ascorbate to form thiols, which were then reacted with a sulfhydryl-specific biotinylating reagent. The biotinylated/S-nitrosylated proteins were subjected to immunoblot analysis with anti-biotin antibodies.

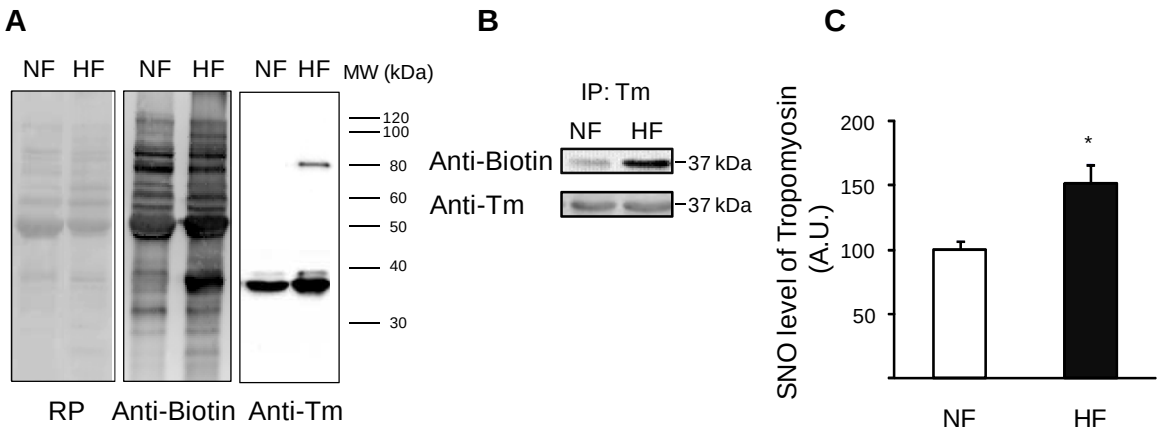

Figure 22. Detection of S-nitrosylated proteins in human left ventricles.
(**A**) MPs were extracted from LV biopsies of HF(n=36)- and NF(n=24)-group and subjected to the biotin-switch assay. To ascertain the identity of the band corresponding to Tm in the anti-biotin blot of panel A the derived biotinylated proteins were immunoprecipitated (IP) with anti-Tm monoclonal antibody. (**B**) Immunoblots of the pellets were stained with anti-Tm, to confirm the IP, and anti-biotin antibodies. The density of the band in the HF-group was markedly increased in the immunoblot probed with anti-biotin antibody indicating the major S-nitrosylation in this group. Equal loading was checked by Red Ponceau staining (RP). (**C**) The amount of S-nitrosylated Tm was given by the ratio between the densitometric values of the S-nitrosylated bands and those of the corresponding bands stained with RP. Values are means ±SEM. * p< 0.05 NF- vs HF-group.

Figure 22A shows that several MPs underwent S-nitrosylation. Most of these proteins were similarly S-nitrosylated in NF- and HF-samples. The major exception was a band at 37 kDa which corresponded to Tm, as shown by immunoblot analysis (Fig. 22A). To provide additional evidence of the identity of the band corresponding to Tm, samples from NF- and HF-group were immunoprecipitated after biotinylation with anti-Tm antibodies (Fig. 22B). The panel of Figure 22B shows an increased biotinylation/S-nitrosylation of Tm in HF-samples. The densitometric analysis of the Tm band in anti-biotin immunoblots, normalized to the corresponding bands in the red Ponceau-stained blots, displayed a significant increase in the HF-group (Fig. 22C) (154±13.1 vs 100±6.09 A.U. in NF-group, $p<0.01$). This finding provides the first evidence of S-nitrosylation of a specific MP, namely Tm, in human failing hearts. However, Tm nitrosylation did not correlate with cTnI and LVEF ($R^2=0.1006$, $p=0.028$ and $R^2=0.0901$, $p=0.038$, respectively). We obtained this result because nitrosylation might have a protective role during

oxidative stress. In recent paper, Murphy and co-workers proposed that S-nitrosylation also protects cysteine residues against potential oxidative damage from ROS during ischemia/reperfusion. Because S-nitrosylation is a transient modification, S-nitrosylation of proteins during ischemic pre-condition could shield cysteine residues from irreversible oxidation during the first few minutes of reperfusion, after which time the S-nitrosylation is removed and normal protein function can resume (168).

The present results demonstrate that human HF, with severe contractile dysfunction as evidenced by poor LVEF that limit cardiac output, involves metabolic stresses that induce specific oxidative covalent changes of actin and Tm thus impeding their molecular function. On the basis of the localisation and crucial role of actin and Tm in the myofilaments, these molecular changes in the MPs are highly predictive of marked interference with myofibrillar contractile performance.

5.4 Oxidative stress by monoamine oxidases is causally involved in myofiber damage in muscular dystrophy.

Muscular dystrophies (MDs) are a heterogeneous group of inherited human disorders primarily affecting skeletal muscles. Several studies documented the key role of oxidative stress and abnormal production of ROS in the pathophysiology of MDs (124,169-171). Mitochondria are generally indicated as a major source of ROS. Besides the respiratory chain, a relevant source of ROS in mitochondria is represented by monoamine oxidases (MAO). Some evidence exists regarding MAO expression in the heart, where MAO-A is the isoform prevalently present and located within the cardiomyocytes. Data available in literature, as well as data

previously obtained in Prof. Di Lisa's laboratory, showed that MAO inhibition is able to prevent cardiac ischemia/reperfusion injury and protect from cardiac hypertrophy by reducing the oxidative stress (55,172).

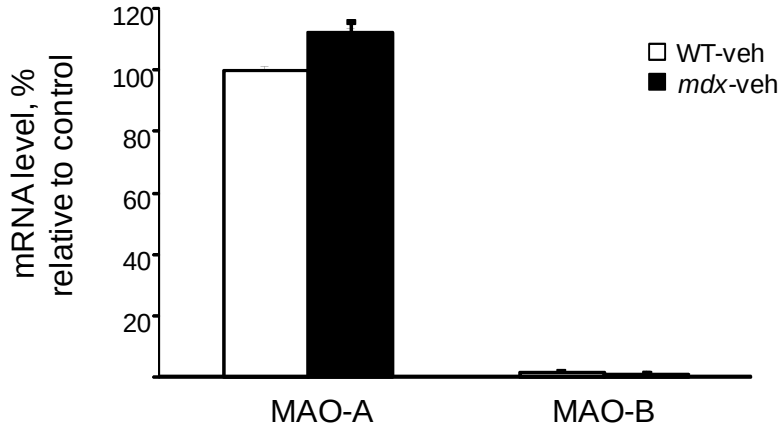

Figure 23. Expression levels of MAO-A and –B mRNA in mouse gastrocnemius.
Total RNA was extracted and reverse transcribed as described in Materials and Methods. Equal amounts of cDNA were amplified by PCR using specific primer for MAO A and MAO B. Gastrocnemius from wild-type mice expresses prevalently MAO-A isoform, while MAO-B expression level is almost negligible. In gastrocnemius from *mdx* mice MAO-A expression increased compared to wild-type littermates, while MAO-B expression did not change in *mdx* mice compared to wild-type. Values are means±SEM.

To study MAO expression in our model, we initially determined the expression level of MAO-A and B in the skeletal muscle from *mdx* and wild-type mice. The mRNA expression of MAO-A and B was determined by RealTime RT-PCR. As shown in Figure 23, gastrocnemius from wild-type mice expresses prevalently MAO-A isoform, while MAO-B expression level is almost negligible. Moreover, in gastrocnemius from *mdx* mice MAO-A expression increased about of 12% compared to wilde-type littermates, while MAO-B expression did not change in *mdx* mice compared to wild-type. However, gene expression level does not necessarily reflect the protein expression level or enzyme activity. Therefore, we measured the activity of these enzymes in skeletal muscle. MAO-A and -B activities were determined measuring the production of H_2O_2 by means of Amplex Red, which is oxidized to resorufin in the presence of H_2O_2. Mitochondria were

incubated with 250 µM tyramine, substrate for MAO-A and B. We found a marked increase in H_2O_2 formation in 5-week-old *mdx* mice as compared to wild-type littermates (Fig. 24A).

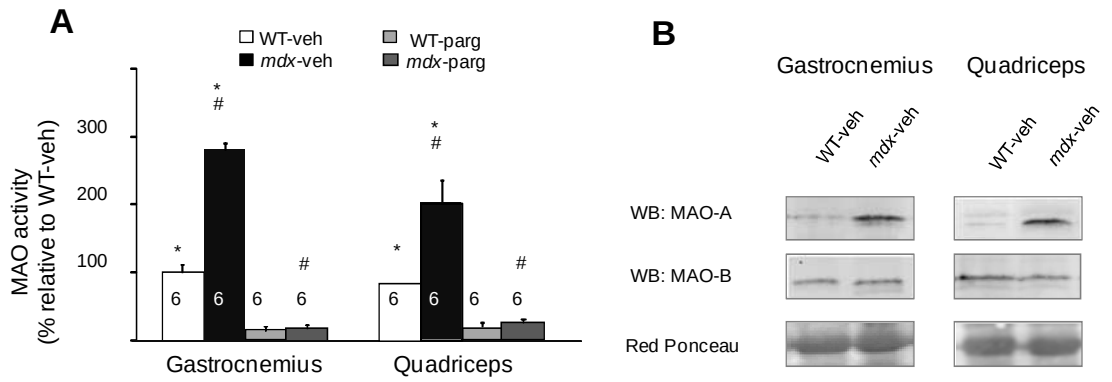

Figure 24. MAO activity increases in *mdx* mice.
(**A**) MAO activity in gastrocnemius and quadriceps muscles from wild-type and *mdx* mice after 1 week of treatment with pargyline or vehicle. The activity increased in *mdx* muscles compared to wild-type, and it was completely abolish after pargyline treatment. (**B**) Representative Western Blots (WB) of MAO-A and MAO-B in gastrocnemius and quadriceps from wild-type (*n*= 6) and *mdx* (*n*= 6) mice. The protein level of MAO-A isoform increased in *mdx* mice compared to wild-type mice. Equal protein loading was indicated by Red Ponceau staining. Parg, pargyline; veh, vehicle; WT, wild-type. $^{*}P< 0.05$ *mdx*-veh versus WT-veh; $^{\#}P< 0.05$ *mdx*-veh versus *mdx*-parg. Error bars represent the s.e.m. The number of mice for each group is indicated inside each bar.

To investigate which isoform was responsible for the increased activity, we measured MAO-A and MAO-B protein levels by Western Blotting. We found that the increased activity was associated with an increase in MAO-A protein levels (Fig. 24B). To assess whether the accumulation of ROS related to MAO activity plays a pivotal role in both loss of cell viability and contractile derangements in skeletal muscle, 5-week-old male *mdx* mice were randomized into groups receiving i.p. treatment with pargyline (50 mg/kg/d), an inhibitor of both MAO-A and MAO-B, or vehicle for one week. MAO activity was abolished after pargyline treatment (Fig. 24A).

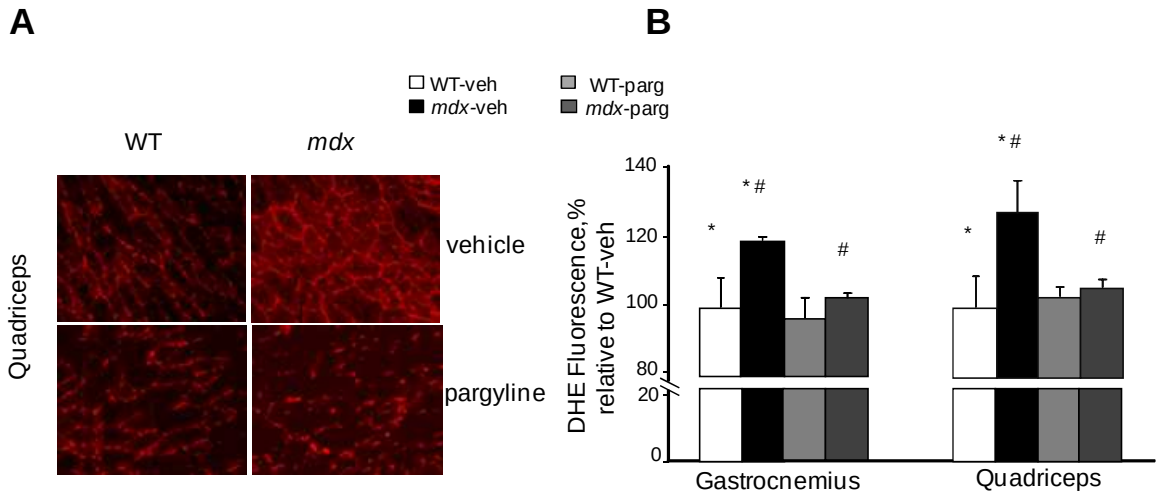

Figure 25. MAO inhibition reduces oxidative stress in *mdx* mice.
(**A**) Oxidative stress assessed by DHE staining in sections of quadriceps from vehicle- or pargyline-treated wild-type and *mdx* mice. Scale bar, 50 µm. (**B**) Quantification of DHE fluorescence in gastrocnemius and quadriceps muscle cryosections from wild-type and *mdx* mice treated with vehicle or pargyline showing the reduced ROS accumulation after pargyline treatment. Parg, pargyline; veh, vehicle; WT, wild-type. **P* < 0.05 *mdx*-veh versus WT-veh; $^{\#}P$ < 0.05 *mdx*-veh versus *mdx*-parg. Error bars represent the s.e.m. The number of mice for each group is indicated inside each bar.

We evaluated whether MAO inhibition could reduce or prevent ROS accumulation in skeletal muscles by means of the DHE staining. As expected, we confirmed that in dystrophic mice there is an increased ROS formation and, interestingly, pargyline significantly decreased oxidative stress in *mdx* muscles (Fig. 25A and B). We investigated whether MAO-dependent ROS accumulation caused oxidative modifications of MPs, as probed by Tm oxidation. Indeed, we previously demonstrated that, among MPs, Tm is particularly susceptible to oxidative stress (76). Immunoblots with anti-Tm displayed additional high molecular mass bands in gastrocnemius and quadriceps from *mdx* (Fig. 26A). The appearance of these bands, which were much fainter in samples obtained from wild-type littermates, reflected DCB formation because they were visible only under non-reducing electrophoresis. The band at 82 kDa was attributed to a dimer of Tm, while the bands with an apparent molecular mass > 220 kDa could reflect high molecular mass complexes among several monomers of Tm, or between Tm and other

proteins. It is worth pointing out that skeletal Tm contains the α- as well as the β-isoform. β-Tm contains two Cys residues, that might result in the covalent aggregation of more than two proteins by means of DCB formation.

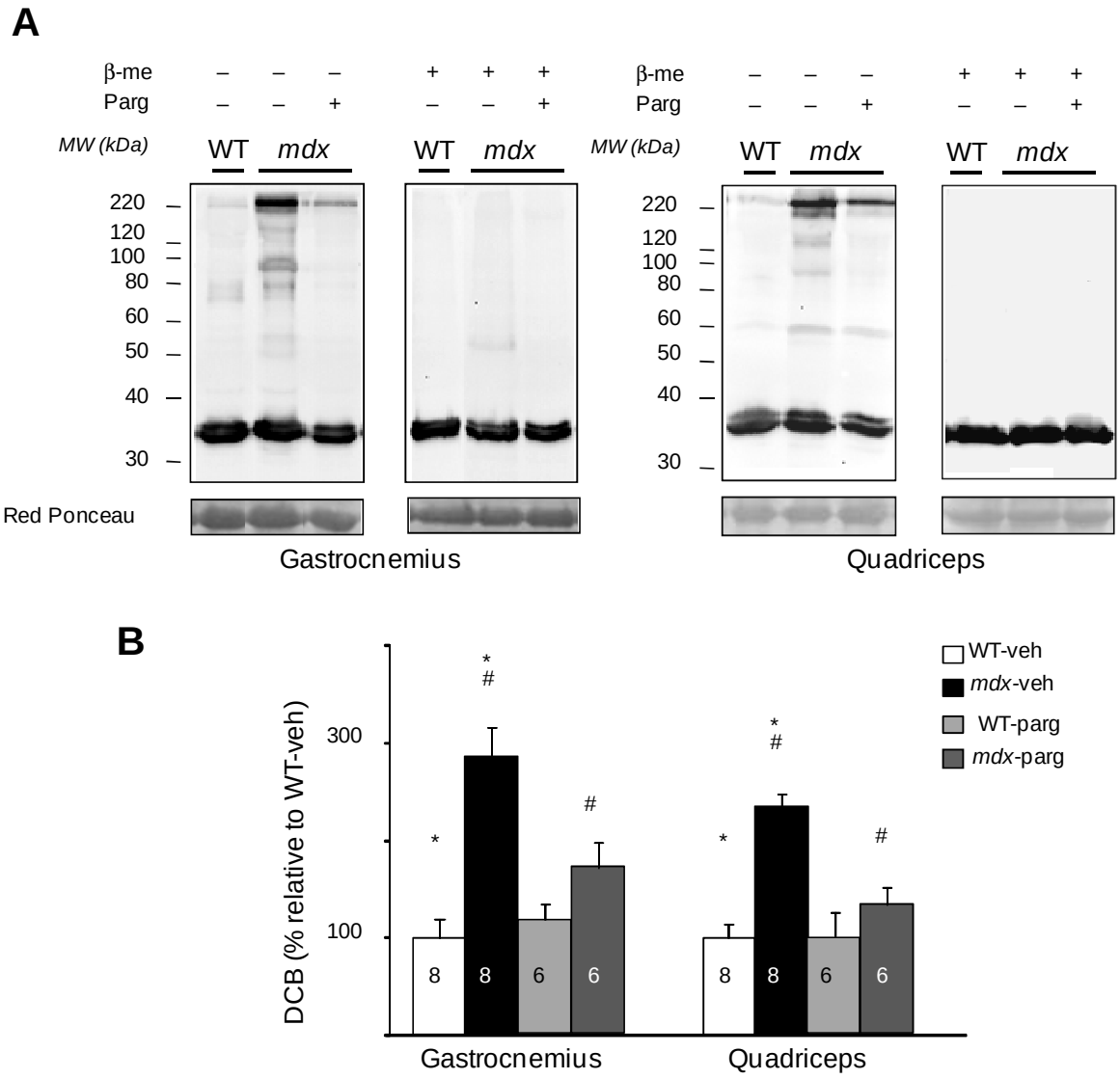

Figure 26. MAO inhibition reduces Tm oxidation in *mdx* mice.
(**A**) Tm oxidation detected as the formation of DCB in gastrocnemius and quadriceps muscles of vehicle- or pargyline-treated wild-type and *mdx* mice. High-molecular-mass peptides were attributed to DCB formation by comparing electrophoreses carried out in the absence or in the presence of β-mercaptoethanol (β-me). Immunoblotting displayed additional high-molecular-mass bands in *mdx* muscles that were reduced by pargyline treatment. (**B**) Quantitative analysis of DCB formation in Tm immunoblots showing a significant decrease in Tm oxidation upon pargyline treatment. Parg, pargyline; veh, vehicle; WT, wild-type. **P* < 0.05 *mdx*-veh versus WT-veh; $^{\#}$*P*< 0.05 *mdx*-veh versus *mdx*-parg. Error bars represent the s.e.m. The number of mice for each group is indicated inside each bar.

Densitomeric analysis showed that DCB increased 2.84±0.31 and 2.34±0.28 folds in gastrocnemius and quadriceps muscle, respectively. Importantly, these oxidative modifications were significantly decreased after i.p. treatment with pargyline for one week (Fig. 26B). Dystrophic mice showed typical signs of myopathy, with focal areas of infiltration by phagocytic cells and a pronounced variation of fiber diameter (Fig. 27A). These pathological signs were markedly reduced in muscles from *mdx* mice treated with pargyline, which showed more uniform fiber size and decreased tissue inflammation. Morphometric analysis of myofiber cross-sectional areas in gastrocnemius muscle confirmed that *mdx* contained myofibers of different sizes, with a significant incidence of small fibers, while pargyline normalized the fiber area distribution (Fig. 27B). Gastrocnemius muscle from *mdx* mice showed the characteristic increase in central nucleation of myofibres that indicates regeneration due to ongoing degeneration, and this regeneration was significantly reduced in pargyline-treated mdx mice (Fig. 27C).

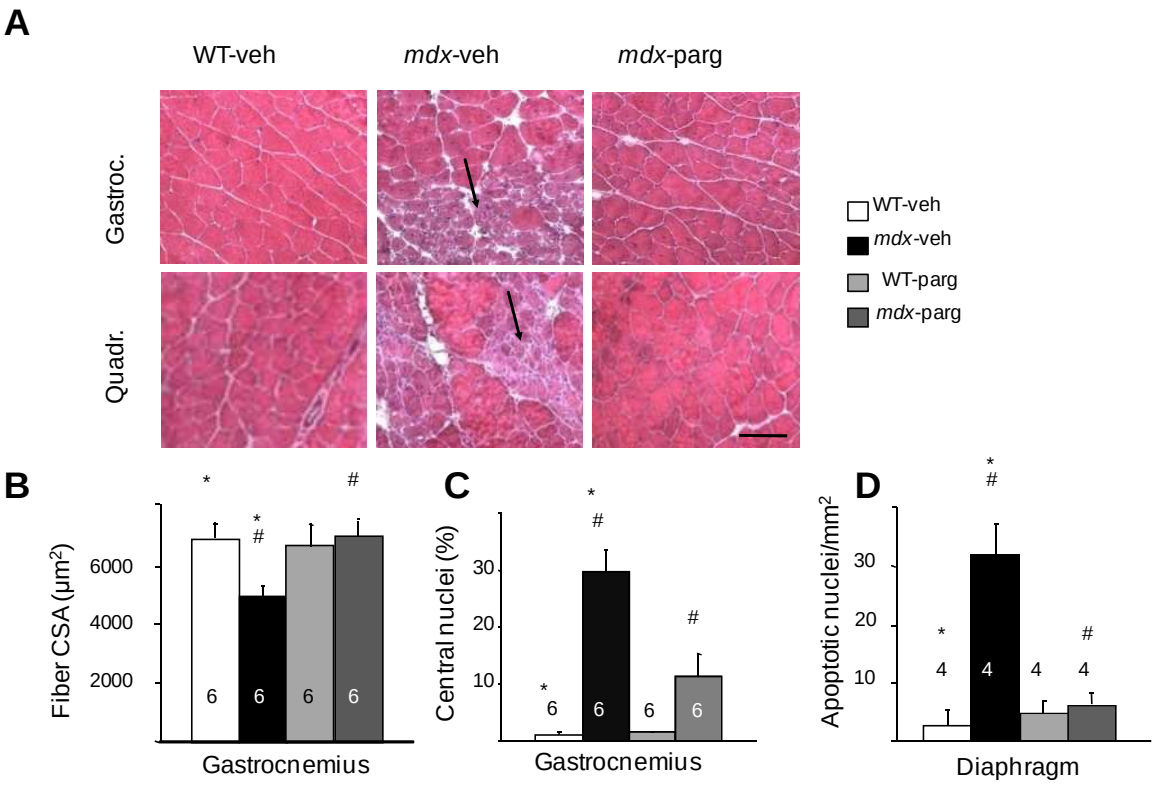

Figure 27. MAO inhibition rescues histological alterations and prevents muscle apoptosis in *mdx* mice.

(**A**) Representative cross-sections of H&E-staining of gastrocnemius (Gastroc.) and quadriceps (Quadr.) muscles from wild-type and *mdx* mice treated with vehicle or with pargyline. *Mdx* muscles showed a large variability in myofiber size and occurrence of inflammatory infiltrates (arrows). On the contrary, *mdx*-treated mice displayed uniform fibers size and absence of inflammatory infiltrates, similarly to wild-type muscles. Scale bar, 100 µm. (**B**) Morphometric analysis of myofiber cross-sectional area (CSA) in gastrocnemius muscles of wild-type and *mdx* mice treated with vehicle or pargyline showed that pargyline treatment normalized the fiber area distribution. (**C**) Gastrocnemius muscle from *mdx* mice showed a higher incidence of fibers with centrally located nucleai that indicates regeneration due to ongoing degeneration, and this percentage was significantly decreased in pargyline-treated *mdx* mice. (**D**) Quantification of apoptotic nuclei by TUNEL assay in diaphragm muscle sections. Pargyline treatment blunted the increased incidence of apoptosis in *mdx* mice. Parg, pargyline; veh, vehicle; WT, wild-type. **P* < 0.05 *mdx*-veh versus WT-veh; $^{\#}P$< 0.05 *mdx*-veh versus *mdx*-parg. Error bars represent the s.e.m. The number of mice for each group is indicated inside each bar. The key in (A) applies to all panels.

Then we investigated whether pargyline treatment was able to improve cell survival and to counteract the apoptotic phenotype observed in *mdx* mice. The frequency of apoptotic nuclei was evaluated *in situ* by using the terminal deoxynucleotidyl transferase-mediated dUTP nick end labeling (TUNEL) method. TUNEL-positive nuclei were readily detected in the diaphragm of *mdx* mice, but not in the corresponding samples of WT and pargyline-treated *mdx* mice. *Mdx*

muscle sections displayed an average of 31.0 ± 6 TUNEL-positive nuclei/mm^2, while the incidence in muscle sections from *mdx*-treated mice was 7 ± 2, which is not significantly different from the value (2.0 ± 1.2) measured in wild-type sections (Fig. 27D). Taken together, these results indicate that in *mdx* mice ROS generated by MAO are relevant to the dystrophic mechanism and that inhibition of MAO protects dystrophic skeletal muscle by reducing myofiber degeneration and ROS production.

Although mutations in components of the dystrophin glycoprotein complex are responsible for the most devastating MDs, mutations of genes coding for extracellular matrix proteins play a causative role in other forms of MDs. Indeed, another group of MDs is due to inherited mutations in genes encoding collagen VI. Collagen VI is a major component of the endomysium, where it is localized just outside the basement membrane of muscle fibers. Mutations of Collagen VI cause two muscle diseases in humans, namely Bethlem myopathy (MIM#158810) and Ullrich congenital muscular dystrophy (UCMD, MIM#254090) (129). Bethlem myopathy is a relatively mild and slowly progressive myopathic disorder, whereas UCMD is a severe and rapidly progressive muscle disease usually causing early death due to respiratory failure.

Several years ago Bonaldo et al. (129) generated a mutant mouse lacking ColVI. The *Col6a1*$^{-/-}$ mouse turned out to be the first and to date the only animal model of ColVI-related disorders, and a key to understand the pathophysiology and to devise and test potential therapies for these diseases. *Col6a1*$^{-/-}$ mice are characterized by muscle necrosis, increased rate of apoptosis accompanied by contractile impairment of muscle fibers and a modest rate of myofiber regeneration (128,129). The alteration appeared early (first week of age), and presented a

limited progression with age. The features displayed by *Col61a*$^{-/-}$ mice are thus similar to those detected in patients with ColVI- related disorders. Previous works provided evidence of mitochondrial involvement in the pathogenesis of the disease (127,128,173).

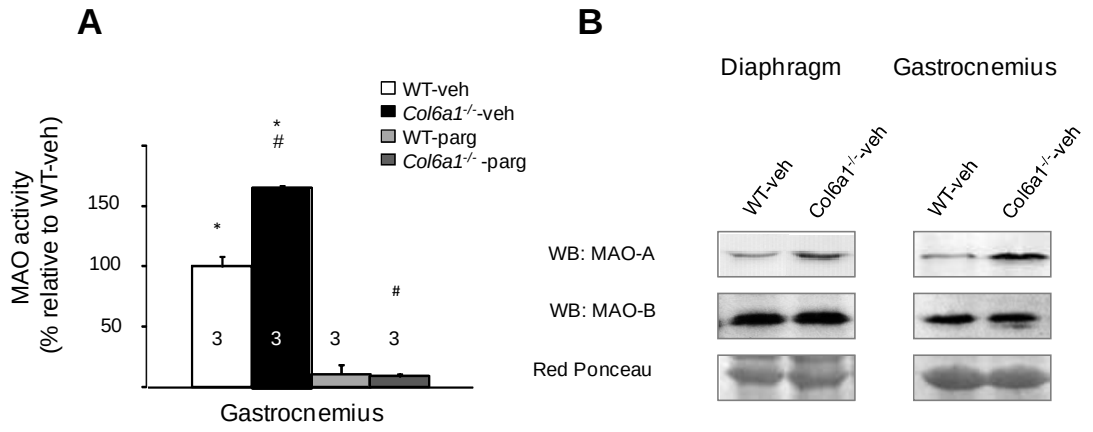

Figure 28. MAO activity increases in *Col6a1*$^{-/-}$ mice.
(**A**) MAO activity in gastrocnemius muscles from wild-type and *Col6a1*$^{-/-}$ mice after one week of treatment with pargyline or vehicle. The activity increased in *Col6a1*$^{-/-}$ muscles compared to wild-type, and it was completely abolish after pargyline treatment. (**B**) Representative western blots (WB) of MAO-A and MAO-B in diaphragm and gastrocnemius from wild-type (n = 6) and *Col6a1*$^{-/-}$ (n = 6) mice. The protein level of MAO-A isoform increased in *Col6a1*$^{-/-}$ mice compared to wild-type mice.Equal protein loading was indicated by red Ponceau staining. Parg, pargyline; veh, vehicle; WT, wild-type. $^{*}P < 0.05$*Col6a1*$^{-/-}$-veh versus WT-veh; $^{\#}P < 0.05$ *Col6a1*$^{-/-}$-veh versus *Col6a1*$^{-/-}$-parg. Error bars represent the s.e.m. The number of mice for each group is indicated inside each bar.

The findings obtained in *mdx* mice prompted us to investigate whether ROS generated by MAO might play a role also in *Col6a1*$^{-/-}$ mice. Interestingly, MAO activity increased in gastrocnemius and quadriceps muscles of *Col6a1*$^{-/-}$ mice along with an increase in MAO-A protein level (Fig. 28A and B), in accordance to what observed in *mdx* mice. Thus, 6-month-old *Col6a1*$^{-/-}$ mice were randomized into groups receiving i.p. treatment with pargyline (50 mg/kg/d), a MAO-A and MAO-B inhibitor, or vehicle for one week. After a week of pargyline the activity of MAO was completely abolish, to confirm the efficacy of the treatment. As expected, dystrophic muscles showed an increased production of ROS compared

to wild-type mice, and pargyline treatment prevent ROS accumulation (Fig. 29A and B).

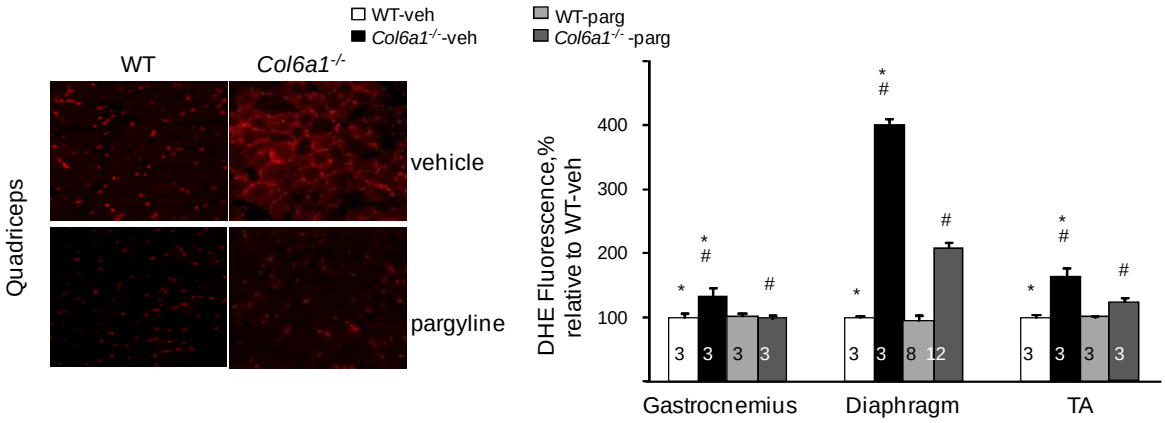

Figure 29. MAO inhibition reduces oxidative stress in *Col6a1*$^{-/-}$ mice.
(**A**) Oxidative stress assessed by DHE staining in sections of quadriceps from vehicle- or pargyline-treated wild-type and *Col6a1*$^{-/-}$ mice. Scale bar, 50 µm. (**B**) Quantification of DHE fluorescence in gastrocnemius, diaphragm and tibialis anterior (TA) muscle cryosections from wild-type and *Col6a1*$^{-/-}$ mice treated with vehicle or pargyline showing the reduced ROS accumulation after pargyline treatment. ROS accumulation increased in *Col6a1*$^{-/-}$ muscles compared to wild-type, and pargyline treatment prevent ROS formation in dystrophic mice. Parg, pargyline; veh, vehicle; WT, wild-type. *$P < 0.05$ *Col6a1*$^{-/-}$-veh versus WT-veh; $^{\#}P < 0.05$ *Col6a1*$^{-/-}$-veh versus *Col6a1*$^{-/-}$-parg. Error bars represent the s.e.m. The number of mice for each group is indicated inside each bar.

Moreover, diaphragm of *Col6a1*$^{-/-}$ mice, which is the most affected muscle in this murine model, displayed a significant increase Tm oxidation (Fig. 30A). DCB content was 3.2±0.4 fold higher in *Col6a1*$^{-/-}$ as compared to wild-type muscles and was significantly reduced by pargyline treatment (Fig. 30B). Mass spectrometric analysis performed on the high molecular mass Tm complexes identified the myosin heavy chain (Table 5). This finding indicates that, in the presence of oxidative stress, Tm form reversible complexes with myosin heavy chain and inhibition of MAO protects dystrophic skeletal muscle by reducing ROS production and protein oxidation.

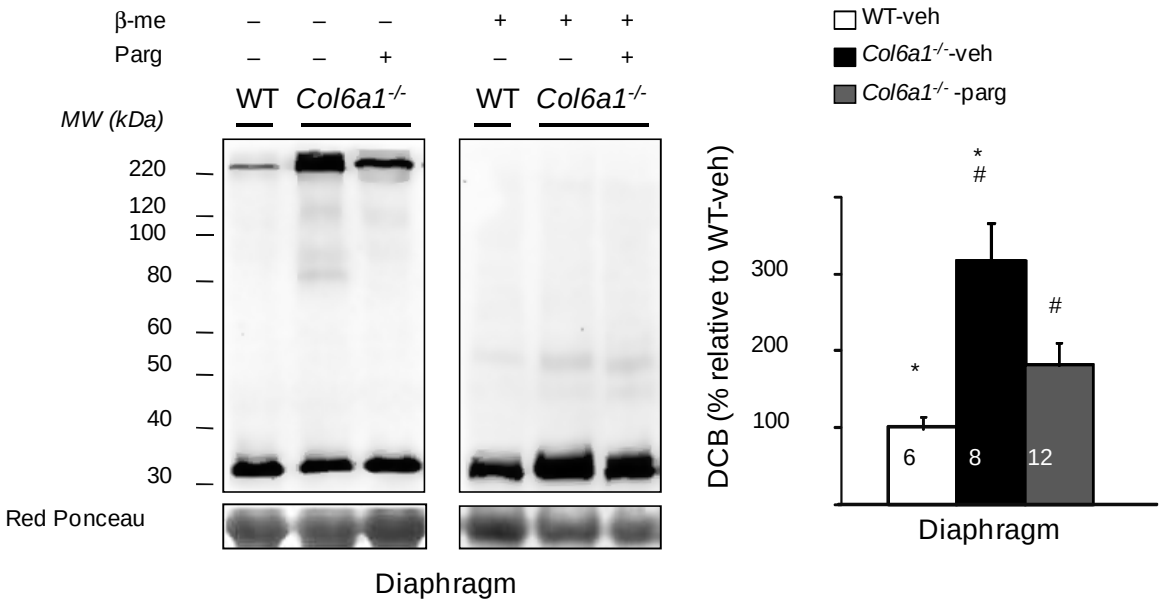

Figure 30. Pargyline treatment reduces Tm oxidation in *Col6a1*$^{-/-}$ mice.
(**A**) DCB formation in Tm detected by immunoelectrophoresis of myofibrillar samples from diaphragm, as detailed in Figure 26A. Immunoblotting analyses showed that the additional high-molecular-mass bands in *Col6a1*$^{-/-}$ muscles were significantly reduced by pargyline treatment (**B**) Quantitative analysis of DCB formation in Tm immunoblots. Parg, pargyline; veh, vehicle; WT, wild-type, β-mercaptoethanol (β-me). * P<0.05 *Col6a1*$^{-/-}$-veh versus WT-veh; # P<0.05 *Col6a1*$^{-/-}$-veh versus *Col6a1*$^{-/-}$-parg. Error bars represent s.e.m. The number of mice for each group is indicated inside each bar.

Morphometric analysis of myofiber cross-sectional areas in tibialis anterior (TA) and diaphragm showed that *Col6a1*$^{-/-}$ muscles contained myofibers of different sizes, with a prevalence of small fibers. This pathological sign was markedly reduced in pargyline-treated *Col6a1*$^{-/-}$ muscles, which showed more uniform fiber size, similarly to wild-type mice (Fig. 31A and B). Then, we investigated whether pargyline treatment was able to counteract the apoptotic phenotype observed in *Col6a1*$^{-/-}$ mice. The occurrence of apoptosis, as detected by TUNEL method, was markedly increased in *Col6a1*$^{-/-}$ mice as compared to wild-type littermates (62.4±2.3 versus 2.7±1.2 nuclei/mm^2), yet pargyline treatment led to a significantly lower incidence in the TUNEL-positive nuclei in dystrophic mice (6.9±1) (Fig.

31C).

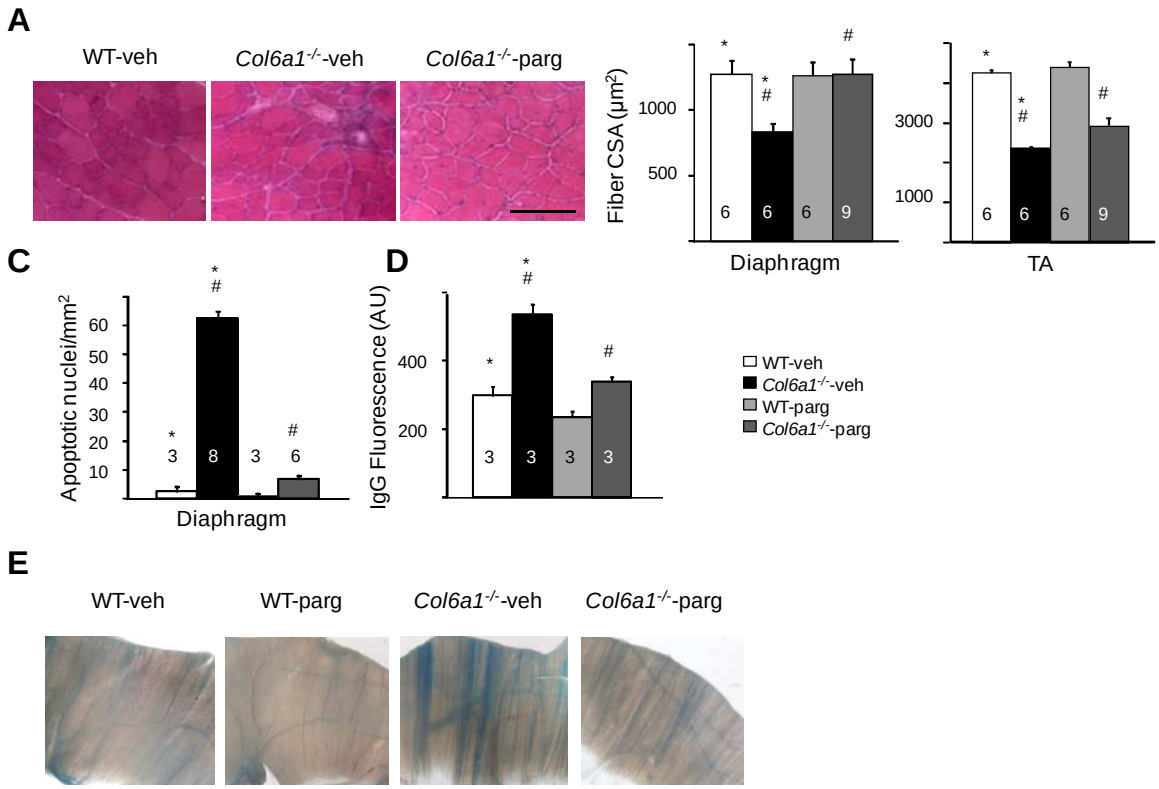

Figure 31. MAO inhibition rescues histological alterations and prevents muscle apoptosis in *Col6a1*$^{-/-}$ mice.
(**A**) Representative cross-sections of H&E-staining from tibialis anterior muscle from wild-type and *Col6a1*$^{-/-}$ mice treated with vehicle or pargyline. *Col6a1*$^{-/-}$ muscles showed a large variability in myofiber size while pargyline-treated *Col6a1*$^{-/-}$ mice displayed uniform myofiber size, similarly to wild-type muscles. Scale bar, 100 μm. (**B**) Analysis of fiber cross-sectional areas (CSA) in diaphragm and tibialis anterior (TA) muscle of pargyline- or vehicle-treated wild-type and *Col6a1*$^{-/-}$ mice. (**C**) Quantification of apoptotic nuclei by TUNEL assay in diaphragm sections. Pargyline treatment prevented the increased incidence of apoptosis in *Col6a1*$^{-/-}$ mice. (**D**) Quantification of the necrotic fibers by means of the immunohistochemical staining for IgG in diaphragm sections. IgG-positive fibers were present in *Col6a1*$^{-/-}$ mice and their number was decreased by pargyline treatment. (**E**) Representative images of diaphragms from wild-type and*Col6a1*$^{-/-}$ mice, following vital staining with Evans blue dye. Diaphragms were isolated from wild-type (n = 5) and *Col6a1*$^{-/-}$ (n = 5) mice treated with vehicle or pargyline and examined by light microscopy. Diaphragms from *Col6a1*$^{-/-}$ mice displayed a marked incidence of damaged fibers, identified by deep blue striations, which was reduced after pargyline treatment. Parg, pargyline; veh, vehicle; WT, wild-type. * P<0.05 *Col6a1*$^{-/-}$-veh versus WT-veh; # P<0.05 *Col6a1*$^{-/-}$-veh versus *Col6a1*$^{-/-}$-parg. Error bars represent s.e.m. The number of mice for each group is indicated inside each bar. The key in **D** applies to all panels.

Membrane permeability of skeletal muscle can also be directly visualized by immunohistochemical staining with IgG antibody. In fact, the circulating IgG can enter the fragile sarcolemma of dystrophic mice and can be detected by anti-mouse FITC-conjugated IgG (141,174). Whereas wild-type mice showed no IgG-

positive fibers in the diaphragm, *Col6a1*$^{-/-}$ mice displayed a high number of IgG-positive fibers that decreased upon pargyline treatment, indicating that the anti-MAO agent was able to stabilize the muscle fibers sarcolemma thus preventing IgG uptake (Fig. 31D). Additional evidence of muscle damage and protection by MAO inhibition was provided by vital staining with Evans blue. Supporting the finding obtained by permeability to IgG, several damaged myofibers stained by Evans blue were found in *Col6a1*$^{-/-}$ but not in wild-type diaphragm, and this alteration was largely reduced in the diaphragm of *Col6a1*$^{-/-}$ mice treated with pargyline (Fig. 31E).

Biochemical and histological analyses were paralleled by functional assessment of the contractile performance of muscles *in vivo* and isolated muscle fibers *in vitro* in collaboration with Prof. Reggiani's group (University of Padova). Single skinned muscle fibers dissected from gastrocnemius muscle were maximally calcium-activated at optimal sarcomere length. *Col6a1*$^{-/-}$ fibers developed lower isometric tension than wild-type fibers, as previously reported (128,175). The contractile impairment disappeared in the fibers of pargyline-treated *Col6a1*$^{-/-}$ mice (Fig. 32A). This *in vitro* evidence was further supported by *in vivo* findings, as pargyline treatment significantly increased the normalized force of gastrocnemius muscle of *Col6a1*$^{-/-}$ mice (Fig. 32B). We finally tested whether treatment with pargyline could improve the voluntary exercise performance of *Col6a1*$^{-/-}$ mice, tested by means of running-wheel. After acclimatizing mice for one week to a wheel placed in their cage, we measured the daily average distance. The pargyline-treated *Col6a1*$^{-/-}$ mice showed a significant improvement in the exercise performance compared to

untreated mice (Fig. 32C).

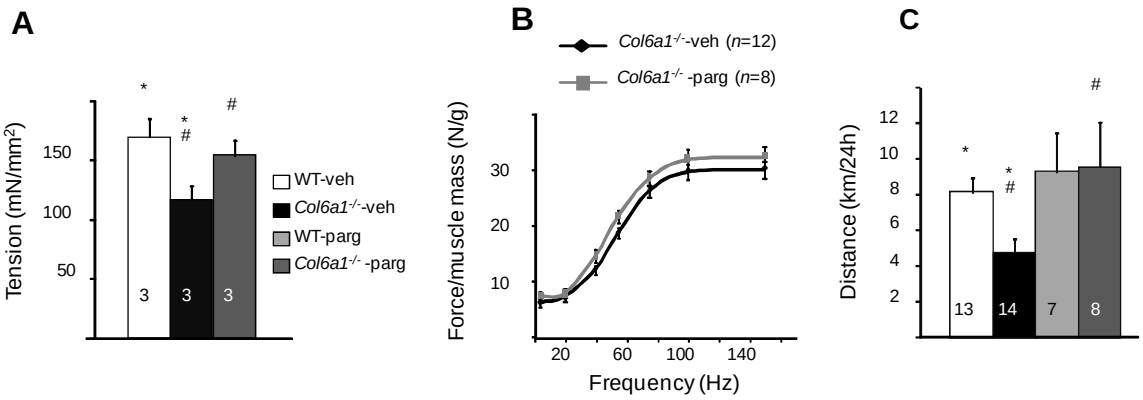

Figure 32. MAO inhibition ameliorates muscle alterations in *Col6a1*$^{-/-}$ mice.
(**A**) Tension development by single skinned fibers of gastrocnemius from vehicle-treated *Col6a1*$^{-/-}$, pargyline-treated *Col6a1*$^{-/-}$ and vehicle-treated wild-type mice. *Col6a1*$^{-/-}$ muscles developed lower isometric tension than wild-type fibers. The contractile impairment disappeared in the fibers of pargyline-treated *Col6a1*$^{-/-}$ mice. n = 22 or more fibers for each group. (**B**) Force-frequency curves of gastrocnemius muscle from vehicle-treated or pargyline-treated *Col6a1*$^{-/-}$ mice showed a significant increase of the normalized force of gastrocnemius muscle upon pargyline treatment. n = 13 or more muscles for each group. *P*=0.0016 by a two-way analysis of variance. (**C**) Locomotor performance measured on the running-wheel as the average distance covered in 24 h. Pargyline-treated *Col6a1*$^{-/-}$ mice showed a significant recovery of the exercise performance. Parg, pargyline; veh, vehicle; WT, wild-type. * *P*<0.05 *Col6a1*$^{-/-}$-veh versus WT-veh; # *P*<0.05 *Col6a1*$^{-/-}$-veh versus *Col6a1*$^{-/-}$-parg. Error bars represent s.e.m. The number of mice for each group is indicated inside each bar or between parentheses for panel **B**.

The present study demonstrates that MAO is a major source of ROS in two murine models of MDs and that its inhibition is able to reduce the occurrence of myofiber defects.

Mitochondria have recently received attention due to the demonstrated role of the permeability transition pore (PTP) in MDs (126,128). Indeed, PTP inhibition was found to limit histological alterations in *Col6a1*$^{-/-}$ (128) as well as *mdx* (126) mice and pilot studies have demonstrated the therapeutic efficacy of PTP inhibitors, namely cyclosporin A and Debio 025 (126,173,176-178). Furthermore, ablation of cyclophilin D, a mitochondrial protein that increases the open probability of the PTP, prevents biochemical and structural alterations observed in different MD models (126,127). However, at present it is difficult to link changes occurring at the level of plasma membrane or even outside the cell, such as loss of collagen VI,

with mitochondrial dysfunction related to processes occurring within the inner mitochondrial membrane, such as PTP opening. Such a link can be provided by oxidative stress. In fact, changes in the composition of extracellular matrix might be sensed by plasma membrane integrins that have been shown to convey intracellular signals resulting in increased ROS formation (179). Besides NADPH oxidase activation, mitochondria have been indicated as the main site for integrin-dependent ROS formation (180,181), although the signaling pathways and the mitochondrial sites have not been elucidated yet. Mitochondrial ROS generation, that according to our data is mostly catalyzed by MAO, is then linked to PTP through a vicious cycle whereby an increased ROS formation increases PTP open probability, and *vice versa* (182). Indeed, while providing further evidence of the pivotal involvement of oxidative stress in MDs, the present findings point to mitochondria as the major site, and MAO as the major source, of ROS formation. Previous studies demonstrated the efficacy of ROS scavenger in ameliorating the muscle pathophysiology of *mdx* mice (183,184). However, these drugs can only reduce the level of ROS that are already formed, pargyline instead acts by preventing ROS formation, thus making this class of inhibitors much more attractive.

In conclusion, this study provides evidence that the MAO-dependent ROS accumulation is responsible for both oxidative modifications of MPs and cell death. Inhibition of MAO protects dystrophic skeletal muscle by reducing ROS production and myofiber degeneration in MDs. The possibility of ameliorating the contractile dysfunction in MDs by using MAO inhibitors appears extremely interesting, since these compounds are already used in clinical settings for the treatment of various

neurological disorders (26). Therefore these findings provide a solid rationale for exploiting MAO inhibition as a novel therapeutic approach in MDs.

Table 5. List of the proteins identified in the band at high molecular mass by LC-MS/MS[a]

Acc. No.	MW (Da)	Protein name	No. of sequenced peptides (Sequence coverage)	Sequence of the tryptic peptides
Q32P18_MOUSE	224116	Myosin, heavy polypeptide 1, skeletal muscle, adult.- Mus musculus (Mouse)	30 (22%)	K.SSVFVVDAK.E R.ENQSILITGESGAGK.T K.MQGTLEDQIISANPLLEAFGNAK.T K.LASADIETYLLEK.S K.AAYLQNLNSADLLK.A K.GQTVQQVYNSVGALAK.A K.NKDPLNETVVGLYQK.S K.TLAYLFSGAAAAAEAESGGGGGK.K K.GSSFQTVSALFR.E K.AGLLGLLEEMR.D K.LAQLITR.T K.DIDDLELTLAK.V K.NLTEEMAGLDETIAK.L K.IEDEQALGMQLQK.K R.IEELEEEIEAER.A R.ELEEISERLEEAGGATSAQIEMNK.K K.HADSVAELGEQIDNLQR.V K.ANSEVAQWR.T R.LQNEVEDLMIDVER.T K.NLQQEISDLTEQIAEGGK.R K.SELQAALEEAEASLEHEEGK.I K.IAEKDEEIDQLKR.N R.VVESMQSTLDAEIR.S R.GQEDLKEQLAMVER.R

				R.ANLLQAEIEELR.A K.IAEQELLDASER.V R.VQLLHTQNTSLINTK.K K.KLETDISQIQGEMEDIVQEAR.N R.LDEAEQLALK.G R.QAEEAEEQSNVNLAK.F
Q5SX41_MOUSE	220513	Myosin, heavy polypeptide 2, skeletal muscle, adult.- Mus musculus (Mouse).	30 (21%)	R.ENQSILITGESGAGK.T R.VIQYFATIAVTGDK.K K.MQGTLEDQIISANPLLEAFGNAK.T K.LASADIETYLLEK.S K.NKDPLNETVVGLYQK.S K.GSSFQTVSALFR.E K.AGLLGLLEEMR.D K.LAQLITR.T K.DIDDLELTLAK.V K.NLTEEMAGLDETIAK.L K.IEDEQAIGIQLQK.K R.IEELEEEIEAER.A R.ELEEISERLEEAGGATSAQIEMNK.K R.LEEAGGATSAQIEMNK.K K.HADSVAELGEQIDNLQR.V K.MEIDDLASNVETVSK.A R.LINDLTTQR.G R.LQTESGEFSR.Q K.ANSEVAQWR.T R.LQNEVEDLMLDVER.T K.NAYEESLDQLETLK.R K.NLQQEISDLTEQIAEGGK.R K.IAEKDEEIDQLKR.N R.VVESMQSTLDAEIR.S R.GQEDLKEQLAMVER.R R.ANLLQAEIEELR.A K.IAEQELLDASER.V

	R.VQLLHTQNTSLINTK.K
	K.KLETDISQIQGEMEDIVQEAR.N
	R.LDEAEQLALK.G

[a] The proteins that were identified in band A are listed with their accession numbers and molecular weights. Protein identification was performed with the MASCOT software searching LC-MS/MS data against the sequences of Rodentia of the MSDB database. The fourth column shows the number of sequenced peptides and within parentheses the sequence coverage of the protein, whereas the fifth column contains a list of the peptides that were sequenced by MS/MS. Several tryptic peptides are identical for the two proteins since they are both myosin and they show a high sequence homology.

6. CONCLUSIONS

The results of this study provide novel evidence that mitochondrial dysfunction and contractile impairment are linked through the myofibrillar protein (MP) oxidation. Oxidative stress underlies many pathologies. At the cardiac level, the involvement of oxidative stress has been demonstrated to contribute to ischemia/reperfusion injury and hypertrophy development, progressively leading to congestive heart failure.

In this project we extended the previous finding obtained in models where the viability of many cells is compromised, such as cardiac ischemia, demonstrating a relationship between MP oxidation and contractile dysfunction in models devoid ischemia and with a minor contribution of cells death.

First, we found an elevated formation of ROS in a HF model obtained by LV pacing in rabbits that is abolished after vitamin treatment. Moreover, Tm oxidation increases in HF compared to sham operated rabbits, suggesting that MP oxidation is a causal link between ROS formation and contractile impairment. It has been investigated also the effect of p38 MAPK inhibition on MP oxidation. Our results indicate that the inhibition of p38 MAPK prevents ROS accumulation, Tm oxidation and the consequent contractile failure, without affecting apoptosis. Thus, p38 MAPK activation appears to be upstream rather than downstream of ROS, which impact on LV function through myofibrillar oxidation. In fact, vitamin treatment does not modify p38 MAPK phosphorylation, indicating that other signals contribute to p38 MAPK activation in failing hearts.

In the second part of this thesis, the contribution of MP oxidation to myocardial dysfunction was studied in clinical setting, analyzing biopsies of patients suffering of severe HF (NYHA, class IV). Our results indicate that protein carbonylation increases in human HF compared to nonfailing hearts. Two proteins, Tm and actin, are carbonylated in HF and both significantly correlate with contractile impairment detected by LVEF. Moreover, protein carbonylation correlates with myocardial cell injury, detected as TnI plasma release. This is the first demonstration that HF is related to oxidative changes of specific MPs in humans.

In addition, reversible modifications have been analyzed in human HF, especially at the level of Tm cysteine, but the correlation between Tm oxidation and contractile impairment is less remarkable compared to the correlation with protein carbonylation. This might be because our study analyzed samples collected at end-stage failure, whereas reversible modification is likely to occur at an earlier stage. In fact, during severe oxidative stress occur irreversible modification, such as carbonylation, while under milder stress, proteins can be oxidatively modified at the level of Cys residues. Then, we demonstrated that Tm is also a target of reactive nitrogen species. In particular, this is the first evidence of S-nitrosylation of Tm in human failing hearts. However, Tm nitrosylation did not correlate with cTnI and LVEF probably because nitrosylation might have a protective role during oxidative stress. In fact, Murphy an co-worker demonstrated that S-nitrosylation is a transient modification and could protect cysteine residues from irreversible oxidation. After damage, the S-nitrosylation can be remove and normal protein function can resume.

The results obtained in the last part of this study provide novel evidence regarding the sources of ROS at mitochondrial level in relation to MDs and confirm that MP

oxidation is an important target of oxidative stress also in skeletal muscle. It is widely accepted that mitochondrial respiratory chain can become a powerful generator of ROS, especially under conditions of increased oxidative stress. It is also becoming increasingly clear that other mitochondrial enzymes play an important role in this process. Here we have demonstrated that MAO is a major source of ROS and that its inhibition can prevents oxidative stress in two murine models of MD. Indeed, It is well known that in skeletal muscle disease, such as MDs, oxidative stress is increased. This increase in ROS production requires the intervention of MAO, as its pharmacological inhibition was able to reduce or completely prevent the oxidative stress in both the MD models. Moreover, the decreased MAO-dependent ROS accumulation ameliorates the dystrophic phenotype, reducing apoptosis, degeneration/regeneration cycling of the fibres, inflammation and normalizing the fibre area distribution and the contractile performance in both the dystrophic models. Interestingly, MAO inhibition prevent Tm oxidation, demonstrating that also in MDs Tm oxidation is a link between ROS production and contractile impairment.

The role of MAO could be interpreted as a trigger necessary to amplify the initial oxidative stimuli and therefore contribute to the instauration of oxidative stress and cellular dysfunction. The results obtained in this study support this hypothesis and reveal that MAO is involved in these processes. Indeed, while providing further evidence of the pivotal involvement of oxidative stress in MDs, the present findings point to mitochondria as the major site, and MAO as the major source, of ROS formation. Recent studies demonstrated that ROS scavenger protects muscle injury in dystrophic mice. However, these drugs can only reduce the level of ROS that are already formed. MAO inhibition instead acts by preventing ROS formation,

thus making this class of inhibitors much more attractive. The possibility of ameliorating the contractile dysfunction and the evolution of dystrophic pathologies by using MAO inhibitors appears appealing. It is worth pointing out that these drugs are already widely used in clinical settings for the treatment of various neurological disorders. Therefore, these findings suggest that MAO inhibition may represent a new therapeutic tool for the treatment of MDs.

In conclusion, the evidence provided in the present work demonstrates the key role of mitochondrial dysfunction in muscle injury. ROS produced in mitochondria alter MPs causing contractile dysfunction in cardiac and skeletal muscle. These results demonstrated that MP oxidation is an important target of ROS. In addition, this study provides evidence that the MAO-dependent ROS accumulation is responsible for both oxidative modifications of MPs and cell death. Inhibition of MAO protects dystrophic skeletal muscle by reducing ROS production and myofiber degeneration. These results demontrate the pivotal role of mitochondria and suggesting a therapeutic potential for MAO inhibition.

7. REFERENCE LIST

1. Stadtman,E.R., Levine,R.L. (2000) Protein oxidation. *Ann. N. Y. Acad. Sci.*, **899**, 191-208.

2. Finkel,T., Holbrook,N.J. (2000) Oxidants, oxidative stress and the biology of ageing. *Nature*, **408**, 239-247.

3. Droge,W. (2002) Free radicals in the physiological control of cell function. *Physiol Rev.*, **82**, 47-95.

4. Davies,M.J. (2003) Singlet oxygen-mediated damage to proteins and its consequences. *Biochem. Biophys. Res. Commun.*, **305**, 761-770.

5. Aikens,J., Dix,T.A. (1991) Perhydroxyl radical (HOO.) initiated lipid peroxidation. The role of fatty acid hydroperoxides. *J. Biol. Chem.*, **266**, 15091-15098.

6. Liochev,S.I., Fridovich,I. (1999) The relative importance of HO* and. *Free Radic. Biol. Med.*, **26**, 777-778.

7. Beckman,J.S., Beckman,T.W., Chen,J., Marshall,P.A., Freeman,B.A. (1990) Apparent hydroxyl radical production by peroxynitrite: implications for endothelial injury from nitric oxide and superoxide. *Proc. Natl. Acad. Sci. U. S. A*, **87**, 1620-1624.

8. Greenacre,S.A., Ischiropoulos,H. (2001) Tyrosine nitration: localisation, quantification, consequences for protein function and signal transduction. *Free Radic. Res.*, **34**, 541-581.

9. Stadtman,E.R., Berlett,B.S. (1991) Fenton chemistry. Amino acid oxidation. *J. Biol. Chem.*, **266**, 17201-17211.

10. Requena,J.R., Chao,C.C., Levine,R.L., Stadtman,E.R. (2001) Glutamic and aminoadipic semialdehydes are the main carbonyl products of metal-catalyzed oxidation of proteins. *Proc. Natl. Acad. Sci. U. S. A*, **98**, 69-74.

11. Balaban,R.S., Nemoto,S., Finkel,T. (2005) Mitochondria, oxidants, and aging. *Cell*, **120**, 483-495.

12. Murphy,M.P. (2009) How mitochondria produce reactive oxygen species. *Biochem. J.*, **417**, 1-13.

13. Turrens,J.F. (2003) Mitochondrial formation of reactive oxygen species. *J. Physiol*, **552**, 335-344.

14. Di Lisa,F., Kaludercic,N., Carpi,A., Menabo,R., Giorgio,M. (2009) Mitochondrial pathways for ROS formation and myocardial injury: the relevance of p66(Shc) and monoamine oxidase. *Basic Res. Cardiol.*, **104**, 131-139.

15. Ago,T., Matsushima,S., Kuroda,J., Zablocki,D., Kitazono,T., Sadoshima,J. (2010) The NADPH oxidase nox4 and aging in the heart. *Aging (Albany. NY)*, **2**, 1012-1016.

16. Cadenas,E., Davies,K.J. (2000) Mitochondrial free radical generation, oxidative stress, and aging. *Free Radic. Biol. Med.*, **29**, 222-230.

17. Votyakova,T.V., Reynolds,I.J. (2001) DeltaPsi(m)-Dependent and -independent production of reactive oxygen species by rat brain mitochondria. *J. Neurochem.*, **79**, 266-277.

18. Boveris,A., Chance,B. (1973) The mitochondrial generation of hydrogen peroxide. General properties and effect of hyperbaric oxygen. *Biochem. J.*, **134**, 707-716.

19. Pelicci,G., Lanfrancone,L., Grignani,F., McGlade,J., Cavallo,F., Forni,G., Nicoletti,I., Grignani,F., Pawson,T., Pelicci,P.G. (1992) A novel transforming protein (SHC) with an SH2 domain is implicated in mitogenic signal transduction. *Cell*, **70**, 93-104.

20. Migliaccio,E., Giorgio,M., Mele,S., Pelicci,G., Reboldi,P., Pandolfi,P.P., Lanfrancone,L., Pelicci,P.G. (1999) The p66shc adaptor protein controls oxidative stress response and life span in mammals. *Nature*, **402**, 309-313.

21. Giorgio,M., Migliaccio,E., Orsini,F., Paolucci,D., Moroni,M., Contursi,C., Pelliccia,G., Luzi,L., Minucci,S., Marcaccio,M.*, et al.* (2005) Electron transfer between cytochrome c and p66Shc generates reactive oxygen species that trigger mitochondrial apoptosis. *Cell*, **122**, 221-233.

22. Pinton,P., Rimessi,A., Marchi,S., Orsini,F., Migliaccio,E., Giorgio,M., Contursi,C., Minucci,S., Mantovani,F., Wieckowski,M.R.*, et al.* (2007) Protein kinase C beta and prolyl isomerase 1 regulate mitochondrial effects of the life-span determinant p66Shc. *Science*, **315**, 659-663.

23. Orsini,F., Migliaccio,E., Moroni,M., Contursi,C., Raker,V.A., Piccini,D., Martin-Padura,I., Pelliccia,G., Trinei,M., Bono,M.*, et al.* (2004) The life span determinant p66Shc localizes to mitochondria where it associates with mitochondrial heat shock protein 70 and regulates trans-membrane potential. *J. Biol. Chem.*, **279**, 25689-25695.

24. Trinei,M., Giorgio,M., Cicalese,A., Barozzi,S., Ventura,A., Migliaccio,E., Milia,E., Padura,I.M., Raker,V.A., Maccarana,M.*, et al.* (2002) A p53-p66Shc signalling pathway controls intracellular redox status, levels of oxidation-damaged DNA and oxidative stress-induced apoptosis. *Oncogene*, **21**, 3872-3878.

25. Edmondson,D.E., Mattevi,A., Binda,C., Li,M., Hubalek,F. (2004) Structure and mechanism of monoamine oxidase. *Curr. Med. Chem.*, **11**, 1983-1993.

26. Youdim,M.B., Edmondson,D., Tipton,K.F. (2006) The therapeutic potential of monoamine oxidase inhibitors. *Nat. Rev. Neurosci.*, **7**, 295-309.

27. Bach,A.W., Lan,N.C., Johnson,D.L., Abell,C.W., Bembenek,M.E., Kwan,S.W., Seeburg,P.H., Shih,J.C. (1988) cDNA cloning of human liver monoamine oxidase A and B: molecular basis of differences in enzymatic properties. *Proc. Natl. Acad. Sci. U. S. A*, **85**, 4934-4938.

28. Chen,Z.Y., Hotamisligil,G.S., Huang,J.K., Wen,L., Ezzeddine,D., ydin-Muderrisoglu,N., Powell,J.F., Huang,R.H., Breakefield,X.O., Craig,I., . (1991) Structure of the human gene for monoamine oxidase type A. *Nucleic Acids Res.*, **19**, 4537-4541.

29. Edmondson,D.E., Binda,C., Mattevi,A. (2004) The FAD binding sites of human monoamine oxidases A and B. *Neurotoxicology*, **25**, 63-72.

30. Abell,C.W., Kwan,S.W. (2001) Molecular characterization of monoamine oxidases A and B. *Prog. Nucleic Acid Res. Mol. Biol.*, **65**, 129-156.

31. Binda,C., Newton-Vinson,P., Hubalek,F., Edmondson,D.E., Mattevi,A. (2002) Structure of human monoamine oxidase B, a drug target for the treatment of neurological disorders. *Nat. Struct. Biol.*, **9**, 22-26.

32. De Colibus,L., Li,M., Binda,C., Lustig,A., Edmondson,D.E., Mattevi,A. (2005) Three-dimensional structure of human monoamine oxidase A (MAO A): relation to the structures of rat MAO A and human MAO B. *Proc. Natl. Acad. Sci. U. S. A*, **102**, 12684-12689.

33. Binda,C., Li,M., Hubalek,F., Restelli,N., Edmondson,D.E., Mattevi,A. (2003) Insights into the mode of inhibition of human mitochondrial monoamine oxidase B from high-resolution crystal structures. *Proc. Natl. Acad. Sci. U. S. A*, **100**, 9750-9755.

34. Kearney,E.B., Salach,J.I., Walker,W.H., Seng,R.L., Kenney,W., Zeszotek,E., Singer,T.P. (1971) The covalently-bound flavin of hepatic monoamine oxidase. 1. Isolation and sequence of a flavin peptide and evidence for binding at the 8alpha position. *Eur. J. Biochem.*, **24**, 321-327.

35. Tipton,K.F., Boyce,S., O'Sullivan,J., Davey,G.P., Healy,J. (2004) Monoamine oxidases: certainties and uncertainties. *Curr. Med. Chem.*, **11**, 1965-1982.

36. Berry,M.D., Juorio,A.V., Paterson,I.A. (1994) The functional role of monoamine oxidases A and B in the mammalian central nervous system. *Prog. Neurobiol.*, **42**, 375-391.

37. Kitahama,K., Maeda,T., Denney,R.M., Jouvet,M. (1994) Monoamine oxidase: distribution in the cat brain studied by enzyme- and immunohistochemistry: recent progress. *Prog. Neurobiol.*, **42**, 53-78.

38. Luque,J.M., Biou,V., Nicholls,J.G. (1998) Three-dimensional visualization of the distribution, growth, and regeneration of monoaminergic neurons in whole mounts of immature mammalian CNS. *J. Comp Neurol.*, **390**, 427-438.

39. Arai,R., Kimura,H., Nagatsu,I., Maeda,T. (1997) Preferential localization of monoamine oxidase type A activity in neurons of the locus coeruleus and type B activity in neurons of the dorsal raphe nucleus of the rat: a detailed enzyme histochemical study. *Brain Res.*, **745**, 352-356.

40. Levitt,P., Pintar,J.E., Breakefield,X.O. (1982) Immunocytochemical demonstration of monoamine oxidase B in brain astrocytes and serotonergic neurons. *Proc. Natl. Acad. Sci. U. S. A*, **79**, 6385-6389.

41. Westlund,K.N., Denney,R.M., Kochersperger,L.M., Rose,R.M., Abell,C.W. (1985) Distinct monoamine oxidase A and B populations in primate brain. *Science*, **230**, 181-183.

42. Westlund,K.N., Denney,R.M., Rose,R.M., Abell,C.W. (1988) Localization of distinct monoamine oxidase A and monoamine oxidase B cell populations in human brainstem. *Neuroscience*, **25**, 439-456.

43. Sivasubramaniam,S.D., Finch,C.C., Rodriguez,M.J., Mahy,N., Billett,E.E. (2003) A comparative study of the expression of monoamine oxidase-A and -B mRNA and protein in non-CNS human tissues. *Cell Tissue Res.*, **313**, 291-300.

44. Saura,J., Kettler,R., Da,P.M., Richards,J.G. (1992) Quantitative enzyme radioautography with 3H-Ro 41-1049 and 3H-Ro 19-6327 in vitro: localization and abundance of MAO-A and MAO-B in rat CNS, peripheral organs, and human brain. *J. Neurosci.*, **12**, 1977-1999.

45. Fowler,J.S., Logan,J., Wang,G.J., Franceschi,D., Volkow,N.D., Telang,F., Pappas,N., Ferrieri,R., Shea,C., Garza,V.*, et al.* (2003) Monoamine oxidase A imaging in peripheral organs in healthy human subjects. *Synapse*, **49**, 178-187.

46. Shih,J.C., Chen,K. (2004) Regulation of MAO-A and MAO-B gene expression. *Curr. Med. Chem.*, **11**, 1995-2005.

47. Edelstein,S.B., Breakefield,X.O. (1986) Monoamine oxidases A and B are differentially regulated by glucocorticoids and "aging" in human skin fibroblasts. *Cell Mol. Neurobiol.*, **6**, 121-150.

48. Youdim,M.B., Banerjee,D.K., Kelner,K., Offutt,L., Pollard,H.B. (1989) Steroid regulation of monoamine oxidase activity in the adrenal medulla. *FASEB J.*, **3**, 1753-1759.

49. Zhu,Q.S., Grimsby,J., Chen,K., Shih,J.C. (1992) Promoter organization and activity of human monoamine oxidase (MAO) A and B genes. *J. Neurosci.*, **12**, 4437-4446.

50. Zhu,Q.S., Chen,K., Shih,J.C. (1994) Bidirectional promoter of human monoamine oxidase A (MAO A) controlled by transcription factor Sp1. *J. Neurosci.*, **14**, 7393-7403.

51. Lenders,J.W., Eisenhofer,G., Abeling,N.G., Berger,W., Murphy,D.L., Konings,C.H., Wagemakers,L.M., Kopin,I.J., Karoum,F., van Gennip,A.H., Brunner,H.G. (1996) Specific genetic deficiencies of the A and B isoenzymes of monoamine oxidase are characterized by distinct neurochemical and clinical phenotypes. *J. Clin. Invest*, **97**, 1010-1019.

52. Brunner,H.G., Nelen,M., Breakefield,X.O., Ropers,H.H., van Oost,B.A. (1993) Abnormal behavior associated with a point mutation in the structural gene for monoamine oxidase A. *Science*, **262**, 578-580.

53. Shih,J.C. (2004) Cloning, after cloning, knock-out mice, and physiological functions of MAO A and B. *Neurotoxicology*, **25**, 21-30.

54. Bianchi,P., Kunduzova,O., Masini,E., Cambon,C., Bani,D., Raimondi,L., Seguelas,M.H., Nistri,S., Colucci,W., Leducq,N., Parini,A. (2005) Oxidative stress by monoamine oxidase mediates receptor-independent cardiomyocyte apoptosis by serotonin and postischemic myocardial injury. *Circulation*, **112**, 3297-3305.

55. Kaludercic,N., Takimoto,E., Nagayama,T., Feng,N., Lai,E.W., Bedja,D., Chen,K., Gabrielson,K.L., Blakely,R.D., Shih,J.C.*, et al.* (2010) Monoamine oxidase A-mediated enhanced catabolism of norepinephrine contributes to adverse remodeling and pump failure in hearts with pressure overload. *Circ. Res.*, **106**, 193-202.

56. Maurel,A., Hernandez,C., Kunduzova,O., Bompart,G., Cambon,C., Parini,A., Frances,B. (2003) Age-dependent increase in hydrogen peroxide production by cardiac monoamine oxidase A in rats. *Am. J. Physiol Heart Circ. Physiol*, **284**, H1460-H1467.

57. Kuroda,J., Ago,T., Matsushima,S., Zhai,P., Schneider,M.D., Sadoshima,J. (2010) NADPH oxidase 4 (Nox4) is a major source of oxidative stress in the failing heart. *Proc. Natl. Acad. Sci. U. S. A*, **107**, 15565-15570.

58. Nordberg,J., Arner,E.S. (2001) Reactive oxygen species, antioxidants, and the mammalian thioredoxin system. *Free Radic. Biol. Med.*, **31**, 1287-1312.

59. Okado-Matsumoto,A., Fridovich,I. (2001) Subcellular distribution of superoxide dismutases (SOD) in rat liver: Cu,Zn-SOD in mitochondria. *J. Biol. Chem.*, **276**, 38388-38393.

60. Fridovich,I. (1995) Superoxide radical and superoxide dismutases. *Annu. Rev. Biochem.*, **64**, 97-112.

61. Ursini,F., Maiorino,M., Brigelius-Flohe,R., Aumann,K.D., Roveri,A., Schomburg,D., Flohe,L. (1995) Diversity of glutathione peroxidases. *Methods Enzymol.*, **252**, 38-53.

62. Urso,M.L., Clarkson,P.M. (2003) Oxidative stress, exercise, and antioxidant supplementation. *Toxicology*, **189**, 41-54.

63. Traber,M.G., Atkinson,J. (2007) Vitamin E, antioxidant and nothing more. *Free Radic. Biol. Med.*, **43**, 4-15.

64. Meister,A. (1994) Glutathione-ascorbic acid antioxidant system in animals. *J. Biol. Chem.*, **269**, 9397-9400.

65. MacLean,P.D., Drake,E.C., Ross,L., Barclay,C. (2007) Bilirubin as an antioxidant in micelles and lipid bilayers: its contribution to the total antioxidant capacity of human blood plasma. *Free Radic. Biol. Med.*, **43**, 600-609.

66. Waring,W.S. (2002) Uric acid: an important antioxidant in acute ischaemic stroke. *QJM.*, **95**, 691-693.

67. Heusch,G., Schulz,R. (2011) A radical view on the contractile machinery in human heart failure. *J Am. Coll. Cardiol.*, **57**, 310-312.

68. Marnett,L.J. (2000) Oxyradicals and DNA damage. *Carcinogenesis*, **21**, 361-370.

69. Pacifici,R.E., Davies,K.J. (1991) Protein, lipid and DNA repair systems in oxidative stress: the free-radical theory of aging revisited. *Gerontology*, **37**, 166-180.

70. Sitte,N., Huber,M., Grune,T., Ladhoff,A., Doecke,W.D., Von,Z.T., Davies,K.J. (2000) Proteasome inhibition by lipofuscin/ceroid during postmitotic aging of fibroblasts. *FASEB J.*, **14**, 1490-1498.

71. Halliwell,B. (1993) The role of oxygen radicals in human disease, with particular reference to the vascular system. *Haemostasis*, **23 Suppl 1**, 118-126.

72. Marian,A.J. (2008) Genetic determinants of cardiac hypertrophy. *Curr. Opin. Cardiol.*, **23**, 199-205.

73. Barreiro,E., Hussain,S.N. (2010) Protein carbonylation in skeletal muscles: impact on function. *Antioxid. Redox. Signal.*, **12**, 417-429.

74. Prochniewicz,E., Lowe,D.A., Spakowicz,D.J., Higgins,L., O'Conor,K., Thompson,L.V., Ferrington,D.A., Thomas,D.D. (2008) Functional, structural, and chemical changes in myosin associated with hydrogen peroxide treatment of skeletal muscle fibers. *Am. J. Physiol Cell Physiol*, **294**, C613-C626.

75. Canton,M., Neverova,I., Menabò,R., Van Eyk,J.E., Di Lisa,F. (2004) Evidence of myofibrillar protein oxidation induced by postischemic reperfusion in isolated rat hearts. *Am. J. Physiol Heart Circ. Physiol*, **286**, H870-H877.

76. Canton,M., Skyschally,A., Menabo,R., Boengler,K., Gres,P., Schulz,R., Haude,M., Erbel,R., Di Lisa,F., Heusch,G. (2006) Oxidative modification of tropomyosin and myocardial dysfunction following coronary microembolization. *Eur. Heart J.*, **27**, 875-881.

77. Lehman,W., Craig,R. (2008) Tropomyosin and the steric mechanism of muscle regulation. *Adv. Exp. Med. Biol.*, **644**, 95-109.

78. Muthuchamy,M., Pajak,L., Howles,P., Doetschman,T., Wieczorek,D.F. (1993) Developmental analysis of tropomyosin gene expression in embryonic stem cells and mouse embryos. *Mol. Cell Biol.*, **13**, 3311-3323.

79. Jagatheesan,G., Rajan,S., Wieczorek,D.F. (2010) Investigations into tropomyosin function using mouse models. *J. Mol. Cell Cardiol.*, **48**, 893-898.

80. Brown,J.H., Kim,K.H., Jun,G., Greenfield,N.J., Dominguez,R., Volkmann,N., Hitchcock-DeGregori,S.E., Cohen,C. (2001) Deciphering the design of the tropomyosin molecule. *Proc. Natl. Acad. Sci. U. S. A*, **98**, 8496-8501.

81. Zot,A.S., Potter,J.D. (1987) Structural aspects of troponin-tropomyosin regulation of skeletal muscle contraction. *Annu. Rev. Biophys. Biophys. Chem.*, **16**, 535-559.

82. Muthuchamy,M., Pieples,K., Rethinasamy,P., Hoit,B., Grupp,I.L., Boivin,G.P., Wolska,B., Evans,C., Solaro,R.J., Wieczorek,D.F. (1999) Mouse model of a familial hypertrophic cardiomyopathy mutation in alpha-tropomyosin manifests cardiac dysfunction. *Circ. Res.*, **85**, 47-56.

83. Hook,J., Lemckert,F., Qin,H., Schevzov,G., Gunning,P. (2004) Gamma tropomyosin gene products are required for embryonic development. *Mol. Cell Biol.*, **24**, 2318-2323.

84. Wieczorek,D.F., Jagatheesan,G., Rajan,S. (2008) The role of tropomyosin in heart disease. *Adv. Exp. Med. Biol.*, **644**, 132-142.

85. Beckman,K.B., Ames,B.N. (1998) Mitochondrial aging: open questions. *Ann. N. Y. Acad. Sci.*, **854**, 118-127.

86. Weinreb,O., Bar-Am,O., Amit,T., Chillag-Talmor,O., Youdim,M.B. (2004) Neuroprotection via pro-survival protein kinase C isoforms associated with Bcl-2 family members. *FASEB J.*, **18**, 1471-1473.

87. Menazza,S., Blaauw,B., Tiepolo,T., Toniolo,L., Braghetta,P., Spolaore,B., Reggiani,C., Di Lisa,F., Bonaldo,P., Canton,M. (2010) Oxidative stress by monoamine oxidases is causally involved in myofiber damage in muscular dystrophy. *Hum. Mol. Genet.*.

88. Canton,M., Menazza,S., Sheeran,F.L., Polverino de L.,P., Di Lisa,F., Pepe,S. (2011) Oxidation of myofibrillar proteins in human heart failure. *J. Am. Coll. Cardiol.*, **57**, 300-309.

89. Schroder,E., Eaton,P. (2008) Hydrogen peroxide as an endogenous mediator and exogenous tool in cardiovascular research: issues and considerations. *Curr. Opin. Pharmacol.*, **8**, 153-159.

90. Mann,D.L., Spinale,F.G. (1998) Activation of matrix metalloproteinases in the failing human heart: breaking the tie that binds. *Circulation*, **98**, 1699-1702.

91. Nakamura,K., Fushimi,K., Kouchi,H., Mihara,K., Miyazaki,M., Ohe,T., Namba,M. (1998) Inhibitory effects of antioxidants on neonatal rat cardiac myocyte hypertrophy induced by tumor necrosis factor-alpha and angiotensin II. *Circulation*, **98**, 794-799.

92. Luo,J.D., Xie,F., Zhang,W.W., Ma,X.D., Guan,J.X., Chen,X. (2001) Simvastatin inhibits noradrenaline-induced hypertrophy of cultured neonatal rat cardiomyocytes. *Br. J. Pharmacol.*, **132**, 159-164.

93. Wang,L., Lopaschuk,G.D., Clanachan,A.S. (2008) H(2)O(2)-induced left ventricular dysfunction in isolated working rat hearts is independent of calcium accumulation. *J. Mol. Cell Cardiol.*, **45**, 787-795.

94. Qin,F., Shite,J., Liang,C.S. (2003) Antioxidants attenuate myocyte apoptosis and improve cardiac function in CHF: association with changes in MAPK pathways. *Am. J. Physiol Heart Circ. Physiol*, **285**, H822-H832.

95. Hool,L.C. (2006) Reactive oxygen species in cardiac signalling: from mitochondria to plasma membrane ion channels. *Clin. Exp. Pharmacol. Physiol*, **33**, 146-151.

96. Li,J.M., Gall,N.P., Grieve,D.J., Chen,M., Shah,A.M. (2002) Activation of NADPH oxidase during progression of cardiac hypertrophy to failure. *Hypertension*, **40**, 477-484.

97. Michel,M.C., Li,Y., Heusch,G. (2001) Mitogen-activated protein kinases in the heart. *Naunyn Schmiedebergs Arch. Pharmacol.*, **363**, 245-266.

98. Avner,B.S., Hinken,A.C., Yuan,C., Solaro,R.J. (2010) H2O2 alters rat cardiac sarcomere function and protein phosphorylation through redox signaling. *Am. J. Physiol Heart Circ. Physiol*, **299**, H723-H730.

99. Little,W.C. (2008) Hypertension, heart failure, and ejection fraction. *Circulation*, **118**, 2223-2224.

100. Carabello,B.A. (2006) Aortic stenosis: from pressure overload to heart failure. *Heart Fail. Clin.*, **2**, 435-442.

101. Maekawa,Y., Ouzounian,M., Opavsky,M.A., Liu,P.P. (2007) Connecting the missing link between dilated cardiomyopathy and viral myocarditis: virus, cytoskeleton, and innate immunity. *Circulation*, **115**, 5-8.

102. Nerheim,P., Birger-Botkin,S., Piracha,L., Olshansky,B. (2004) Heart failure and sudden death in patients with tachycardia-induced cardiomyopathy and recurrent tachycardia. *Circulation*, **110**, 247-252.

103. Lehnart,S.E., Maier,L.S., Hasenfuss,G. (2009) Abnormalities of calcium metabolism and myocardial contractility depression in the failing heart. *Heart Fail. Rev.*, **14**, 213-224.

104. Neumann,T., Ravens,U., Heusch,G. (1998) Characterization of excitation-contraction coupling in conscious dogs with pacing-induced heart failure. *Cardiovasc. Res.*, **37**, 456-466.

105. de Tombe,P.P., Solaro,R.J. (2000) Integration of cardiac myofilament activity and regulation with pathways signaling hypertrophy and failure. *Ann. Biomed. Eng*, **28**, 991-1001.

106. Heusch,G., Neumann,T. (1998) Calcium responsiveness in canine pacing-induced heart failure. *J. Mol. Cell Cardiol.*, **30**, 1605-1613.

107. LeWinter,M.M. (2005) Functional consequences of sarcomeric protein abnormalities in failing myocardium. *Heart Fail. Rev.*, **10**, 249-257.

108. Giordano,F.J. (2005) Oxygen, oxidative stress, hypoxia, and heart failure. *J. Clin. Invest*, **115**, 500-508.

109. Qin,F., Liang,M.C., Liang,C.S. (2005) Progressive left ventricular remodeling, myocyte apoptosis, and protein signaling cascades after myocardial infarction in rabbits. *Biochim. Biophys. Acta*, **1740**, 499-513.

110. Wang,Y. (2007) Mitogen-activated protein kinases in heart development and diseases. *Circulation*, **116**, 1413-1423.

111. Tenhunen,O., Rysa,J., Ilves,M., Soini,Y., Ruskoaho,H., Leskinen,H. (2006) Identification of cell cycle regulatory and inflammatory genes as predominant targets of p38 mitogen-activated protein kinase in the heart. *Circ. Res.*, **99**, 485-493.

112. Baines,C.P., Molkentin,J.D. (2005) STRESS signaling pathways that modulate cardiac myocyte apoptosis. *J. Mol. Cell Cardiol.*, **38**, 47-62.

113. Kerkela,R., Force,T. (2006) p38 mitogen-activated protein kinase: a future target for heart failure therapy? *J. Am. Coll. Cardiol.*, **48**, 556-558.

114. Wang,M., Tsai,B.M., Turrentine,M.W., Mahomed,Y., Brown,J.W., Meldrum,D.R. (2005) p38 mitogen activated protein kinase mediates both death signaling and functional depression in the heart. *Ann. Thorac. Surg.*, **80**, 2235-2241.

115. Liu,Y.H., Wang,D., Rhaleb,N.E., Yang,X.P., Xu,J., Sankey,S.S., Rudolph,A.E., Carretero,O.A. (2005) Inhibition of p38 mitogen-activated protein kinase protects the heart against cardiac remodeling in mice with heart failure resulting from myocardial infarction. *J. Card Fail.*, **11**, 74-81.

116. Ren,J., Zhang,S., Kovacs,A., Wang,Y., Muslin,A.J. (2005) Role of p38alpha MAPK in cardiac apoptosis and remodeling after myocardial infarction. *J. Mol. Cell Cardiol.*, **38**, 617-623.

117. Haq,S., Choukroun,G., Lim,H., Tymitz,K.M., del,M.F., Gwathmey,J., Grazette,L., Michael,A., Hajjar,R., Force,T., Molkentin,J.D. (2001) Differential activation of signal transduction pathways in human hearts with hypertrophy versus advanced heart failure. *Circulation*, **103**, 670-677.

118. Butter,C., Rastogi,S., Minden,H.H., Meyhofer,J., Burkhoff,D., Sabbah,H.N. (2008) Cardiac contractility modulation electrical signals improve myocardial gene expression in patients with heart failure. *J. Am. Coll. Cardiol.*, **51**, 1784-1789.

119. Liao,P., Wang,S.Q., Wang,S., Zheng,M., Zheng,M., Zhang,S.J., Cheng,H., Wang,Y., Xiao,R.P. (2002) p38 Mitogen-activated protein kinase mediates a negative inotropic effect in cardiac myocytes. *Circ. Res.*, **90**, 190-196.

120. Braz,J.C., Bueno,O.F., Liang,Q., Wilkins,B.J., Dai,Y.S., Parsons,S., Braunwart,J., Glascock,B.J., Klevitsky,R., Kimball,T.F.*, et al.* (2003) Targeted inhibition of p38 MAPK promotes hypertrophic cardiomyopathy through upregulation of calcineurin-NFAT signaling. *J. Clin. Invest*, **111**, 1475-1486.

121. Schulz,R., Gres,P., Skyschally,A., Duschin,A., Belosjorow,S., Konietzka,I., Heusch,G. (2003) Ischemic preconditioning preserves connexin 43 phosphorylation during sustained ischemia in pig hearts in vivo. *FASEB J.*, **17**, 1355-1357.

122. Schulz,R., Belosjorow,S., Gres,P., Jansen,J., Michel,M.C., Heusch,G. (2002) p38 MAP kinase is a mediator of ischemic preconditioning in pigs. *Cardiovasc. Res.*, **55**, 690-700.

123. Clark,J.E., Sarafraz,N., Marber,M.S. (2007) Potential of p38-MAPK inhibitors in the treatment of ischaemic heart disease. *Pharmacol. Ther.*, **116**, 192-206.

124. Rando,T.A. (2002) Oxidative stress and the pathogenesis of muscular dystrophies. *Am. J. Phys. Med. Rehabil.*, **81**, S175-S186.

125. Disatnik,M.H., Dhawan,J., Yu,Y., Beal,M.F., Whirl,M.M., Franco,A.A., Rando,T.A. (1998) Evidence of oxidative stress in mdx mouse muscle: studies of the pre-necrotic state. *J. Neurol. Sci.*, **161**, 77-84.

126. Millay,D.P., Sargent,M.A., Osinska,H., Baines,C.P., Barton,E.R., Vuagniaux,G., Sweeney,H.L., Robbins,J., Molkentin,J.D. (2008) Genetic and pharmacologic inhibition of mitochondrial-dependent necrosis attenuates muscular dystrophy. *Nat. Med.*, **14**, 442-447.

127. Palma,E., Tiepolo,T., Angelin,A., Sabatelli,P., Maraldi,N.M., Basso,E., Forte,M.A., Bernardi,P., Bonaldo,P. (2009) Genetic ablation of cyclophilin D

rescues mitochondrial defects and prevents muscle apoptosis in collagen VI myopathic mice. *Hum. Mol. Genet.*, **18**, 2024-2031.

128. Irwin,W.A., Bergamin,N., Sabatelli,P., Reggiani,C., Megighian,A., Merlini,L., Braghetta,P., Columbaro,M., Volpin,D., Bressan,G.M.*, et al.* (2003) Mitochondrial dysfunction and apoptosis in myopathic mice with collagen VI deficiency. *Nature Genetics*, **35**, 367-371.

129. Bonaldo,P., Braghetta,P., Zanetti,M., Piccolo,S., Volpin,D., Bressan,G.M. (1998) Collagen VI deficiency induces early onset myopathy in the mouse: an animal model for Bethlem myopathy. *Human Molecular Genetics*, **7**, 2135-2140.

130. Lang,R.M., Bierig,M., Devereux,R.B., Flachskampf,F.A., Foster,E., Pellikka,P.A., Picard,M.H., Roman,M.J., Seward,J., Shanewise,J.S.*, et al.* (2005) Recommendations for chamber quantification: a report from the American Society of Echocardiography's Guidelines and Standards Committee and the Chamber Quantification Writing Group, developed in conjunction with the European Association of Echocardiography, a branch of the European Society of Cardiology. *J. Am. Soc. Echocardiogr.*, **18**, 1440-1463.

131. Schulz,R., Aker,S., Belosjorow,S., Konietzka,I., Rauen,U., Heusch,G. (2003) Stress kinase phosphorylation is increased in pacing-induced heart failure in rabbits. *Am. J. Physiol Heart Circ. Physiol*, **285**, H2084-H2090.

132. Aker,S., Snabaitis,A.K., Konietzka,I., van de Sand,A., Bongler,K., Avkiran,M., Heusch,G., Schulz,R. (2004) Inhibition of the Na+/H+ exchanger attenuates the deterioration of ventricular function during pacing-induced heart failure in rabbits. *Cardiovasc. Res.*, **63**, 273-282.

133. Towbin,H., Staehelin,T., Gordon,J. (1979) Electrophoretic transfer of proteins from polyacrylamide gels to nitrocellulose sheets: procedure and some applications. *Proc. Natl. Acad. Sci. U. S. A.*, **76**, 4350-4354.

134. Stanley,B.A., Van Eyk,J.E. (2007) A solubility optimization protocol for two-dimensional gel electrophoresis of cardiac tissue. *Methods Mol. Biol.*, **357**, 59-65.

135. Conrad,C.C., Choi,J., Malakowsky,C.A., Talent,J.M., Dai,R., Marshall,P., Gracy,R.W. (2001) Identification of protein carbonyls after two-dimensional electrophoresis. *Proteomics.*, **1**, 829-834.

136. Janssen-Heininger,Y.M., Mossman,B.T., Heintz,N.H., Forman,H.J., Kalyanaraman,B., Finkel,T., Stamler,J.S., Rhee,S.G., van,d., V (2008) Redox-based regulation of signal transduction: principles, pitfalls, and promises. *Free Radic. Biol. Med.*, **45**, 1-17.

137. Jaffrey,S.R., Snyder,S.H. (2001) The biotin switch method for the detection of S-nitrosylated proteins. *Sci. STKE.*, **2001**, L1.

138. Smillie,L.B. (1982) Preparation and identification of alpha- and beta-tropomyosins. *Methods Enzymol.*, **85 Pt B**, 234-241.

139. Schagger,H., von,J.G. (1987) Tricine-sodium dodecyl sulfate-polyacrylamide gel electrophoresis for the separation of proteins in the range from 1 to 100 kDa. *Anal. Biochem.*, **166**, 368-379.

140. Rossi,R., Bottinelli,R., Sorrentino,V., Reggiani,C. (2001) Response to caffeine and ryanodine receptor isoforms in mouse skeletal muscles. *Am. J. Physiol Cell Physiol*, **281**, C585-C594.

141. Blaauw,B., Mammucari,C., Toniolo,L., Agatea,L., Abraham,R., Sandri,M., Reggiani,C., Schiaffino,S. (2008) Akt activation prevents the force drop induced by eccentric contractions in dystrophin-deficient skeletal muscle. *Hum. Mol. Genet.*, **17**, 3686-3696.

142. Bleumink,G.S., Knetsch,A.M., Sturkenboom,M.C., Straus,S.M., Hofman,A., Deckers,J.W., Witteman,J.C., Stricker,B.H. (2004) Quantifying the heart failure epidemic: prevalence, incidence rate, lifetime risk and prognosis of heart failure The Rotterdam Study. *Eur. Heart J.*, **25**, 1614-1619.

143. Lloyd-Jones,D.M., Larson,M.G., Leip,E.P., Beiser,A., D'Agostino,R.B., Kannel,W.B., Murabito,J.M., Vasan,R.S., Benjamin,E.J., Levy,D. (2002) Lifetime risk for developing congestive heart failure: the Framingham Heart Study. *Circulation*, **106**, 3068-3072.

144. Neumann,T., Biermann,J., Erbel,R., Neumann,A., Wasem,J., Ertl,G., Dietz,R. (2009) Heart failure: the commonest reason for hospital admission in Germany: medical and economic perspectives. *Dtsch. Arztebl. Int.*, **106**, 269-275.

145. Liang,C.S., Delehanty,J.D. (2009) Increasing post-myocardial infarction heart failure incidence in elderly patients a call for action. *J. Am. Coll. Cardiol.*, **53**, 21-23.

146. Ide,T., Tsutsui,H., Kinugawa,S., Suematsu,N., Hayashidani,S., Ichikawa,K., Utsumi,H., Machida,Y., Egashira,K., Takeshita,A. (2000) Direct evidence for increased hydroxyl radicals originating from superoxide in the failing myocardium. *Circ. Res.*, **86**, 152-157.

147. Li,Y., Huang,T.T., Carlson,E.J., Melov,S., Ursell,P.C., Olson,J.L., Noble,L.J., Yoshimura,M.P., Berger,C., Chan,P.H.*, et al.* (1995) Dilated cardiomyopathy and neonatal lethality in mutant mice lacking manganese superoxide dismutase. *Nat. Genet.*, **11**, 376-381.

148. Nojiri,H., Shimizu,T., Funakoshi,M., Yamaguchi,O., Zhou,H., Kawakami,S., Ohta,Y., Sami,M., Tachibana,T., Ishikawa,H.*, et al.* (2006) Oxidative stress causes heart failure with impaired mitochondrial respiration. *J. Biol. Chem.*, **281**, 33789-33801.

149. Duncan,J.G., Ravi,R., Stull,L.B., Murphy,A.M. (2005) Chronic xanthine oxidase inhibition prevents myofibrillar protein oxidation and preserves

cardiac function in a transgenic mouse model of cardiomyopathy. *Am. J. Physiol Heart Circ. Physiol*, **289**, H1512-H1518.

150. Lombardi,R., Rodriguez,G., Chen,S.N., Ripplinger,C.M., Li,W., Chen,J., Willerson,J.T., Betocchi,S., Wickline,S.A., Efimov,I.R., Marian,A.J. (2009) Resolution of established cardiac hypertrophy and fibrosis and prevention of systolic dysfunction in a transgenic rabbit model of human cardiomyopathy through thiol-sensitive mechanisms. *Circulation*, **119**, 1398-1407.

151. Bergamini,C.M., Signorini,M., Barbato,R., Menabò,R., Di Lisa,F., Gorza,L., Beninati,S. (1995) Transglutaminase-catalyzed polymerization of troponin in vitro. *Biochem. Biophys. Res. Commun.*, **206**, 201-206.

152. Gorza,L., Menabò,R., Vitadello,M., Bergamini,C.M., Di Lisa,F. (1996) Cardiomyocyte troponin T immunoreactivity is modified by cross- linking resulting from intracellular calcium overload. *Circulation*, **93**, 1896-1904.

153. Rabkin,S.W., Klassen,S.S., Tsang,M.Y. (2007) Sodium nitroprusside activates p38 mitogen activated protein kinase through a cGMP/PKG independent mechanism. *Life Sci.*, **81**, 640-646.

154. Pan,J., Singh,U.S., Takahashi,T., Oka,Y., Palm-Leis,A., Herbelin,B.S., Baker,K.M. (2005) PKC mediates cyclic stretch-induced cardiac hypertrophy through Rho family GTPases and mitogen-activated protein kinases in cardiomyocytes. *J. Cell Physiol*, **202**, 536-553.

155. Ueno,H. (1984) Local structural changes in tropomyosin detected by a trypsin-probe method. *Biochemistry*, **23**, 4791-4798.

156. Michele,D.E., Metzger,J.M. (2000) Physiological consequences of tropomyosin mutations associated with cardiac and skeletal myopathies. *J. Mol. Med.*, **78**, 543-553.

157. Schagger,H., von Jagow,G. (1991) Blue native electrophoresis for isolation of membrane protein complexes in enzymatically active form. *Anal. Biochem.*, **199**, 223-231.

158. Heusch,P., Canton,M., Aker,S., van de Sand,A., Konietzka,I., Rassaf,T., Menazza,S., Brodde,O.E., Di,L.F., Heusch,G., Schulz,R. (2010) The contribution of reactive oxygen species and p38 mitogen-activated protein kinase to myofilament oxidation and progression of heart failure in rabbits. *Br. J Pharmacol*, **160**, 1408-1416.

159. Heusch,P., Aker,S., Boengler,K., Deindl,E., van de Sand,A., Klein,K., Rassaf,T., Konietzka,I., Sewell,A., Menazza,S.*, et al.* (2010) Increased inducible nitric oxide synthase and arginase II expression in heart failure: no net nitrite/nitrate production and protein S-nitrosylation. *Am. J Physiol Heart Circ. Physiol*, **299**, H446-H453.

160. Levine,R.L., Williams,J.A., Stadtman,E.R., Shacter,E. (1994) Carbonyl assays for determination of oxidatively modified proteins. *Methods Enzymol.*, **233**, 346-357.

161. DalleDonne,I., Rossi,R., Giustarini,D., Gagliano,N., Lusini,L., Milzani,A., Di Simplicio,P., Colombo,R. (2001) Actin carbonylation: from a simple marker of protein oxidation to relevant signs of severe functional impairment. *Free Radic. Biol. Med.*, **31**, 1075-1083.

162. Peacock,W.F., De,M.T., Fonarow,G.C., Diercks,D., Wynne,J., Apple,F.S., Wu,A.H. (2008) Cardiac troponin and outcome in acute heart failure. *N. Engl. J. Med.*, **358**, 2117-2126.

163. Horwich,T.B., Patel,J., MacLellan,W.R., Fonarow,G.C. (2003) Cardiac troponin I is associated with impaired hemodynamics, progressive left ventricular dysfunction, and increased mortality rates in advanced heart failure. *Circulation*, **108**, 833-838.

164. Miettinen,K.H., Eriksson,S., Magga,J., Tuomainen,P., Kuusisto,J., Vanninen,E.J., Turpeinen,A., Punnonen,K.R., Pettersson,K., Peuhkurinen,K.J. (2008) Clinical significance of troponin I efflux and troponin autoantibodies in patients with dilated cardiomyopathy. *J. Card Fail.*, **14**, 481-488.

165. Fenton,K.E., Sable,C.A., Bell,M.J., Patel,K.M., Berger,J.T. (2004) Increases in serum levels of troponin I are associated with cardiac dysfunction and disease severity in pediatric patients with septic shock. *Pediatr. Crit Care Med.*, **5**, 533-538.

166. Skyschally,A., Gres,P., van,C.P., van de Sand,A., Boengler,K., Schulz,R., Heusch,G. (2008) Reduced calcium responsiveness characterizes contractile dysfunction following coronary microembolization. *Basic Res. Cardiol.*, **103**, 552-559.

167. Hess,D.T., Matsumoto,A., Kim,S.O., Marshall,H.E., Stamler,J.S. (2005) Protein S-nitrosylation: purview and parameters. *Nat. Rev. Mol. Cell Biol.*, **6**, 150-166.

168. Kohr,M.J., Sun,J., Aponte,A., Wang,G., Gucek,M., Murphy,E., Steenbergen,C. (2010) Simultaneous Measurement of Protein Oxidation and S-Nitrosylation During Preconditioning and Ischemia/Reperfusion Injury With Resin-Assisted Capture. *Circ. Res.*.

169. Whitehead,N.P., Yeung,E.W., Allen,D.G. (2006) Muscle damage in mdx (dystrophic) mice: role of calcium and reactive oxygen species. *Clin. Exp. Pharmacol. Physiol*, **33**, 657-662.

170. Tidball,J.G., Wehling-Henricks,M. (2007) The role of free radicals in the pathophysiology of muscular dystrophy. *J. Appl. Physiol*, **102**, 1677-1686.

171. Messina,S., Bitto,A., Aguennouz,M., Mazzeo,A., Migliorato,A., Polito,F., Irrera,N., Altavilla,D., Vita,G.L., Russo,M.*, et al.* (2009) Flavocoxid

counteracts muscle necrosis and improves functional properties in mdx mice: a comparison study with methylprednisolone. *Exp. Neurol.*, **220**, 349-358.

172. Di Lisa,F., Kaludercic,N., Carpi,A., Menabo,R., Giorgio,M. (2009) Mitochondria and vascular pathology. *Pharmacol. Rep.*, **61**, 123-130.

173. Tiepolo,T., Angelin,A., Palma,E., Sabatelli,P., Merlini,L., Nicolosi,L., Finetti,F., Braghetta,P., Vuagniaux,G., Dumont,J.M.*, et al.* (2009) The cyclophilin inhibitor Debio 025 normalizes mitochondrial function, muscle apoptosis and ultrastructural defects in Col6a1(-/-) myopathic mice. *Br. J. Pharmacol.*, **157**, 1045-1052.

174. Weller,B., Karpati,G., Carpenter,S. (1990) Dystrophin-deficient mdx muscle fibers are preferentially vulnerable to necrosis induced by experimental lengthening contractions. *J. Neurol. Sci.*, **100**, 9-13.

175. Blaauw,B., Agatea,L., Toniolo,L., Canato,M., Quarta,M., Dyar,K.A., Danieli-Betto,D., Betto,R., Schiaffino,S., Reggiani,C. (2010) Eccentric contractions lead to myofibrillar dysfunction in muscular dystrophy. *J. Appl. Physiol*, **108**, 105-111.

176. Angelin,A., Tiepolo,T., Sabatelli,P., Grumati,P., Bergamin,N., Golfieri,C., Mattioli,E., Gualandi,F., Ferlini,A., Merlini,L.*, et al.* (2007) Mitochondrial dysfunction in the pathogenesis of Ullrich congenital muscular dystrophy and prospective therapy with cyclosporins. *Proc. Natl. Acad. Sci. U. S. A*, **104**, 991-996.

177. Reutenauer,J., Dorchies,O.M., Patthey-Vuadens,O., Vuagniaux,G., Ruegg,U.T. (2008) Investigation of Debio 025, a cyclophilin inhibitor, in the dystrophic mdx mouse, a model for Duchenne muscular dystrophy. *Br. J. Pharmacol.*, **155**, 574-584.

178. Merlini,L., Angelin,A., Tiepolo,T., Braghetta,P., Sabatelli,P., Zamparelli,A., Ferlini,A., Maraldi,N.M., Bonaldo,P., Bernardi,P. (2008) Cyclosporin A corrects mitochondrial dysfunction and muscle apoptosis in patients with collagen VI myopathies. *Proc. Natl. Acad. Sci. U. S. A*, **105**, 5225-5229.

179. Svineng,G., Ravuri,C., Rikardsen,O., Huseby,N.E., Winberg,J.O. (2008) The role of reactive oxygen species in integrin and matrix metalloproteinase expression and function. *Connect. Tissue Res.*, **49**, 197-202.

180. Werner,E., Werb,Z. (2002) Integrins engage mitochondrial function for signal transduction by a mechanism dependent on Rho GTPases. *J. Cell Biol.*, **158**, 357-368.

181. Taddei,M.L., Parri,M., Mello,T., Catalano,A., Levine,A.D., Raugei,G., Ramponi,G., Chiarugi,P. (2007) Integrin-mediated cell adhesion and spreading engage different sources of reactive oxygen species. *Antioxid. Redox. Signal.*, **9**, 469-481.

182. Di Lisa,F., Bernardi,P. (2009) A CaPful of mechanisms regulating the mitochondrial permeability transition. *J. Mol. Cell Cardiol.*, **46**, 775-780.

183. Whitehead,N.P., Pham,C., Gervasio,O.L., Allen,D.G. (2008) N-Acetylcysteine ameliorates skeletal muscle pathophysiology in mdx mice. *J. Physiol*, **586**, 2003-2014.

184. Dorchies,O.M., Wagner,S., Vuadens,O., Waldhauser,K., Buetler,T.M., Kucera,P., Ruegg,U.T. (2006) Green tea extract and its major polyphenol (-)-epigallocatechin gallate improve muscle function in a mouse model for Duchenne muscular dystrophy. *Am. J. Physiol Cell Physiol*, **290**, C616-C625.